LBL-22827 c.2

Lawrence Berkeley Laboratory
UNIVERSITY OF CALIFORNIA

RECEIVED
MAR 17 1987
LIBRARY AND
DOCUMENTS SECTION

CHEMICAL BIODYNAMICS DIVISION

PICOSECOND SPECTROSCOPIC STUDIES OF ENERGY TRANSFER IN PHYCOBILIPROTEINS AND MODEL DYE SYSTEMS

S.C. Switalski
(Ph.D. Thesis)

February 1986

TWO-WEEK LOAN COPY
This is a Library Circulating Copy which may be borrowed for two weeks.

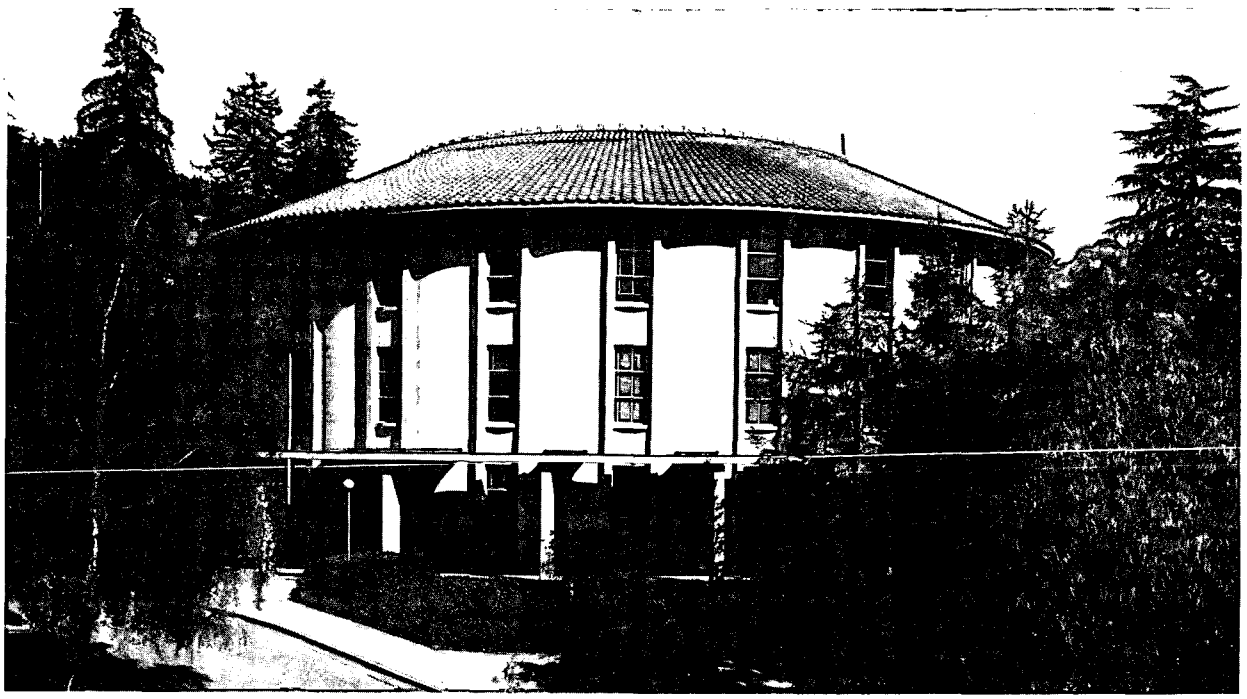

LBL-22827 c.2

Prepared for the U.S. Department of Energy under Contract DE-AC03-76SF00098

DISCLAIMER

This document was prepared as an account of work sponsored by the United States Government. While this document is believed to contain correct information, neither the United States Government nor any agency thereof, nor the Regents of the University of California, nor any of their employees, makes any warranty, express or implied, or assumes any legal responsibility for the accuracy, completeness, or usefulness of any information, apparatus, product, or process disclosed, or represents that its use would not infringe privately owned rights. Reference herein to any specific commercial product, process, or service by its trade name, trademark, manufacturer, or otherwise, does not necessarily constitute or imply its endorsement, recommendation, or favoring by the United States Government or any agency thereof, or the Regents of the University of California. The views and opinions of authors expressed herein do not necessarily state or reflect those of the United States Government or any agency thereof or the Regents of the University of California.

Picosecond Spectroscopic Studies of Energy Transfer in Phycobiliproteins and Model Dye Systems

Steven Casimir Switalski

Ph.D. Thesis

Lawrence Berkeley Laboratory
University of California
Berkeley, California 94720

February 1987

This work was supported by the U.S. Department of Energy under Contract Number DE-AC03-76SF00098.

dichroism spectra were studied to determine the aggregation state of the protein.

The subunits and monomer of C-phycocyanin exhibit biexponential fluorescence decay kinetics. The biexponential decay kinetics of the α subunit fluorescence (1.4 ns and 0.4 ns) is unexpected, because there is only one chromophore and no possibility of energy transfer. Changes in buffer components, protein concentration, and excitation and emission wavelength do not affect the decay parameters. Conformational heterogeneity is proposed as the source of the biexponential kinetics.

A microchannel plate detector was developed for use in the single-photon timing system and a time resolution of 10-14 ps was achieved. The decay kinetics of the αβ monomer of R-phycocyanin from Porphyridium cruentum, were biexponential and similar to those obtained from C-phycocyanin. R-phycocyanin dimer, with and without linker protein, was studied to determine the effect of the linker on the conformational heterogeneity of the chromophores. Lifetimes for R-phycocyanin with the linker were longer (1.4 ns, 0.3 ns) and the relative fluorescence yield of the long component higher (95%) than R-phycocyanin without the linker (1.2 ns, 0.3 ns; 91%), indicating that the linker alters the amounts of the heterogeneous conformations. We conclude that energy transfer is faster than 10-14 ps in the subunits, monomer, and dimer of phycobiliproteins.

Digested or denatured C-phycocyanin exhibits 3

resolvable decay components. The mean lifetime is shorter than that of the native protein. The chromophore appears to have increased conformational heterogeneity due to the disruption of the protein-chromophore interaction.

The fluorescence decay kinetics of triphenylmethane dyes were studied as a function of viscosity. This dye system provided a calibration of the microchannel plate time resolution, and allowed us to study the effect of molecular conformation on the competition between non-radiative relaxation and fluorescence decay rates. Contrary to previous literature results, we found no regime in which the log of the fluorescence decay lifetimes of TPM dyes has a linear dependence on the log of the viscosity. Rather, a curve with a continuously varying slope fits the results, with different low and high viscosity lifetime asymptotes for malachite green and crystal violet and with different viscosities at which the inflection points of similarly shaped curves appear. In addition, we obtained two lifetimes for crystal violet and three for malachite green, all with different asymptotes and inflection points. The preexponential factors are not in a constant ratio, but vary as a function of viscostiy and the number of lifetimes resolved. Decay kinetics in various solvents did not indicate any solvent effect; nor was there any dependence on excitation and emission wavelength. Our results resolve the discrepancies among the literature values for the slope of the log lifetime vs. log viscosity dependence.

DEDICATION

To my one and only, to Barb.

ACKNOWLEDGEMENTS

First, and foremost, I would like to acknowledge the support and guidance provided by Ken Sauer, my research director. I would like to thank the Sauer research group as a whole, but I would also like to mention a few special individuals. Much of my knowledge of picosecond laser spectroscopy came from profitable experiments conducted with Kerry Karukstis, Sara Hoover, and Paul Reisberg.

I am most grateful for the cultures and protein samples provided by Alex Glazer and Bruce Watson. I was assisted in protein characterization by Steve Worland and Kris Zsebo.

I would like to thank the members of my thesis committee. In particular, fruitful discussions with Alex Glazer gave important direction to my work.

In addition, I was privileged to work with an excellent scientist and superb human being, Ken Rousslang. Our collaboration and close friendship provided a motivating force to finish this work and continue a career in chemistry.

I would like to acknowledge my parents for their unswerving support of my education through all these many years.

And finally, I would like to thank the most important person in my life, my wife, Barb, for her emotional support during my graduate career; her typing; proofing and editing of this manuscript; and the time and effort she committed to my career.

ABBREVIATIONS

APC	allophycocyanin
APC-B	allophycocyanin B
APC I	allophycocyanin I
b-PE	b-phycoerythrin
B-PE	B-phycoerythrin
CD	circular dichroism
chl a	chlorophyll a
chl b	chlorophyll b
C-PC	C-phycocyanin
C-PE	C-phycoerythrin
f	fluorescing
FWHM	full width, half maximum
MCP	microchannel plate
PAGE	polyacrylamide gel electrophoresis
PMT	photomultiplier tube
PS I	photosystem I
PS II	photosystem II
PB	phycobilin
PBP	phycobiliprotein
PBS	phycobilisome
PC	phycocyanin
PCB	phycocyanobilin
PE	phycoerythrin
PEB	phycoerythrobilin
PEC	phycoerythrocyanin
PUB	phycourobilin
RC	reaction center
R-PC	R-phycocyanin
R-PE	R-phycoerythrin
s	sensitizing

TABLE OF CONTENTS

ABSTRACT

DEDICATION.....i

ACKNOWLEDGEMENTS.....ii

ABBREVIATIONS.....iii

TABLE OF CONTENTS.....iv

GOALS.....vii

I. INTRODUCTION.....1

A. Motivation.....1

B. Phycobiliproteins.....2

II. PHYCOBILIPROTEINS.....3

A. Introduction.....3

1. Structure.....3

a) Chromophores.....4

(1) Chromophore structure, diversity.....4
(2) Chromophore bound to protein - covalent interaction.....12
(3) Chromophore bound to protein - noncovalent interaction.....13
(4) Chromophore conformation.....14

b) Protein.....17

(1) Primary sequence.....17
(2) Tertiary conformation.....17
(3) Subunits.....18

c) Aggregation.....18

(1) Monomer.....18
(2) Trimer.....19
(3) Hexamer.....19
(4) Linker.....20
(5) Rods.....21
(6) Core.....21
(7) Phycobilisomes.....22

d) Association to thylakoids and photosystems....26
e) Biosynthesis and chromatic adaption....26
f) Evolution....28

2. Function....29

a) Chromophores....30

(1) chromophore structure, diversity....30
(2) Chromophore bound to protein - covalent interaction....31
(3) Chromophore bound to protein - noncovalent interaction....31
(4) Chromophore conformation....32

b) Protein....34

(1) Primary sequence....34
(2) Subunits....35

c) Aggregation....37

(1) Monomer....37
(2) Trimer....38
(3) Hexamer....38
(4) Linker....39
(5) Rods....39
(6) Core....40
(7) Phycobilisomes....40

B. Materials and Methods....43

1. Protein preparation....43

a) Monomer....43
b) Subunits....44
c) Dimer....45

2. Steady-state spectroscopy....47
3. Picosecond single-photon timing....48

a) Instrumentation....48
b) Data collection....61
c) Analysis....66

C. Results and Discussion....70

1. Steady-state spectroscopy....70

a) Absorption....70
b) Fluorescence excitation....87

c) Fluorescence emission.....92
d) Fluorescence excitation polarization.....95
e) Circular dichroism.....101

2. Time-resolved spectroscopy.....106

a) Monomer and subunits.....106
b) Dimer.....122

D. Conclusion.....127

III. TRIPHENYLMETHANE DYES.....141

A. Introduction.....141

1. Structure.....142
2. Photophysics.....145

B. Materials and methods.....160
C. Results.....164
D. Discussion.....184
E. Conclusion.....191

IV. CONCLUSIONS AND FUTURE EXPERIMENTS.....194

A. Methods and instrumentation.....194

1. Deconvolution.....194
2. Component analysis.....196
3. Wavelength-resolved decay kinetics.....198
4. Time resolution.....199

B. Triphenylmethane dyes.....200

1. Separation of temperature, viscosity, and solvent dependence of fluorescence decay kinetics.....201
2. Time-resolved Raman spectroscopy.....202
3. Transient absorption spectroscopy.....203

C. Phycobiliproteins.....203

1. Effect of temperature on decay kinetics.....204
2. Time-resolved Raman spectroscopy.....205
3. Methods and instrumentation.....206

GOALS

The goal for this thesis was to utilize structural, steady-state, and picosecond spectroscopic techniques to investigate energy transfer in a biophysical system. The system chosen for study was the phycobiliproteins. In conjunction with these investigations, the time resolution of the picosecond single-photon timing technique was improved by using microchannel plate photomultiplier tube detection and the system calibrated with triphenylmethane dyes. The triphenylmethane dyes proved to have very interesting photophysical properties as a function of solvent viscosity, and these were also investigated.

CHAPTER I

INTRODUCTION

I.A Motivation

Photosynthetic organisms provide the most important examples of efficient utilization of solar energy. Utilizing the energy of the sun requires the absorption of the spectrally disperse light energy and its transformation into some useable energy form. These organisms physically divide the two processes. A variety of antenna (accessory light-harvesting pigment) systems collect (absorb) the light, and transfer electronic excitation energy to reaction centers. These special enzymatic sites transform the electronic excitation energy into chemical energy via a primary charge separation. The energy transfer is a radiationless process and not a trivial emission and then reabsorption of a photon. The size, structure, location, and composition for this light harvesting function of the antenna is widely varied. Reaction centers are always located in the membrane; but the antennae may be membranous, attached to the membrane, or in separate particles or vesicles.

In cyanobacteria and eukaryotic organisms, the reaction center chlorophylls represent < 1% of the chlorophyll within the thylakoid.[36] Generally, the light-harvesting apparatus of bacteria, algae, and higher plants has a higher proportion

of pigment and a large extent than the reaction center, which befits its function.[39] Green plants and algae use carotenoids and various chlorophylls (a,b) to harvest light. As a result, photons in the 500-600 nm region are not absorbed effectively. Other algae have accessory pigments to take advantage of this portion of the useable solar spectrum. In particular, the Cyanophyta (cyanobacteria), Rhodophyta (red algae), and Cryptophyceae (cryptomonads) use phycobilin-containing proteins for the light-harvesting function. These organisms do not have chlorophyll b as part of their antenna.

I.B Phycobiliproteins

Phycobiliproteins serve as an excellent model for the study of energy transfer in a biological system. The phycobiliproteins are water-soluble and easily detached from the photosynthetic lamellae constituents. The antenna array, called a phycobilisome, can be purified intact, or the various constituents can be isolated pure and studied separately. At the molecular level, phycobilisomes and their constituent phycobiliproteins remain the best understood photosynthetic antenna array available for study.

The hierarchical nature of the phycobiliprotein aggregates and arrays is also important. Specifically, different chromophore type, number, orientation, and conformation allow us to study energy transfer at different levels of complexity and possibly involving different energy transfer mechanisms.

CHAPTER II.

PHYCOBILIPROTEINS

II.A Introduction

II.A1 Structure

Phycobiliproteins are the antenna or light harvesting proteins of cyanobacteria, red algae, and cryptomonads. Phycobiliproteins compose as much as 24% of the dry weight of algal cells and 40-60% of the soluble cell protein.[2,3,88,30] Cyanobacteria and red algae have their characteristic colors because of the phycobiliproteins. "Phyco" denotes a seaweed and "bili" indicates the relation of the tetrapyrrole prosthetic pigments to the bile pigments, biliverdin and bilirubin, of mammals.[38,68] The hierarchical structure of these proteins provides the appropriate framework for discussion. Therefore, the order of topics will be the structure of the chromophores, protein, and aggregated protein and how this relates to their function and evolution.

Cryptomonad phycobiliproteins are sufficiently distinct from the cyanobacterial and red algal phycobiliproteins studied that they will be discussed sparingly and usually only with respect to their differences.

In addition to the information and references that follow, many excellent, informative reviews on

phycobiliproteins and phycobilisomes are available. (See references 93, 94, 6, 96, 11, 36, 37, 24, 26, 38, 106, 81, 124, 39, 40, and 41.)

II.Ala Chromophores

II.Ala(1) Chromophore structure, diversity

Open-chain or "linear" (extended as opposed to cyclic) tetrapyrroles are the prosthetic pigments of phycobiliproteins. Chromophore cleavage reactions yield different pigments depending on the method used.[106] Methods include hydrolysis with HCL at room temperature, methanolysis, and cleavage with HBr in trifluoroacetic acid at 75°C. The five major isomers assigned to the native pigment are phycocyanobilin, phycoerythrobilin, phycourobilin, a phycobiliviolin-type chromophore, and a chromophore present in cryptomonads whose structure is unknown. These names apply to the bound pigment. One distinction between phycobiliproteins is based on the type and number of phycobilins attached to the protein. The first conclusive assignment of the number and type of phycobilins present was determined by Glazer and Fang, based on the observation of O'hEocho that the spectra of the bound chromophores under denaturing conditions matched more closely the spectra of the free phycobilin and could be correlated to the structure of free bili pigment.[95,46,47] In 8M urea at pH 3.0, the absorption spectra of bound phycobilins are independent of the attached polypeptide chain. From measurements of molar absorption spectra,

protein concentrations from amino acid analysis, and amino acid sequence, the bilin content of many biliproteins has been determined (see Fig. II.A-1). The prefixes C-, R-, etc. can be dated to similarities with the first isolated proteins: C- for Cyanophycean, R- for Rhodophycean, and B-, b- for Bangiophycean, a subgroup of Rhodophycean.[7,26]

The absorption spectra arise predominantly from the bilin content, and on this basis the phycobiliproteins of cyanobacteria and red algae can be divided into three major types: the phycoerythrins, absorbing from 480-580 nm; the phycocyanins, absorbing from 570-630 nm; and the allophycocyanins, absorbing from 610-670 nm (Fig. II.A-2)

As seen in Fig. II.A-1, the 2 predominant chromophores are phycocyanobilin and phycoerythrobilin (shown in Fig. II.A-3). Phycocyanin appears to be present in phycochromes (photoreversible pigments involved in regulation of phycobiliprotein biosynthesis, (see Section II.Ale), and a chromophore similar to phycocyanobilin occurs in phytochromes.[91,92] The structure for phycourobilin is also shown in Fig. II.A-3.[41] Phycoerythrocyanin has a red chromophore of unknown structure (Bryant et al., 1978).[11] Two other chromophores are present in Cryptophytan biliproteins.[44,61,84,106]

All cyanobacteria described to date contain allophycocyanin and C-phycocyanin. All red algae contain allophycocyanin and R-phycocyanin or C-phycocyanin. Some cyanobacteria and red algae contain phycoerythrin. Some

Fig. II.A-1: The nature and distribution of bilin prosthetic groups among the subunits of the various biliproteins, and the numbers present in higher aggregates of each protein. For example, R-phycocyanin, $(\alpha\beta)_3$, contains six phycocyanobilin and three phycoerythrobilin groups per trimer; each α subunit carries one phycocyanobilin, whereas each β subunit carries one phycocyanobilin and one phycoerythrobilin. The absorption and fluorescence emission maxima are given for the higher aggregate of each of the biliproteins, i.e.; in the case of R-phycocyanin, the values refer to the $(\alpha\beta)_3$ aggregate. PEB, phycoerythrobilin; PUB, phycourobilin; PCB, phycocyanobilin; PXB, bilin of undetermined structure. Fig. 3 from Ref. 40, with the kind permission of Dr. A. Glazer.

	Allophycocyanin B	R-Phycocyanin	b-Phycoerythrin
	$(\alpha\beta)_3$ 6 PCB	$(\alpha\beta)_3$ 6 PCB, 3 PEB	$(\alpha\beta)_n$
			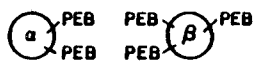
λ_{max} (nm)	670, 618	618, 555	563 (s), 545
λ^F_{max} (nm)	680	636	570

	Allophycocyanin	Phycoerythrocyanin	B-Phycoerythrin
	$(\alpha\beta)_3$ 6 PCB	$(\alpha\beta)_3$ 6 PCB, 3 PXB	$(\alpha\beta)_6\gamma$ 32 PEB, 2 PUB
			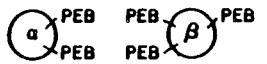
λ_{max} (nm)	650	590 (s), 568	563, 545, 498 (s)
λ^F_{max} (nm)	660	625	575

	C-Phycocyanin	C-Phycoerythrin	R-Phycoerythrin
	$(\alpha\beta)_6$ 18 PCB	$(\alpha\beta)_6$ 36 PEB	$(\alpha\beta)_6\gamma$ 25 PEB, 9 PUB
	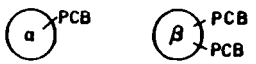	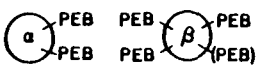	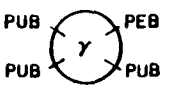
λ_{max} (nm)	620	564	567, 540, 498
λ^F_{max} (nm)	648	577	578

Fig. II.A-2: Spectroscopic characteristics of native cyanobacterial and rhodophytan phycobiliproteins at neutral pH. The main absorption maximum in the visible region of the room temperature spectrum is indicated for each protein by a thick vertical line; subsidiary maxima are indicated by thinner vertical lines. Broken vertical lines represent shoulders. The horizontal lines cover the portion of the spectrum over which the absorption of the particular protein is ≧ 20% of that at its absorption maximum. PCB, phycocyanobilin; PEB, phycoerythrobilin; PUB, phycourobilin; PXB, bilin of undetermined structure. The abbreviation indicates the bile pigment which makes the major contribution at each maximum or shoulder. Provided by Dr. A. Glazer.

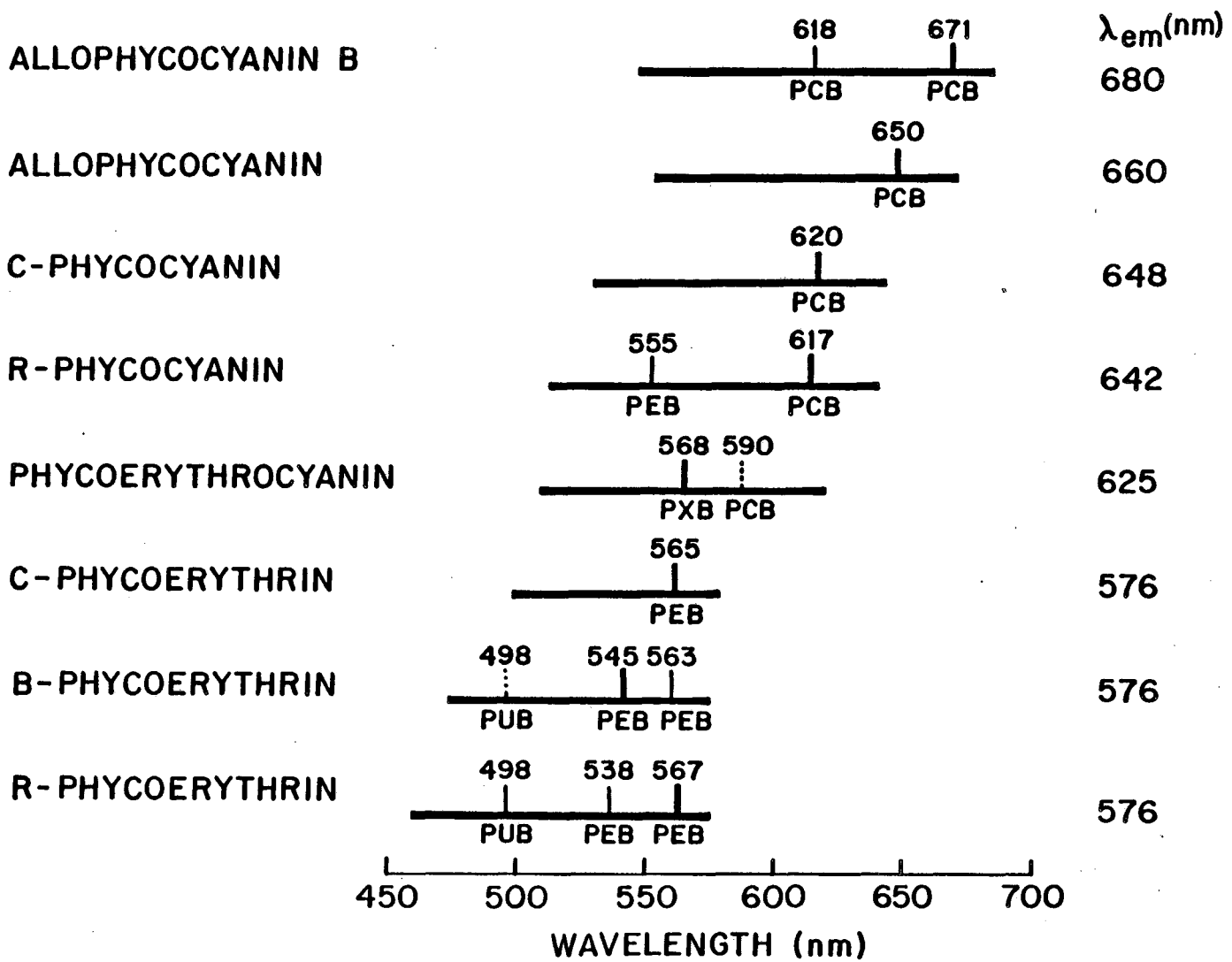
ALLOPHYCOCYANIN B
618
671
PCB
PCB
λem(nm)
680
ALLOPHYCOCYANIN
650
PCB
660
C-PHYCOCYANIN
620
PCB
648
R-PHYCOCYANIN
555
617
PEB
PCB
642
PHYCOERYTHROCYANIN
568 590
PXB PCB
625
C-PHYCOERYTHRIN
565
PEB
576
B-PHYCOERYTHRIN
498
545 563
PUB
PEB PEB
576
R-PHYCOERYTHRIN
498
538 567
PUB
PEB PEB
576
450
500
550
600
650
700
WAVELENGTH (nm)

Fig. II.A-3: Bilin-peptide linkages in biliproteins. (A) phycocyanobilin linked through ring A (ref. 69); (B) phycocyanobilin linked through ring D (J. Bishop, J. C. Lagarias, A. N. Glazer, H. Rapoport, unpublished results); (C) phycoerythrobilin linked through ring A (79, 102, 104); (D) doubly linked phycoerythrobilin (79, 103); (E) phycourobilin linked through ring A; and (F) doubly linked phycourobilin (A. V. Klotz, A. N. Glazer, J. Nagy, J. Bishop, H. Rapoport, unpublished results). Fig. 3 of Ref. 41, with the kind permission of Dr. A. Glazer.

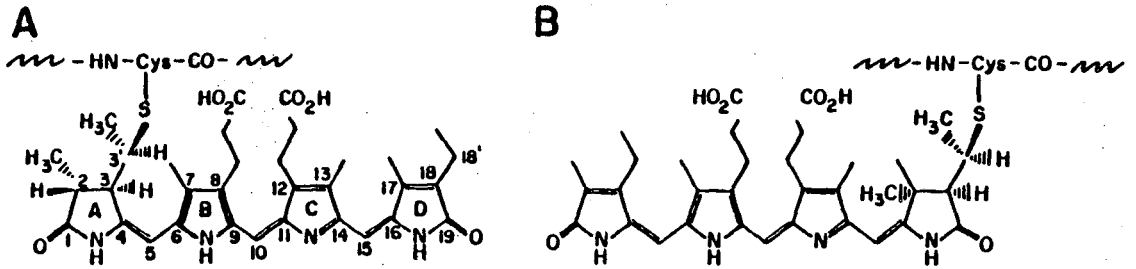

Peptide-linked PHYCOCYANOBILINS

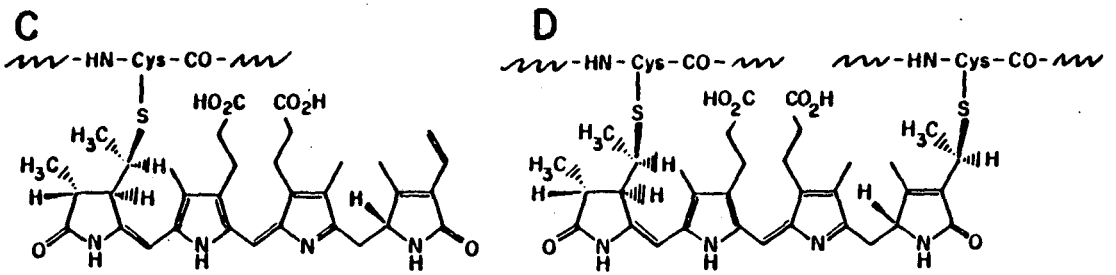

Peptide-linked PHYCOERYTHROBILINS

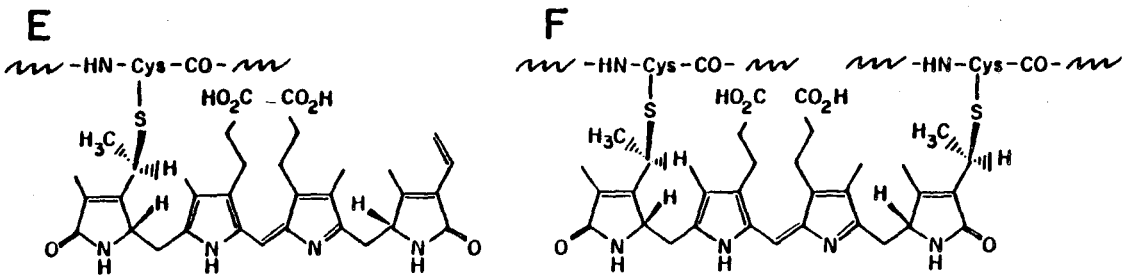

Peptide-linked PHYCOUROBILINS

cyanobacteria contain phycoerythrocyanin. It should be noted that the chromophore content of phycoerythrin from cryptomonads is different, containing only phycoerythrobilin, and the phycocyanin from cryptomonads is more complex than that of blue-green or red algae. For example, phycocyanobilin and phycobiliviolin are present in C-phycocyanin from Hemiselmis virescens Plymouth 157.[97,44] The phycocyanin from Hemiselmis virescens Millport 64 has 3 different bilins; phycocyanobilin, phycobiliviolin (cryptoviolin), and an unknown bilin with absorption λ_{max}= 694 and 368 nm on the α subunit. Allophycocyanin seems to be missing from cryptomonads, and it is proposed that chlorophyll-c fulfills the energy transfer role of allophycocyanin.

II.Ala(2) Chromophore bound to protein - covalent interaction

The tetrapyrroles are covalently bound to the proteins. There is direct support for a single thioether linkage to ring A of the phycocyanobilin in Synechococcus 6301 C-phycocyanin, based on NMR studies performed by Lagarias et al. (Fig. II.A-3).[69] One and two thioether linkages in other phycobilins have subsequently been supported by NMR and chemical studies.[79,102,103,104] The mechanism of bilin attachment is unknown, but the presence of a cysteine is not a sufficient condition for attachment, implying some attachment specificity. However, cysteine has been shown to be a necessary amino acid for binding in the structure studies so

far (see review references, especially References 27, 28, and 88, for a listing of sequence studies). These sequence studies show that every bilin is attached to cysteinyl residues.

The stereospecificity is known from modified chromic acid digestion, model studies of succinimides, and NMR investigations.[69,63,78]

Other linkages have been proposed, including an ester bond of the β-carboxyl group of an aspartyl residue and the hydroxyl group of the enol form of ring A and also the carbonyl group of ring B and C, but there is no evidence for such linkages.

II.Ala(3) Chromophore bound to protein - noncovalent interaction

Physical and immunological results suggest that the tetrapyrrole is enveloped by the polypeptide. For example, allophycocyanin and C-phycocyanin, which both carry phycocyanobilin groups, do not cross react, and a tryptic digest of R-phycoerythrin, which has 2 types of tetrapyrroles, does not inhibit the cross reaction of this protein with its homologous antibody.[38]

The differences in characteristics between the denatured and the native structures are due to noncovalent protein-chromophore and chromophore-chromophore interactions. From the absorption and CD spectral changes, Figs. II.A-4a and b are the proposed structures for the denatured and

native conformations, respectively, and can be ascribed to protein-chromophore interaction.[107]

II.Ala(4) Chromophore conformation

Phototautomerization has also been suggested to occur in bili pigments (Falk et al.[19], Holzwarth et al.[57]) from photochemical holeburning experiments by Friedrich et al.[22,23] The mechanism proposed involves a proton transfer in triplet intermediates.

The conformation of the chromophore changes as a result of aggregation of the phycobiliproteins and has been proposed to increase in rigidity, as evidenced by the increase in fluorescence quantum yield out of the terminal emitting chromophore and the increased efficiency of energy transfer (up to 99% to chlorophyll a).[100,108,52,53] In general, therefore, the chromophores are isolated from the amino acid backbone in terms of excitation energy transfer losses, but they have a strong interaction in terms of conformation.[106]

The claim has been made that free bili pigments and denatured biliproteins have broader spectra than native phycobiliproteins and that these spectra result from rapidly interconverting forms in equilibrium.[22,23,57,107] However, biliverdin ester was shown by Braslavsky et al. to exist in solution as 3-4 isomers that are not in equilibrium.[9] The suggestion has been made that the breadth of the native phycobiliprotein spectra is not due to equilibrium conformations but to a number of specific conformations fixed by the

Fig. II.A-4: Proposed structures for the denatured (a) and native (b) chromophore conformations of phycobiliproteins, based on spectra in Ref. 107. From Fig. 10 of Ref. 106.

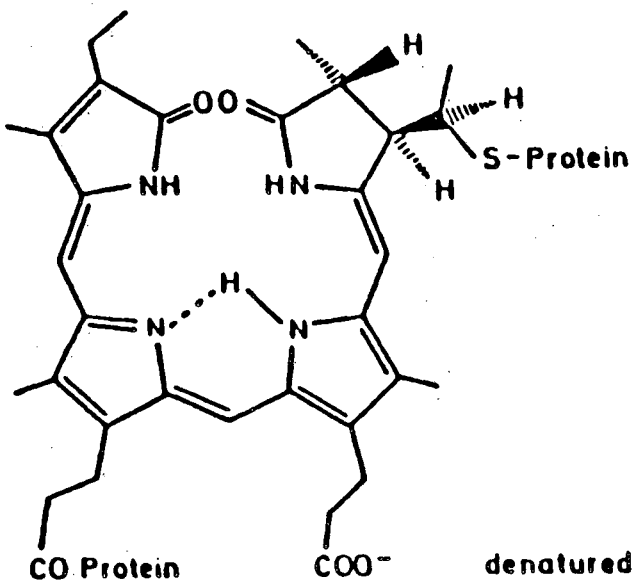

denatured

a

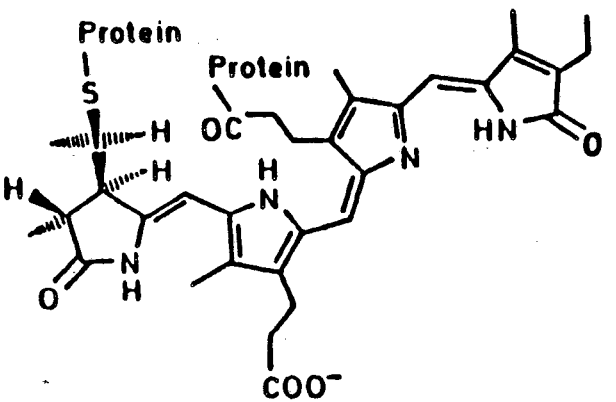

native

b

protein. The spectral and chemical evidence for this will be discussed later (see Section II.A2a[4]).

II.Alb Protein

II.Alb(1) Primary sequence

N-terminal sequences have been determined for all of the classes of protein except the subunits of R-phycoerythrin.[38,49] The amino acid sequence about the site of bilin attachment has been determined in several phycobiliproteins. The complete amino acid sequence has been determined for many phycobiliproteins; for example C-phycocyanin from Mastigocladus laminosus, the α subunit of C-phycocyanin from Cyanidium caldarium, and the β subunit of C-phycocyanin from Synechococcus 6301. The molecular weights in some cases were determined by gel electrophoresis and calibrated with globular proteins. However, phycobiliproteins have been suggested to interact with the resins and stable aggregates of phycobiliproteins are disc shaped, implying that the molecular weights reported in the older literature may have large errors associated with them.[38] The isoelectric points of phycobiliproteins range from 4.2-5.5. The most predominant amino acids are aliphatic and acidic residues, with alanine and aspartic acid the most abundant.

II.Alb(2) Tertiary conformation

The high degree of conservation in primary structure is

reflected in the conserved tertiary structure. Even hybrid proteins, with an α-subunit from one species and a β-subunit from another species, are possible (see Section II.Alb[3]). This tertiary structure conservation is also necessary for the higher aggregation states.

II.Alb(3) Subunits

The phycobiliproteins always have at least 2 subunits, denoted α and β. In B- and R-phycoerythrin a third type of subunit, the γ subunit, is present.[49,112,30]

Subunits can be separated by denaturation. Neutral or alkaline pH results in colored degradation products. Cation exchange chromatography of phycobiliproteins in urea solutions at pH 3.0 results in separation, and recovered subunits can be successfully renatured and reconstituted. Such reconstituted proteins are indistinguishable from the native with respect to chromatography, isoelectric point, absorption and CD spectra, PAGE, and electron microscopy of reconstituted hexamers.[47,48,18]

II.Alc Aggregation

II.Alc(1) Monomer

Aggregation is affected by pH, ionic strength, protein concentration, presence or absence of linker protein, algal source, and temperature. High pH, high ionic strength, high protein concentration, and the presence of linker protein favor aggregation. In addition, aromatic compounds,

deuterium substitution, inorganic and organic salts (chaotropic agents), and nonionic detergents affect aggregation states. Hydrophobic interactions have been concluded to be the major driving force for aggregation.[106] Monomers, composed of one α and one β subunit and denoted (αβ), trimers $(\alpha\beta)_3$, and hexamers, $(\alpha\beta)_6$, are common aggregation states *in vitro* and *in vivo* (see Fig. II.A-1).

II.Alc(2) Trimer

Trimers are ≈ 30 A° thick disks of ≈ 120 A° diameter. They consist of 3 αβ monomers arranged in a ring shape. One proposal has the α subunit of one monomer closest to the β subunit of the next monomer in a circle, having a hole in the center of the ring.[86]

II.Alc(3) Hexamer

Hexamers are ≈ 60 A° double disks with a weak ≈ 30 A° spacing between 2 trimers.[128,129] They are essentially 2 trimers stacked on their broad faces. Trimers and hexamers are the major building blocks of the phycobilisomes and of crystals of phycobiliproteins; they are the most common aggregation states for cyanobacterial and red algal phycobiliproteins.[112]

Cryptomonad phycobiliproteins aggregate into dimers *in vitro*, and do not aggregate further as readily as cyanobacterial and red algal phycobiliproteins.[25] *In vivo*, the aggregation form is unknown.

II.Alc(4) Linker

Tandeau de Marsac and Cohen-Bazire showed that the presence or absence of "uncolored" polypeptides (linker polypeptides) in phycobilisomes is related to the change in the content of phycocyanin and phycoerythrin in chromatic adapters, organisms that change the phycocyanin/phycoerythrin ratio (see Section II.Ale).[114] These linkers represent approximately 15% of the protein content of the phycobilisomes. They come in 2 classes, weighing 70,000-120,000 daltons for Group I and 25-35,000 for Group II. Group I polypeptides are strongly associated to the thylakoid membrane. Certain polypeptides in Group II interact with individual biliproteins. Linkers fill the hole in the center of trimers, except in the case of the γ subunit of B- and R-phycoerythrins. More recently, linkers have been found that have a phycobilin chromophore and that participate in energy transfer. For example, the 75 kD protein of Synechococcus 6301 phycobilisomes has been shown to contain a chromophore that emits at 680 nm (see Section II.Alc[6]).[128] (A review of phycobilisomes and phycobiliproteins by A. Glazer has an extensive discussion of linkers and a proposed nomenclature.[41])

Lundell et al. have isolated three (33, 30, and 27 kilodaltons) polypeptides of Group II from Synechococcus 6301 and have deduced linker function for these.[80] The 33 kd and 30 kd polypeptides are rod extenders and the 27 kd is a rod core linker. It is now clear that linkers are necessary for

the *in vivo* assembly process. Linker proteins can affect aggregation, conformation, spectral characteristics, and assembly. Ironically, they can be viewed as a variable component or contamination in previous pure biliprotein experiments and may partially explain conflicting results for aggregation and spectral studies.

II.Alc(5) Rods

Rods are composed of stacks of hexamers with strong spacings at 60A° and weak at 30A°.[128,129] They commonly include from two to six hexamers *in vivo*. However, Lundell et al. showed that without terminating linker proteins, the length is purely a matter of solution equilibrium and can be in the range of 20-30 hexamers *in vitro*.

II.Alc(6) Core

The inner core of a phycobilisome consists of rods from 1-3 hexamer disks long. In the case of *Rhodella violacea*, the rods are 1 hexamer disk long, and there are 3 rods arranged in a triangular fashion.[66,85]

It has been proposed that APC-B and a linker protein of 75,000 daltons, which is not colorless, are the terminal emitters in phycobilisomes.[27] In addition, the 75,000 Da protein is apparently the anchor, or foot, for the phycobilisome in the membrane near the reaction center of photosystem II.[120]

II.Alc(7) Phycobilisome

Phycobiliproteins are organized *in vivo* into supramolecular arrays called phycobilisomes, which are attached to the outer surface of the photosynthetic membranes (thylakoids). They can be isolated intact from the membranes of broken cells using high ionic strength buffer (0.75 M salt) at pH 7 and the nonionic detergent Triton X-100. The phycobilisomes are separated free from chlorophyll by centrifugation on a sucrose step gradient. Molecular weights are > 10^7 Da. In salt concentrations < 0.50 M, the phycobilisomes dissociate, and phycobiliproteins can then be purified (see Section II.B1).

The phycobilisomes are sometimes seen as 30-40 nm diameter particles, 6-33 nm in thickness, spaced 40-50 nm apart in regular arrays on the stroma side of photosynthetic lamellae. Glutaraldehyde-fixed red algal cells were shown to have this regular array of granules in 1966 by Gantt and Conti, providing the first structural evidence for these supramolecular arrays.[28,29]

The size and shape of phycobilisomes differ from one organism to another, from spherical or globular to disk-shaped (hemidiscoidal), in long cylinders, and in all intermediate shapes. For instance, in *Griffithsia pacifica*, the phycobilisomes are prolate or block-shaped.[26]

Purity of phycobilisomes can be checked by exciting into the phycoerythrin absorption band. In intact phycobilisomes, > 99% of the emission yield occurs from

allophycocyanin I or APC-B at 680 nm, demonstrating the functional integrity of the energy transfer.[75]

Cyanobacterial phycobilisomes consist of a core from which radiate 6 rods of varying length in a hemispherical array. The core consists of 2 or 3 cylinders perpendicular to the hemispherical array. The outer rods consist of phycoerythrin or phycoerythrocyanin on the exterior and phycocyanin on the interior, or core side. The cores consist of allophycocyanin and APC-B (Fig. II.A-5). This has been deduced both by steady state optical spectroscopy, immunoelectron microscopy, and the controlled disruption of intact phycobilisomes, observing the kinetics and the absorption and fluorescence emission spectra.[32,31] Purified phycobilisomes do not contain chlorophyll pigments.[62] The phycobilisomes always follow this arrangement of having allophycocyanin at the core, the phycocyanin further out, and the phycoerythrocyanin or phycoerythrin, when present, at the periphery.

Self-assembly of phycobiliproteins into phycobilisomes seems to be controlled by the relative concentrations of different biliproteins and linker proteins, which are controlled by their biosynthesis and degradation, and modulated by at least the factors of light (intensity and/or color), nitrogen supply, and sulfur compounds.

In healthy growing cyanobacteria and red algae, essentially all of the phycobiliproteins are associated into phycobilisomes.[37] However, the phycobiliproteins of cryptomonads are located in the intrathylakoidal space.[123] The

Fig. II.A-5: Schematic of the Synechocystis 6701 phycobilisome, showing the location and composition of the complexes making up the rods. PE, phycoerythrin, PC, phycocyanin. From Fig. 13 of Ref. 40, with the kind permission of Dr. A. Glazer.

SYNECHOCYSTIS 6701 WILD TYPE

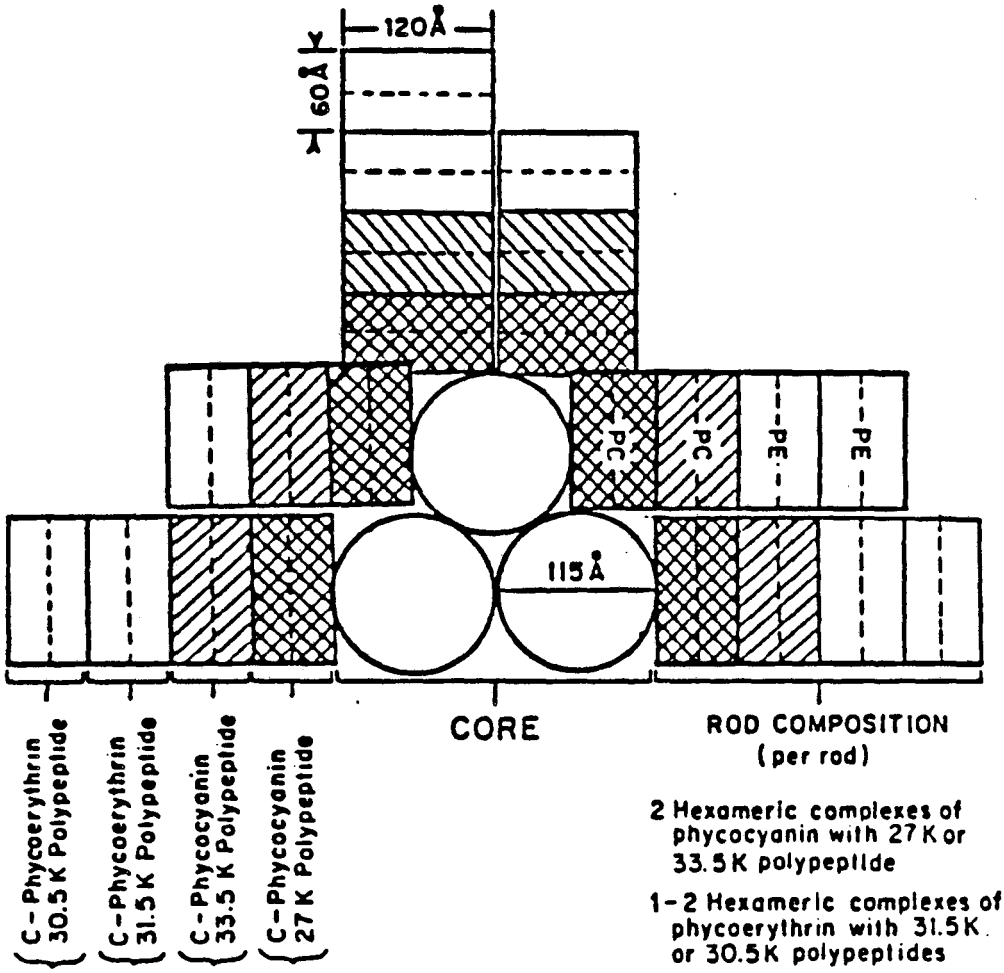

aggregation state here is unknown. The intrathylakoidal space is proposed to provide close-packing of pigments and efficient energy transfer.[25]

II.Ald Association to thylakoids and photosystems

Phycobilisomes feed energy mostly to photosystem II and are related to the presumed regular arrays of Photosystem II seen in freeze-etched preparations on the EFu fracture face of chloroplasts.[74,119,76] The phycobilisomes may be associated with more than one photosystem. The ratio of phycobilisomes/particles has been found to range from 0.25-2.0.[76,111]

Phycobilisomes are not necessary to maintain the activity of PS I or PS II. Mutants lacking phycobiliproteins can carry out normal photosynthesis.[89] In nitrogen-starved or otherwise nitrogen depleted cells, chlorophyll a functions as the principal light-harvesting pigment.[71]

II.Ale Biosynthesis and chromatic adaption

The bili pigments of animals and the phycobilins are derived from protoporphyrin IX, in which the macrocycle is opened at the C-5 position.[116] Very little is known about the biosynthesis of the protein-chromophore covalent linkage. The synthesis is photoregulated, and there is evidence that it is strongly linked to chlorophyll biosynthesis.[106]

Scheer has suggested that phycochromes controlling the photoregulation are not separate pigments but may be slightly denatured phycobiliproteins or some subpopulation of them.[106]

This is consistent with the hypothesis that slight denaturation might provide for photochemical activity without allowing internal conversion and destruction of the pigment, which can still be protected by the protein matrix. This is also consistent with the stepwise denaturation observed in phycobiliproteins.[107,92]

Detectable quantities of free apoprotein or free chromophore have not been observed *in vivo*.

In all phycobiliprotein-containing organisms, phycobiliprotein content is affected by light intensity. In other words, the amount of biliprotein relative to chlorophyll increases with a decrease in light intensity. In some red algae, a change occurs in the number of phycobilisomes, not in the composition of the rods. But in certain cyanobacteria and red algae, called chromatic adapters, phycobiliproteins serve to tune the spectral bandwidth used for photosynthesis.[7,5] They do this at the level of the phycobilisome, where the composition of the rod changes from generation to generation as the color of light is changed.[113] Phycobilisome shape remains the same but composition of the rods responds to changes in the illumination wavelength.

In chromatically adapting organisms, phycoerythrin is the dominant protein in green light, and phycocyanin is the dominant protein in red light. There are 3 groups of organisms: those that don't chromatically adapt, those that adapt through phycoerythrin synthesis, and those that adapt through phycoerythrin and phycocyanin synthesis.[113] Organisms

belonging to Group III have a second phycocyanin that is produced under the red light.[10]

There is good correlation between the phycobiliproteins in a particular organism and the location (water depth) and the color of light available to that organism. The chromatic adaptability is probably another function of phycobiliproteins that has evolved in response to the changing wavelength of light and light intensity.

II.Alf Evolution

Fossils structurally indistinguishable from present species of cyanobacteria have been found in geological formations from 2.6-3 billion years old. Phycobiliproteins are probably at least as old as this. Phycobiliproteins cross the gap between prokaryotic and eukaryotic cells. As with other important proteins with conformationally dependent functions, like cytochrome C, it is reasonable to propose that the need to provide the special environment and conformation to the phycobilin restricts the variation allowed in phycobiliproteins. In addition, the complex interaction of phycobiliproteins in aggregates and between different phycobiliproteins in the light-harvesting array of the phycobilisomes further specifies the amino acid sequence.

Immunological studies have determined 3 clusters of phycobiliproteins in red and blue-green algae. Cluster I consists of allophycocyanin and APC-B; Cluster II of C-phycocyanin, R-phycocyanin, and phycoerythrocyanin; and cluster

III of C-phycoerythrin, B-phycoerythrin, b-phycoerythrin, and R-phycoerythrin.[38] Within the clusters, immunological cross-reactivity is observed. There is very little cross-reactivity between members of different clusters. There clusters relate to the spectroscopic classes of Section II.Ala(1).[38] This has been taken to imply that the divergence into spectroscopically distinct classes was an ancient event with very little change in biliprotein surface characteristics since that time.

The α and β subunits of all phycobiliproteins of red algae and cyanobacteria are homologous. (However, Agmenellum quadruplicatum [cyanobacteria, Fox 1980] shows pronounced sequence divergences.)[38,43] The phycobiliproteins, therefore, are a family of proteins descended from a common ancestral gene. It is presumed that divergence of an ancestral gene resulted in the α and β subunits. This hypothesis is supported by the preparation of stable hybrid phycobiliproteins in high yield.

Immunochemical studies show very little relation between cryptomonad and cyanobacteria or red algal phycobiliproteins.[45] The β subunit of cryptomonads is homologous to cyanobacteria and red algal biliproteins, but no obvious homology is observed for the α subunit.[42]

II.A2 Function

The main function of phycobiliproteins, of course, is the energy transfer of absorbed photosynthetic energy to the

reaction center. This is the main function with regard to the organism and also the main concern of this thesis. There are some additional subfunctions (e.g. chromatic adaptation and nitrogen storage) previously covered in Section II.A1.

The energy transfer will be discussed in terms of the spectral properties and evidence for transfer mechanisms at each level of structural hierarchy previously defined in the structure section. This is a reasonable scheme to follow, because the spectral properties of phycobiliproteins depend on the following structural factors: the nature of the phycobilin, the covalent linkage of the chromophore to the protein, the conformation and environment of the chromophore in the protein, and the chromophore and protein interaction in higher aggregation states.

II.A2a Chromophore

II.A2a(1) Chromophore structure, diversity

Absorption by the chromophores of phycobiliproteins spans the range of visible light, with maxima occurring between 450-650 nm. This allows these organisms to take advantage of niches left open by other photosynthetic species. Assigning the phycobiliproteins to 3 main classes (allophycocyanin, phycocyanin, and phycoerythrin) does not reveal the full complexity of the proteins. The same cell from a give species (so far, only chromatic adaptors) may contain different phycoerythrins, different allophycocyanins, etc.[38]

The large shifts in absorption λ_{max} can be generated by small changes in chromophore structure. Structural isomers of the same phycobilin can result in large band shape changes. Even phycoerythrobilin and phycocyanobilin are structural isomers of each other (see Fig. II.A-3).

The requirement of efficient absorption and transfer of energy and the use of phycobiliproteins to fulfill this requirement have dramatically affected the evolution of cyanobacteria and red algae and contributed to their diversity and abundance.

II.A2a(2) Chromophore bound to protein - covalent interaction

The conjugation length does not extend into the covalent bond with the protein. This led to some problems in early spectral characterization, because chromophores isolated by different methods have conjugation lengths different from those of the bound chromophores.[107] Although linkage does not affect the conjugation length, it does affect the conformation of the chromophore and, hence, its spectral properties (see Section II.A2a[4]).

II.A2a(3) Chromophore bound to protein - noncovalent interaction

It is clear that most of the spectroscopic properties and function of chromophores accrues through interactions with the protein other than by the covalent linkage. The denatured protein absorption and fluorescence spectra more closely match the free chromophore spectra. Upon

renaturation, the spectra revert to those observed for native phycobiliproteins.[67,107,46,47] In addition, the absorption is red shifted and the extinction coefficient and fluorescence quantum yield dramatically increase for the native protein conformation. There is also an absolute increase in the visible/near UV extinction ratio upon renaturation: In the denatured or free phycocyanobilin, A_{612}/A_{360} is approximately 0.5, but in monomeric C-phycocyanin this ratio is approximately 6.0.[48,95] Bands for native phycobiliproteins are generally narrower than for the denatured forms. All of these effects can be ascribed to the structure that the chromophore assumes upon interaction with the amino acid backbone of the protein, and the protein-protein interactions that provide the environment for the chromophore site. (The exact nature of these interactions is not known.) The final result is to provide an efficiently absorbing pigment, with most of the energy directed into fluorescence or energy transfer, depending upon the availability of an acceptor.

II.A2a(4) Chromophore conformation

The main feature of protein-induced chromophore structure that has been proposed to account for the unique spectral features is the extended, more rigid structure in the native phycobiliprotein as compared to a cyclic conformation in the denatured phycobiliprotein.[31,106] The cyclic conformation of the chromophore in the denatured

protein has a large conformational heterogeneity at room temperature.[106] The more rigid structure of the native chromophore should minimize the internal conversion routes of decay and possibly, along with the protective protein envelope, minimize the destructive photochemical redox pathways. In general, the chromophore is stabilized with respect to effects of O_2 or external chemical agents (see Section II.C1). The extended conformers are not thermodynamically stable, however, so the energy for unfolding must be provided by the protein.[67]

The shoulders in the absorption spectra of native phycobiliproteins that narrow upon lowering the temperature have been assigned to distinct conformations of the chromophore. It has been claimed that these forms are not in equilibrium.[105,132,134] From protein primary sequences, distinct environments for each chromophore in a phycobiliprotein have been found which are conserved from one phycobiliprotein to another. This conservation implies that at least the range of conformational mobility is under the control of some protein-chromophore interaction.[20,21,134] Photochemical hole-burning, partial denaturation, and chemical modification support the assignment of at least 2 different absorption bands to the main long wavelength absorption band in C-phycocyanin and C-phycoerythrin. These results indicate, however, varying degrees of conformational mobility for the sets of chromophores.[22,23,107,67]

The decrease of mobility imposed by the protein-chromophore interaction results in a decrease in radiationless internal conversion and an increase in fluorescence (analogous to triphenylmethane dyes in highly viscous solutions). In addition, it is clear that photochemical channels are also controlled by the protein: Phytochromes and phycochromes have important photochemical channels but native phycobiliproteins do not.[5,105]

It is interesting to note that allophycocyanin and phycocyanin have been shown to acquire photoreversible photochemical properties upon partial denaturation and that these changes resemble changes in phycochromes.[92,91] Indeed, it has been proposed that phycochromes are not separate pigments but rather slightly denatured states of phycobiliproteins.

II.A2b Protein

II.A2b(1) Primary sequence

It is not clear to what extent the side groups of the amino acids interact with the chromophore. The high conservation of amino acids near the bilin site may indicate that important non-covalent interactions, even to the extent of charged groups, are involved in maintaining chromophore conformation and absorption and fluorescence spectral properties.

II.A2b(2) Subunits

The sum of the absorption spectra of the separated α and β subunits at pH 7.0 is superimposable on the absorption spectrum of the αβ monomer of C-phycocyanin. The circular dichroism (CD) maximum of the sum also corresponds to that of the monomer.[47,48] It has been concluded that the combination of α and β subunits does not result in a "major" perturbance of the protein-chromophore interaction.

However, Stadnichuk and others have shown that absorption spectra of (αβ) monomers may be analyzed as a sum of Gaussian bands, which they have attributed to strongly coupled chromophores involved in an exciton interaction.[109,110]

Here it is appropriate to concern ourselves with the model presented for energy transfer between 2 or more phycobilin chromophores, because this is the first level in the structural hierarchy where 2 chromophores are present that may interact through energy transfer.

The change of fluorescence excitation polarization across the absorption band for solutions of mixed aggregation state has been attributed by Dale and Teale to energy transfer between sensitizing (s) and fluorescing (f) chromophores.[16,115] In this model the ratio of s to f chromophores and the extent of energy transfer increases with increasing aggregation state.

The polarization decreases with increasing number of chromophores in the aggregation state. These results are

consistent with the model of s and f chromophores. In this model, s chromophores, absorbing on the blue side of the absorption band, transfer absorbed energy to f chromophores. The subsequent fluorescence from f chromophores becomes depolarized because of energy transfer involving the s chromophore emission transition moment and the differently oriented f chromophore absorption transition moment. By exciting f chromophores directly on the red side of the absorption band, fluorescence should result which is not so depolarized, due to a lack of energy transfer.

This model has been applied particularly at the monomer level where the 2 chromophores on the β subunit absorbing at 608 nm were assigned to s-chromophores and the single chromophore on the α subunit, absorbing at 620 nm, was assigned to the f-chromophore.[48] CD bands were observed at 620 for α and 598 for β, corresponding well with the absorption maxima. This s-f assignment based on wavelength is consistent with the deconvolution of the absorption spectra based on the polarization experiments performed by Teale and Dale and Vernotte.[115,118] However, this model has not been confirmed by time-resolved spectroscopy at the level of the subunits or monomer (see Section II.C2 and II.D).

The energy transfer of the separated subunits, monomer, and higher aggregation states up to the phycobilisome have been analyzed in terms of the Forster resonance induced dipole-induced dipole mechanism. The strong coupling exciton mechanism has not been applied to cyanobacteria or red algae

and certainly would not be consistent with an s-f transfer mechanism. In an exciton mechanism, the energy states are considered to be delocalized over the ensemble of interacting chromophores under consideration, and the terms "sensitizer" or "fluorescor" would not be applicable.

Strong coupling has been implied in a crytophytan phycocyanin. A transient absorption component of $\leqq$ 8 ps has been resolved that has been assigned to energy transfer among tightly coupled chromophores.[61,65] The mechanisms of energy transfer will be treated in more detail in the Results and Discussion, Section II.C.

II.A2c Aggregation

II.A2c(1) Monomer

Aggregation of monomeric phycobiliproteins results in a red shift of the long wavelength absorption and fluorescence λ_{max} and an increase of the extinction coefficient and fluorescence quantum yield. In some cases, the band shape changes when the extinction coefficients of the long wavelength maxima are enhanced with respect to the shorter wavelength shoulders (see Section II.C2). In addition, the CD spectra of many of the phycobiliproteins, for example C-phycocyanin and allophycocyanin, show evidence of interactions that have been attributed to exciton coupling of chromophores. The ratio of the area under the visible band to that in the near UV absorption spectrum continues to rise

with aggregation, increasing to 2.5 for hexamers. (See references 106, 12, 82, 70, and 84.)

II.A2c(2) Trimer

The dramatic changes in spectral properties begin to occur even at the level of trimer. In particular, MacColl et al. have attributed the CD changes in allophycocyanin from monomer to trimer to an exciton interaction between the chromophore on an α subunit of one monomer unit interacting with a chromophore on a β subunit of another monomeric unit within the trimer.[83] Strong coupling between chromophores in trimers and in other aggregation states has been neglected in most treatments of the energy transfer. Intermediate coupling has been suggested in this allophycocyanin trimer by MacColl et al. (1980).[83]

The most dramatic example of a spectral shift upon aggregation is the shift of the absorption λ_{max} of the allophycocyanin trimer with respect to that of the allophycocyanin monomer. Here the λ_{max} changes from 620 to 650 nm and increases in intensity with respect to the monomer. However, the visible/near UV absorption cross-section ratio does not change.[14]

II.A2c(3) Hexamer

The $\alpha\beta$ monomer has a CD λ_{max} at approximately 600 nm which diminishes upon aggregation to hexamer, while a new band appears at 636 nm, in experiments by Glazer et al.[48] Under the conditions used, a clear isosbestic point was

observed, correlated to the interconversion between the monomer and hexamer. Moreover, the absorption λ_{max} during this aggregation changes from 614 to 621 nm. These changes suggest, along with changes seen in other aggregation states, that chromophore coupling interactions occur upon aggregation. The hexamer also shows a very low fluorescence polarization ($P < 0.1$), consistent with efficient and extensive energy transfer.[16,115]

II.A2c(4) Linker

The characteristics of the in vivo spectra of phycobiliproteins is first seen at the levels of trimer, hexamer, and higher aggregation states in combination with linker polypeptides. Phycobiliprotein aggregation with linker polypeptides causes many of the spectroscopic changes seen in Section II.A2c(2) and (3) (higher quantum yields, red shifts of maxima, etc.). Different linkers interacting with the same biliprotein result in different absorption and fluorescence maximum shifts.[80] These wavelength shifts are consistent with achieving a thermodynamically favored energy transfer in a vector toward the terminal emitters of the phycobilisome (i.e. linker-biliprotein aggregates are located in order of decreasing excitation energy toward the core of the phycobilisome).[41]

II.A2c(5) Rods

Rods probably serve the function of preventing multiple excitations from interacting and dissipating the energy

through exciton-exciton annihilation. The energy is efficiently confined to a trimer disk because each disk toward the core has a longer excitation wavelength than the one preceding it. This minimizes random walks that occur in random arrangements of chromophores or in an arrangement of equal excitation wavelength chromophores (see Section II.A2c[7]). The rods serve to confine the energy in a vector toward the reaction center and prevent lateral hops to neighboring pools of pigment in other rods due to the distance dependence of the energy transfer mechanism.

II.A2c(6) Core

The core serves as a pool of pigment to collect energy from the rods and direct it to the final emitter(s), APC-B and/or APC-I (the 75,000 kD polypeptide that extends into the membrane), which bridge the gap between the phycobilisomes and the reaction center and its associated antenna chlorophyll.

II.A2c(7) Phycobilisomes

The work of Searle et al. showed conclusively that the order for energy transfer in algae and phycobilisomes is PE → R-PC → APC → Chl-a.[100,108] In this primary experiment, 580 nm picosecond flashes of light were used to excite phycoerythrin, and the risetime for fluorescence was monitored for each of the pigment beds. The rise of B-phycoerythrin emission at 576 nm was instantaneous; the emission at 640 nm had a 12 ps risetime, at 661 nm a 22 ps risetime,

and at 685 nm a 52 ps risetime. These observations are consistent with the ordering of the pigment beds in phycobilisomes and their relation with Photosystem II reaction centers if a Forster transfer mechanism is operative (Fig. II.A.-5). The organization at this supramolecular level reflects the requirement of minimizing the donor-acceptor separation, the $1/R^6$ dependence of the rate, and the efficiency of energy transfer.

The results of Searle at al. have been confirmed many times (see Section I.A1 for a list of reviews that summarize the picosecond results on phycobilisomes). (Care must be taken in interpreting the results of early literature. The interpretation is complicated by singlet-singlet exciton annihilation at high light intensities, the integrity of the phycobilisomes, the presence or absence of linker protein in phycobiliprotein preparations, and the inability to resolve kinetic subcomponents of the fluorescence decays.) All of the results point to the general conclusion that energy absorbed in any part of the phycobilisome is transferred to a few terminal emitters with an efficiency greater than 93%. Most of the data indicate that the disk-to-disk energy transfer is the rate-limiting step in phycobilisomes.[41] The best supported model has a disk-to-disk transfer time of 25 ps.[50] The phycobilisome functions as a linear, five-point array. Therefore, the energy absorbed by any part of the phycobilisome reaches the terminal emitters, on the average, in approximately five or fewer distinct kinetic steps. The

current literature concerning picosecond time-resolved experiments on isolated phycobiliproteins, our results, and their application to energy transfer will be discussed in Section II.C and II.D.

II.B Materials and Methods

II.B1 Protein preparation

Culture of Anabaena variabilis and initial samples of C-phycocyanin were provided through the kindness of Professor A. Glazer (Microbiology, University of California, Berkeley). Samples of C-phycocyanin from Anacystis nidulans and R-phycocyanin from Porphyridium cruentum were also provided by Professor A. Glazer. Further cultures were grown using the algal growth medium BG11 as presented by Rippka et al. (1979).[99] R-phycocyanin dimers from Griffithsia tenuis, with and without linker, were provided by Dr. B. Watson of the University of Washington.[122]

II.B1a Monomer

All buffers contained 0.001 M β-mercaptoethanol and 0.001 M NaN_3 unless otherwise noted. A suspension of cells in 0.05 M ammonium acetate at pH 6.0, homogenized and broken with a French pressure cell or freeze-thaw cycle, was centrifuged. The pooled supernatants were brought to 65% of saturation with $(NH_4)_2SO_4$. The precipitate was collected by centrifugation at 25,000 g for 15 min, resuspended in 0.005 M potassium phosphate, pH 7.0, and dialyzed against the same buffer at 4°C. The protein solution was centrifuged and separated on a DEAE-cellulose column. Anabaena variabilis C-phycocyanin crystallized in fractions eluting from the column at potassium phosphate concentrations near 0.1 M.

In the case of C-phycocyanin from Anacystis nidulans, Crystal Chan and Dan Lundell developed a procedure to separate linker from the C-phycocyanin. The linker and C-phycocyanin from Anacystis nidulans coseparate under conditions in which C-phycocyanin from Anabaena variabilis is separated pure from its linker polypeptide. The preparation is identical to that described above for C-phycocyanin from Anabaena variabilis, but, in addition, the isolated protein is developed on another DEAE-cellulose column with 3.0 M urea at pH 3.0.

Both C-phycocyanin from Anabaena variabilis and Anacystis nidulans were shown to lack linker proteins and to consist only of α and β subunit polypeptides by sodium dodecyl sulfate--polyacrylamide gel electrophoresis.

R-phycocyanin from Porphyridium cruentum was isolated by Glazer using methods presented in reference 49a.

II.B1b Subunits

To obtain separated subunits, a solution of C-phycocyanin in 0.1 M potassium phosphate at pH 7.0 was adjusted to pH 3.0 with glacial acetic acid, and β-mercaptoethanol was added to give a final concentration of 10 mM. This solution was applied to a Biorex 70 cation exchange column, preequilibrated with 0.4% acetic acid in distilled water. Subunits were separated by a urea step gradient, the α subunit eluting from the column at 8 M urea and the β subunit at 9 M urea (Glazer and Fang, 1973).[47] After exhaustive

dialysis and lyophilization, the separated subunits were placed in polyethylene vials and stored over anhydrous calcium chloride at -20°C. This procedure is equally successful for C-phycocyanin from Anabaena variabilis and Anacystis nidulans. All samples were shown to lack linker proteins and consist only of a single subunit polypeptide by sodium dodecyl sulfate--polyacryamide gel electrophoresis.

II.B1c Dimer

The description of the preparation of the R-phycocyanin dimer with and without linker that follows is a summary of the procedure submitted by Watson et al.[122]

Phycobilisomes from Griffithsia tenuis (Anotrichium tenue) were isolated by a modified procedure of Gantt et al. (1979).[33] Phycobilisomes were pooled and dialyzed overnight (2°C) against ST buffer (0.05 M NaCl, 10 mM Tris, 1 mM β-mercaptoethanol, 0.02% NaN_3, pH 7.5).

The phycobilisomes were loaded onto a DEAE Biogel A column (2.6 X 40 cm) equilibrated in ST buffer. The biliproteins were retained on the first few cm of the column. The biliproteins were eluted with salt gradient of 0.05 M to 0.20 M NaCl in 10 mM Tris, 1 mM β-mercaptoethanol, 0.02% NaN_3, pH 7.5.

Hydroxylapatite chromatography. Pooled fractions from ion exchange were further purified by chromatography on short (3-10 cm) columns of hydroxylapatite (HAP). All biliproteins adsorbed well to HAP in ST buffer and were eluted by step

gradients of phosphate buffer (5-100 mM KH_2PO_4, 0.1 M NaCl, 0.02% NaN_3, 1 mM β-mercaptoethanol, pH adjusted to 7.0 with KOH). HAP chromatography was performed at room temperature.

Gel filtration chromatography. Gel filtration chromatography was performed both as a purification step and to characterize the molecular weight of the biliproteins. This was carried out at 2° in ST buffer on Sephacryl S-200 (1.5 X 90 cm). Flow rates of approximately 4 cm/h were used. The elution volume vs. molecular weight characteristic of this column was calibrated by the elution of proteins of known molecular weight.

Hydrophobic interaction chromatography. Dimer without linker protein ($R\text{-}PC_{617}$) fractions were purified by chromatography on Phenyl Sepharose. The protein was loaded either in ST buffer (following gel filtration) or in phosphate buffer (following HAP chromatography). In either case, the phycocyanin was adsorbed to the top cm of a 1.0 X 3.0 cm column. $R\text{-}PC_{617}$ was eluted at room temperature with 0.02 M Tris-HCl, pH 8.2. Contaminating biliproteins were retained on the column under these elution conditions. The salt concentration of the eluate was brought immediately to 0.1 M by the addition of solid NaCl to stabilize the phycocyanin against dissociation. Molecular weights of the dimer with ($R\text{-}PC_{625}$) and without ($R\text{-}PC_{617}$) linker protein were also determined by Bruce Watson using ultracentrifugation on a 5-15% linear sucrose gradient in 0.05 M potassium phosphate

buffer, pH 7.0 (37,500 rpm, 27 hrs, 4°C, r_{av} = 112.7 nm, g (r_{av}) = 173,000 g). This determination was based on the methods of Yu, et al.[131] The interpolated molecular weights were 115.4 and 77.6 kD for R-PC_{625} and R-PC_{617}. These molecular weights are consistent with the designation of dimer with and without a 30 kD linker protein for R-PC_{625} and R-PC_{617}, respectively.

II.B2 Steady-state spectroscopy

Absorption spectra were recorded using a Cary model 118 (Varian) UV-visible absorption spectrophotometer. Fluorescence emission spectra and fluorescence excitation polarization measured at 90° to the excitation direction were obtained using an instrument described by Bolt and Sauer (1981).[8] The excitation bandwidth (full width, half maximum) was 6 nm and the emission bandwidth was 3 nm. Emission spectra were corrected for the wavelength-dependent response of the detection system (Parker, 1968)[98], a minor correction under our conditions (Bolt and Sauer, 1981).[8]

Fluorescence polarization was defined as

$$P = \frac{I_{\parallel} - I_{\perp}}{I_{\parallel} + I_{\perp}}$$

where $I_{\parallel}$ is the fluorescence intensity measured parallel and $I_{\perp}$ is the fluorescence intensity measured perpendicular to the direction of the electric field vector of the plane-polarized excitation light.

Unless otherwise noted, monomer and subunit samples for

fluorescence spectroscopy had an absorbance of 0.05 (path-length = 1 cm) at the visible absorption maximum in a buffer containing 0.001 M NaN_3, 0.001 M β-mercaptoethanol, and 0.005 M potassium phosphate, pH 7. The only change in dimer samples was that 100 mM phosphate buffer was used instead of 0.005 M.

Additional information on the use of steady state spectroscopy to study energy transfer phenomena is presented in the Results and Discussion, Section II.C.

II.B3 Picosecond single-photon timing

II.B3a Instrumentation

Fluorescence decay kinetics were measured using the single-photon timing instrument previously described.[55,117] Modifications are illustrated in the schematic in Fig. II.B-1, and only these modifications will be discussed extensively. A microchannel plate (MCP) photomultiplier tube (PMT) detector was incorporated to improve the time resolution. In addition, a sample chamber was equipped with optics to minimize scatter.

The instrument response E(t) (see Section II.B3c) from most fast photomultiplier tube systems is on the order of 300-600ps full width at half maximum (FWHM) (Fig. II.B-2). Much of this width is the result of jitter in the photoelectrons because of the random deviations in the initial kinetic energy and trajectory of the primary photoelectrons, resulting in a spread in photoelectron transit time and

Fig II.B-1: Diagram of the single-photon timing system used for time-resolved fluorescence. Abbreviations: ADC, analog-to-digital converter; BS, beam splitter; CFD, constant fraction discriminator; Fl, neutral density filter; Lev. Disc., level discriminator; MCA, multichannel analyzer; MCP, microchannel plate photomultiplier tube; M. L., mode locker; P. D., photodiode; TAC, time-to-amplitude converter. Modification of Fig. 1 of Ref. 55.

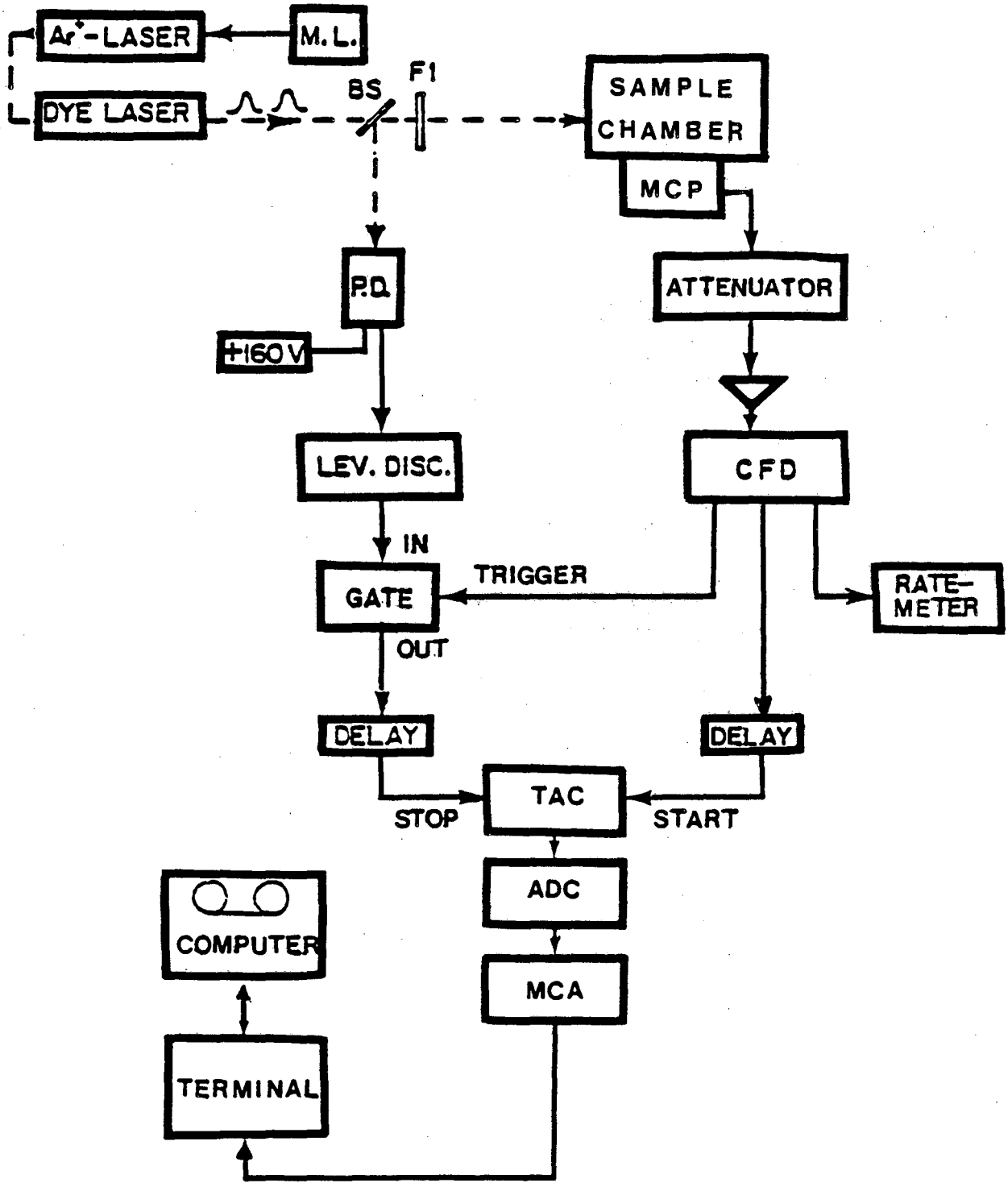
Ar⁺-LASER
M.L.
DYE LASER
BS
F1
SAMPLE CHAMBER
MCP
P.D.
+160 V
ATTENUATOR
LEV. DISC.
CFD
IN
GATE
TRIGGER
RATE-METER
OUT
DELAY
DELAY
TAC
STOP
START
ADC
COMPUTER
MCA
TERMINAL

Fig. II.B-2: Instrument response of single-photon timing system using a RCA C31034A photomultiplier tube at 2200V and a solution of non-dairy coffee creamer. Counts in the 1024 channels of a MCA are uncorrected for noise.

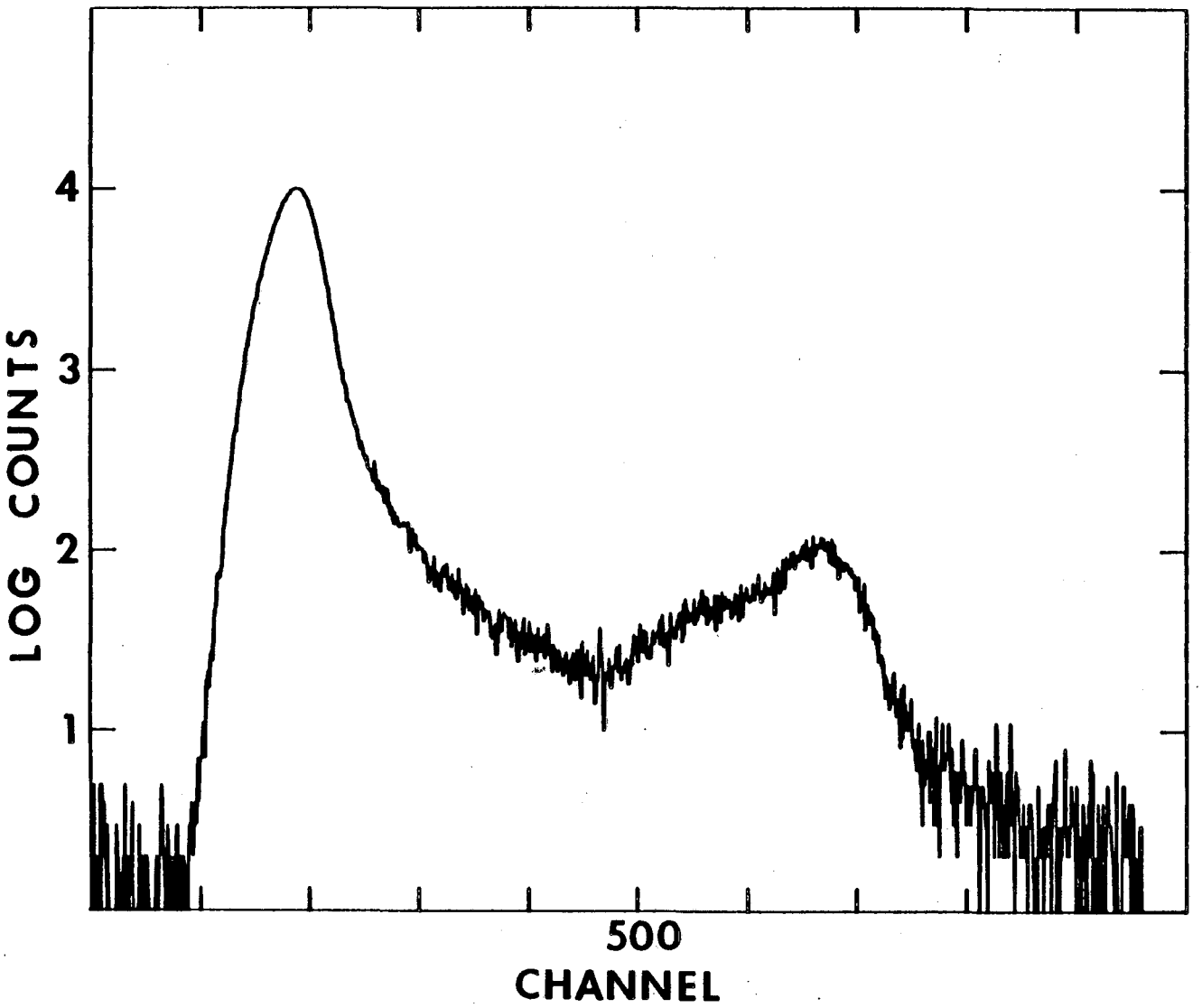
LOG COUNTS
4
3
2
1
500
CHANNEL

pathlength. We have implemented the MCP detector to narrow the instrument response FWHM.

A MCP consists of tens of thousands to a million channels formed from solid glass cylinders with etchable cores, pulled, fused, and pulled again. The cores are etched to form hollow cylinders or channels of approximately 10-20 μm diameter, separated by 20-40 μm (Fig. II.B-3).[72] Each channel is coated with semiconductor, the bundle cut into wafers < 1 mm thick, and then a voltage gradient is provided from the front to the rear face of the channel bundle. The result is a two dimensional array of distinct, parallel electron multipliers with < 50 μm separation. This arrangement provides excellent spatial resolution, on the order of a single channel (Section IV.A3 contains a description of how this spatial resolution might be used in time-resolved emission spectroscopy).[15]

Each channel is a continuous glass tube with an inside secondary electron-emitting surface.[73,99] Primary photoelectrons are accelerated by the potential gradient and collide with the walls of the channels. The wafer is cut at an angle to the normal of the channels to increase the initial collision cross section. The accelerating potential assures that the electrons have multiple collisions with the channel walls before reaching the rear face of the bundle. The voltage gradient is adjusted to ensure that more than one secondary electron is released at each collision.

Fig. II.B-3: Single microchannel plate wafer indicating the direction of incoming signal and amplified output. Fig. 2 of Ref. 72.

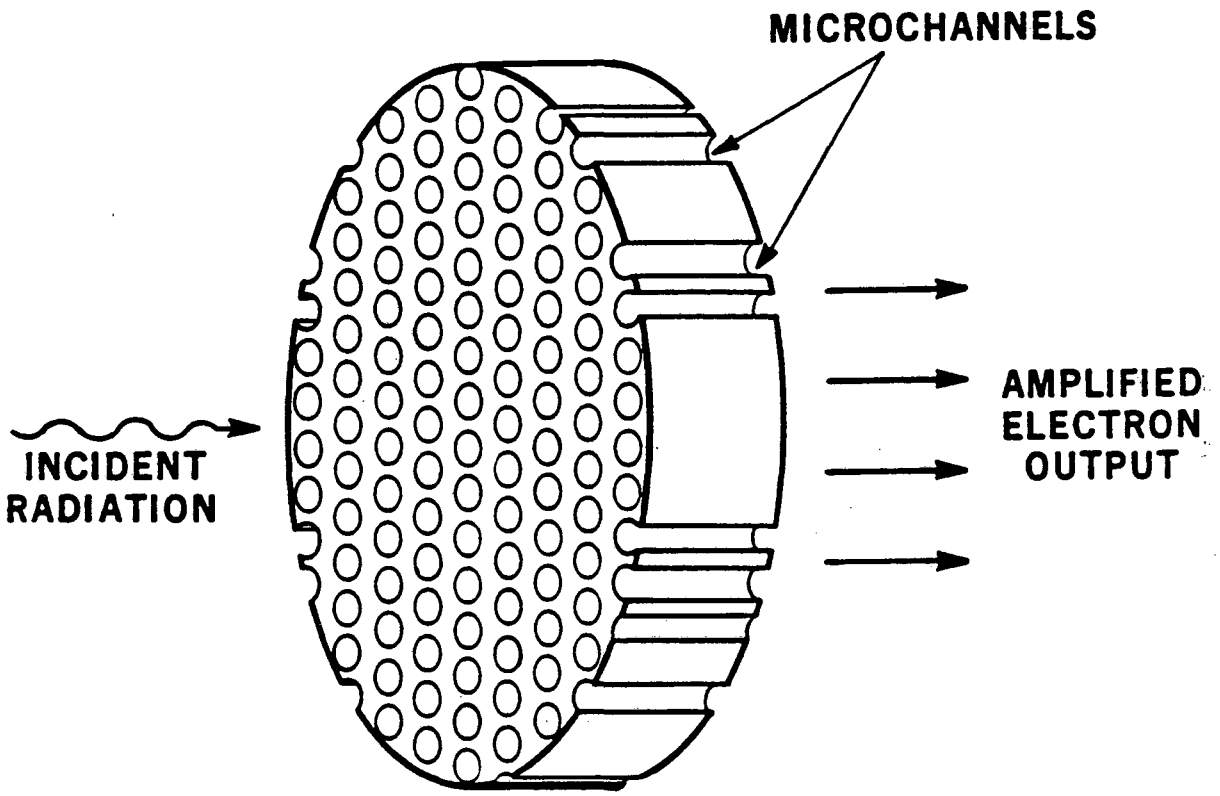
MICROCHANNELS
INCIDENT RADIATION
AMPLIFIED ELECTRON OUTPUT

The amplified electron pulse can be collected by a single anode, an anode array, or a phosphor screen. The small channel size, the high voltage, and the shorter electron path (due to the < 1 mm wafer thickness), as compared to multi-dynode PM tubes, shortens the electron transit time. The shorter transit time results in less jitter and a transit time spread of ≈ 100 ps.[77,13,87,130] However, the statistical nature of the photon-to-photoelectron conversion and of the secondary emission process causes the output signal to vary, even with a constant number of incident photons.[72] We have observed that this variance of pulse height is greater for the MCP than for the conventional PM tubes we have used. For this reason, constant fraction discrimination of the signal from the MCP is not as effective as for the PMT.

The problem with straight channels is that the charge built up on the back of the channels allows for ionization of residual gas molecules that have not been evacuated. The positive ions are accelerated toward the front face of the MCP and can impact with the channel wall or the photocathode to cause secondary electron events and photocathode damage. These secondary electron events result in afterpulses, noise, a broadening of the FWHM, and shorten the life of the tube. Operating straight channels at gains of 10^4 produces positive ion feedback and places a practical limit on the obtainable gain because repetitive electron pulses charge the walls of the tube and cause gain saturation.[72]

Curving the channels or stacking MCP wafers in a "chevron" or "V" configuration can reduce positive ion feedback.[58] The low kinetic energy ions travel only a short distance before striking the channel wall and do not produce a large number of secondary electron events. The angle is such that the passage of secondary electrons, due to initial photoelectrons, is not inhibited. This design can be carried a step further to a "Z" configuration, composed of 3 stacked MCP wafers. Gains of 10^6-10^7 have been achieved with this configuration.[58,73,77,13]

Our MCP is Z-type,ITT F4129f, with a usual operating voltage of 2900 V between the multialkali photocathode and the collection anode. The sample chamber has a variable aperture allowing the dye laser beam to enter and traverse the sample cuvette in the cell holder (Fig. II.B-4). The fluorescence is collected at right angles with a biconvex lens and focused on the face of the MCP. Between the lens and MCP are a shutter and 2 apertures. The apertures are adjusted to eliminate reflected light. The cell holder is separated from the detector by a wall with an opening to prevent the reflected laser light from entering the detector side of the chamber. With the system of Fig. II.B-1, the minimum wavelength separation between the excitation wavelength and emission wavelength, before scatter and reflected light becomes significant (above 0.1% of the counts in the peak channel), is 10 nm, an improvement of 20-30 nm over the previous system.[55,117] This improvement is attributable to

Fig.II.B-4: Diagram of the sample chamber used with the MCP photomultiplier tube.

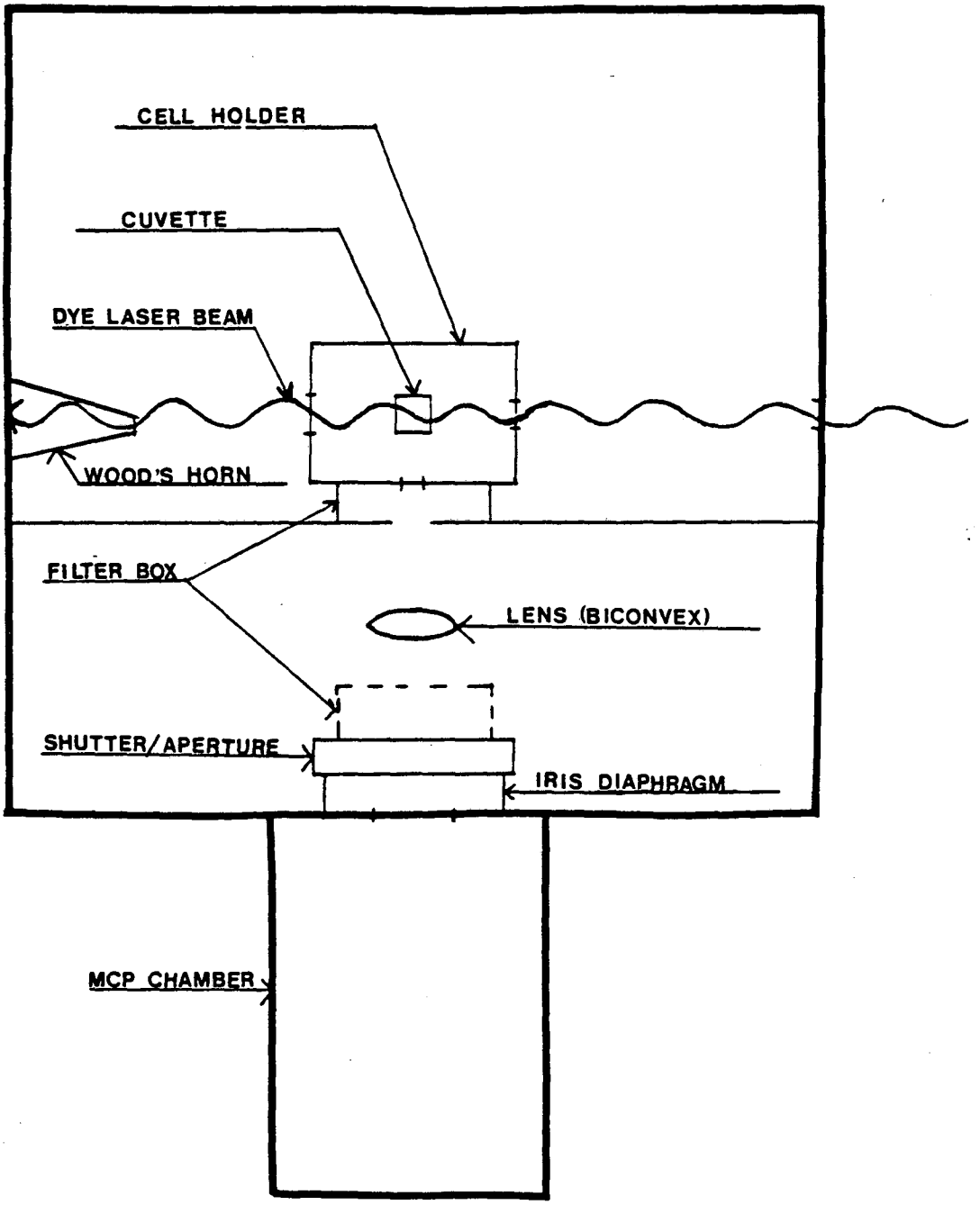
CELL HOLDER
CUVETTE
DYE LASER BEAM
WOOD'S HORN
FILTER BOX
LENS (BICONVEX)
SHUTTER/APERTURE
IRIS DIAPHRAGM
MCP CHAMBER

the cell holder and the full utilization of the right-angle design with a modified Wood's horn (Fig. II.B-4). The present design uses the dye laser beam directly, eliminating the fiber optic cable, which can widen the excitation response function (FWHM, see Section II.B3b). Furthermore, by drastically reducing the scatter and reflected light, the full power of the dye laser can be used, improving the signal-to-noise ratio in cases where the quantum yield, or the concentration of fluorescor, is low. The cell holder is constructed from a brass block equipped with channels and an inlet and outlet port, allowing the use of a fluid to control the temperature. Dr. Ken Rousslang (University of Puget Sound, Dept. of Chemistry) collaborated in the design of this housing and the collection of data presented in the results section.

The output of the MCP is amplified with a Miteq amplifier. Pulse inversion and amplification is necessary after the constant-fraction discriminator to operate the ratemeter. A typical operating photocurrent of 15 nA results in a signal count-to-dark count ratio of 50:1. The signal-to-noise ratio is generally better than this, however, because noise counts are randomly distributed among the channels, and the fluorescence counts have a Poisson distribution (see Section II.B3b).

We have successfully narrowed the FWHM of the instrument response using the MCP. The FWHM obtained have ranged from 105-167 ps, with an average range of 133-140 ps

(Fig. II.B-5). We have not succeeded in eliminating the shoulder (afterpulse?) on the main peak of the instrument response. This shoulder does not depend on laser power, scattered light, count rate, MCP voltage, discriminator settings, etc., but did increase with age of the MCP. From simulations and our triphenylmethane dye data (Section III.C), the time resolution of this system is estimated to be 10-14 ps. This is consistent with the theoretical limit due to single-photon counting Poisson statistics of 7-10% of the FWHM.

II.B3b Data collection

Fluorescence decay kinetics can be studied by observing the response of a chemical system to either continuous, modulated excitation or to a series of discrete exciting pulses. In both cases, modification of the time profile of the excitation due to the time lag caused by the finite lifetime of the excited state provides the information needed to determine the decay kinetics.

The pulse method relies on the statistical nature of the decay. For example, in a simple case, the fluorescence decay can be described as a sum of exponential decay terms:

$$I(t) = \Sigma_i \ \alpha_i e^{-k_i t} = \Sigma_i \ \alpha_i e^{-t/\tau_i}$$

where I(t) represents the true fluorescence decay law, α_i is the preexponential factor or amplitude, k_i is the fluorescence decay rate constant, and τ_i is the measured fluorescence decay lifetime. The measured fluorescence decay

Fig. II.B-5: Instrument response of single-photon timing system using a ITT F4129f MCP-PMT at 2900 V and a solution of non-dairy coffee creamer. Counts in the 1024 channels (7.4 ps/channel) of the MCA are uncorrected for noise. FWHM = 140 ps.

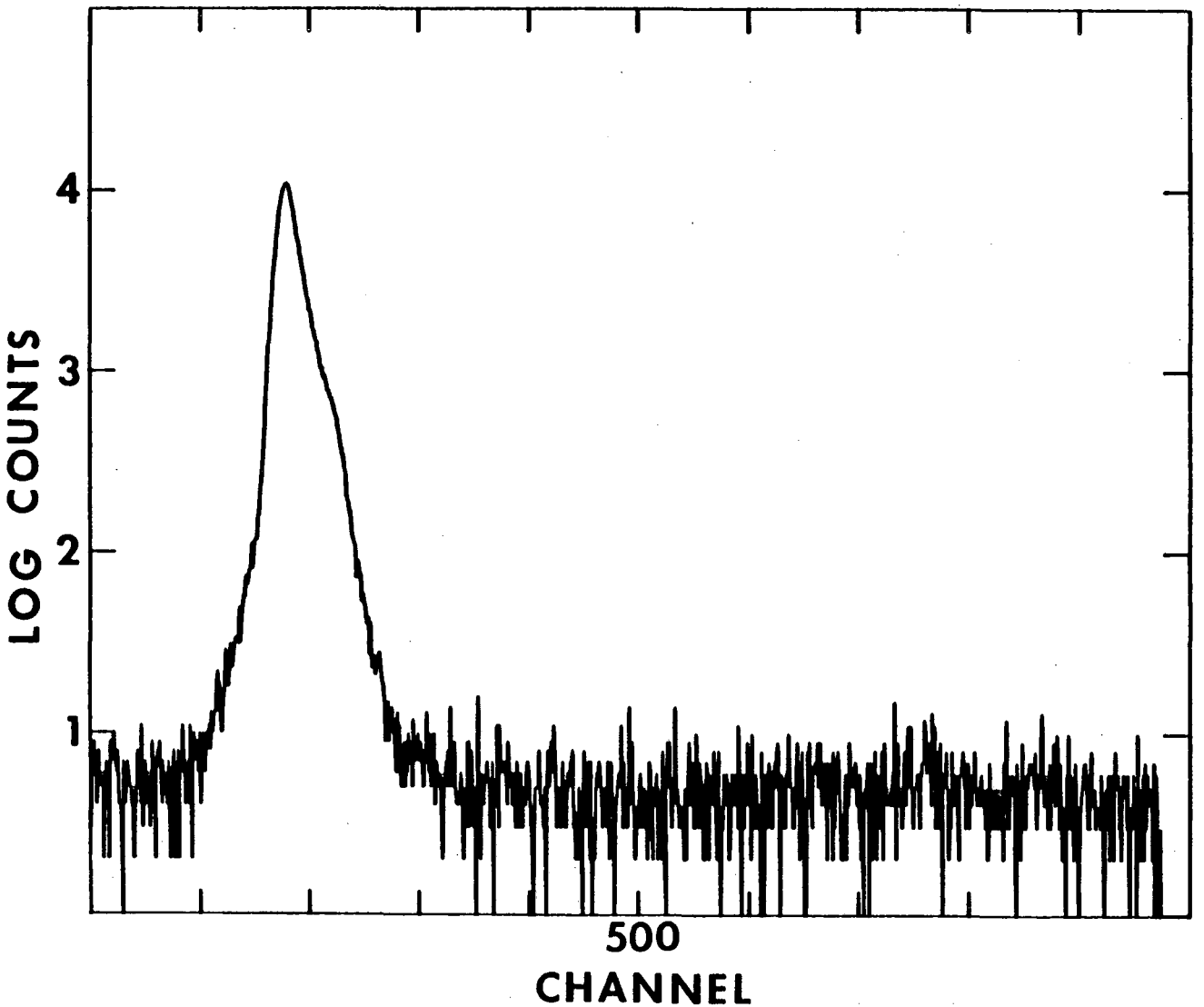
LOG COUNTS
4
3
2
1
500
CHANNEL

lifetime τ is decreased from the natural lifetime τ_o by competitive decay processes (quenching, excited state reaction, internal conversion, etc.). The natural lifetime is related to the intrinsic decay rate of fluorescence k_f,

$$\tau_o = 1/k_f$$

As the quantum yield Q approaches unity, the measured lifetime approaches the natural lifetime, and the relationships can be summarized as follows:

$$Q = \tau/\tau_o$$

$$\tau = 1/(k_f + k_d)$$

$$Q = k_f/(k_f + k_d)$$

where k_d is the rate constant for the competing decay processes. The exponential decay law is obtained by summing the photons of the potentially fluorescent molecules over a time interval after a delta-pulse excitation. In the limit of the time interval approaching zero, I(t) becomes proportional to the number of excited molecules emitting at time t after excitation.

In single-photon timing, only one photon is accepted for each exciting light pulse. The photon arrival is timed relative to the excitation pulse. A histogram of a large number of these statistical photon detection events represents the true fluorescence decay. The criteria are that only the first arriving photon is accepted and that all possible arrival times are equally represented.[121,1] Therefore, forward single-photon timing is essentially a statistical interval timing method.

Reverse single-photon timing is the method we used to collect data for our analysis. In essence, fluorescence photons start the clock and the next laser pulse (the one after the excitation pulse) stops the clock. Since the jitter in the laser pulses is < 5 ps, the data can be treated like forward single-photon timing data after the time axis has been reversed. In a typical scenario, the fluorescence photon is detected by the MCP and the resultant current pulse attenuated to prevent saturation of the fast amplifier (Fig. II.B-1). The amplified signal is discriminated from noise with the constant fraction discriminator (CFD) and sent to a count ratemeter to monitor the fluorescence intensity, to the time-to-amplitude convertor (TAC) to start a voltage ramp, and to a gate box to allow a stop pulse from the laser to reach the TAC. The gate box prevents laser stop pulses from entering the TAC when no fluorescence photons are detected and interacting with subsequent start-stop TAC events. (This interference would be highly probable without the gate box because the laser pulse repetition rate is 80 MHz and the fluorescence count rate is a maximum of 10 kHz.) When a fluorescence photon starts the voltage ramp, a laser pulse (detected by a photodiode--level discriminator combination) is allowed to stop the voltage ramp.

The analog voltage is converted to a digital count by an analog to digital convertor (ADC), a channel of a multichannel analyzer (MCA) is addressed, and the count recorded. Fluorescence is usually measured until there are ≧ 10,000

counts in the peak channel of the MCA. The technique is thus a time interval measurement, a conversion to an analog signal, and a conversion back to digital form. The time resolution is determined predominantly by the time interval measured, which is the process that must occur on a picosecond time scale. The data are transferred from the MCA to a VAX 11/780 for analysis. The data are read into the analysis program in reverse order to reverse the time axis.

II.B3c Analysis

The fluorescence decay that would be obtained with excitation by a theoretical delta function light pulse is called the true fluorescence decay I(t). Experimentally, the excitation pulse E(t) has a finite width. The experimentally measured fluorescence decay F(t) is a convolution of the true decay I(t) and the excitation pulse E(t).[1]

In an attempt to understand the physical nature of the convolution, consider the excitation pulse to be composed of discrete pulses whose width is equal to the channel width in a multichannel analyzer.[1,64,17] These can be approximated as n delta-pulses in n discrete channels (since the channel width defines the smallest discrete time limit of the system). The intensity of the excitation pulse in a particular channel, E(i-j+1) can be considered to contribute E(i-j+1)I(j) to the fluorescence in channel i, where I(j) is the fluorescence intensity j channels after the delta excitation pulse. Each delta pulse would contribute some amount to

the ith channel. Each delta pulse produces a true fluorescence decay but the sum of the delta excitation pulses (which describe the intensity distribution of the light source with respect to time) produces the experimentally observed fluorescence F(i) in the ith channel. To labor the point, the experimentally measured fluorescence intensity is

$$F(i) = E(i)I(1) + E(i-1)I(2) + \ldots + E(i-j+1)I(j) + \ldots + E(1)I(i)$$

The series limits are determined by the physics of the situation: No fluorescence can be produced prior in time to its parent delta excitation pulse ($i \geqq j$).

A discrete convolution of the true fluorescence decay and the excitation pulse can be obtained by allowing i to vary from 1 to n. This can be expressed as

$$F(i) = \Sigma\, E(i-j+1)I(j) \quad (i=1,2, \ldots n)$$

If an infinite number of channels were present the convolution could be expressed as an integral

$$F(t) = {}^{t}\!\int_{0} E(t-t')\, I(t')\, dt$$

This is a well-known convolution integral equation. In the case where F(t) and E(t,t') are step functions, as in the experimental case under consideration, then the solution seeking I(t) is not well-defined and is subject to large oscillations with small errors in the data.[64] The results of this treatment are also applicable to the description of the convolution of the delta pulse with other functions, such as an instrument time response.

[To avoid confusion, it should be noted that some authors treat t as the time associated with a fluorescence response induced by an excitation pulse at time t'. The integral then becomes

$$F(t) = {}^{t}\int_{0} E(t')\ I(t-t')\ dt'$$

A change of variables is all that is represented, since t' is a dummy variable.[1,17]]

Solving the convolution integral equation for I(t) by deconvolution can be accomplished with methods that work in a transformed domain rather than in the real time domain. These include Laplace transform, Fourier transform, and the method of moments operators. Most of these methods suffer from truncation problems.[1] Other methods have been attempted without much deconvolution success (Knight and Selinger).[64]

The real time method usually used is the convolution of the measured excitation pulse E(t) (obtained with a scattering solution of commercial non-dairy creamer or Ludox [Dupont] as the sample) with a model for the true fluorescence dacay I(t). Usually, a sum of exponentials is assumed for the model for I(t);

$$I(t) = \Sigma_i\ \alpha_i e^{-t/\tau_i}$$

(as defined in Section II.B3b). The calculated F(t), $F(t)_{cal}$, is compared to the experimental F(t), $F(t)_{exp}$. The preexponential factors and lifetimes are allowed to vary until the best fit is obtained. We have used a nonlinear least squares fitting method with a modified Marquardt algorithm as presented by Bevington and tested by Grinvald and

Steinberg.[4,54] In the Marquardt algorithm, a solution search is performed on the ^{2} surface, where ^{2} is defined as

$$\chi^2 = \Sigma^n_{i=1} W_i[F(t)_{exp} - F(t)_{calc}]^2$$

where $W_i = 1/F(t)_{exp}$, $F(t)_{exp}$ is the experimentally measured intensity in counts, and $F(t)_{calc}$ is the calculated intensity in counts.

The fits are judged by the superimposed fit, the residuals $(F(t)_{exp} - F(t)_{calc})$, the weighted residuals $([F(t)_{exp}-F(t)_{calc}]/F(t)exp)$, and the reduced χ^2_ν ($\chi^2_\nu = \chi^2/_\nu$, where ν = degrees of freedom = the number of channels in the analysis + 2i-1, and i is the number of components; a reduced chi square of exactly 1 is considered the best fit). The autocorrelation function of the residuals has been used by other workers. In general, inspection of the weighted residuals provides the same information without the extra computer time investment.[58]

The relative fluorescence quantum yield ϕ_i where

$$\phi_i = \alpha_i \tau_i$$

was also calculated. This yield represents the integrated number of photons emitted in the ith component and is normalized to 1 for the sum of all components in a given experimental decay curve. The α_i are also normalized to 1.

II.C Results and discussion

II.C1 Steady-state spectroscopy

II.C1a Absorption

Absorption and fluorescence emission spectra are shown in Figs. II.C-1a, b, and c for the αβ monomer, separated β, and separated α subunits of C-phycocyanin from Anabaena variabilis, respectively. When the absorption spectra of the separated subunits are added, the resultant normalized spectrum is superimposable with that of the αβ monomer. This is consistent with results of Glazer et al. The absorption maxima for the α (620 nm) and β (605 nm) subunits are similar to maxima for the subunits of C-phycocyanin from other cyanobacteria (Glazer et al., 1973).[48] Based on these maxima, Glazer et al. proposed that the f chromophore is the single chromophore on the α subunit and the s chromophores are the 2 chromophores on the β subunit. These assignments were also based on the deconvolution, by Dale and Teale, of the absorption band into sensitizing and fluorescing chromophores.[16,115] This, in turn, was based on use of the Forster energy transfer mechanism to explain energy transfer in phycobiliproteins. In the Forster mechanism, the rate of energy transfer is dependent on three main factors: the spectral overlap of the donor normalized fluorescence and the acceptor molar absorption; the orientation of the donor emission transition dipole moment and the acceptor absorption transition dipole moment; and the inverse of the sixth power

Fig. II.C-1: Absorption (——) and fluorescence (---) spectra for C-phycocyanin from Anabaena variabilis in 0.005 M potassium phosphate, pH 7, 0.001 M NaN_3, 0.001 M β-mercaptoethanol. Absorbance is 0.05 at the absorption wavelength maximum; fluorescence excitation at 550 nm. (a) αβ monomer, absorption λ_{max} = 614 nm, fluorescence emission λ_{max} = 640 nm. (b) β subunit, absorption λ_{max} = 604 nm, fluorescence emission λ_{max} = 640 nm. (c) α subunit, absorption λ_{max} = 620 nm, fluorescence emission λ_{max} = 640 nm.

Absorption (—) and Fluorescence Emission (---) of C-phycocyanin from *Anabaena variabilis*.

A_{max} = 0.05 , λex = 550nm.

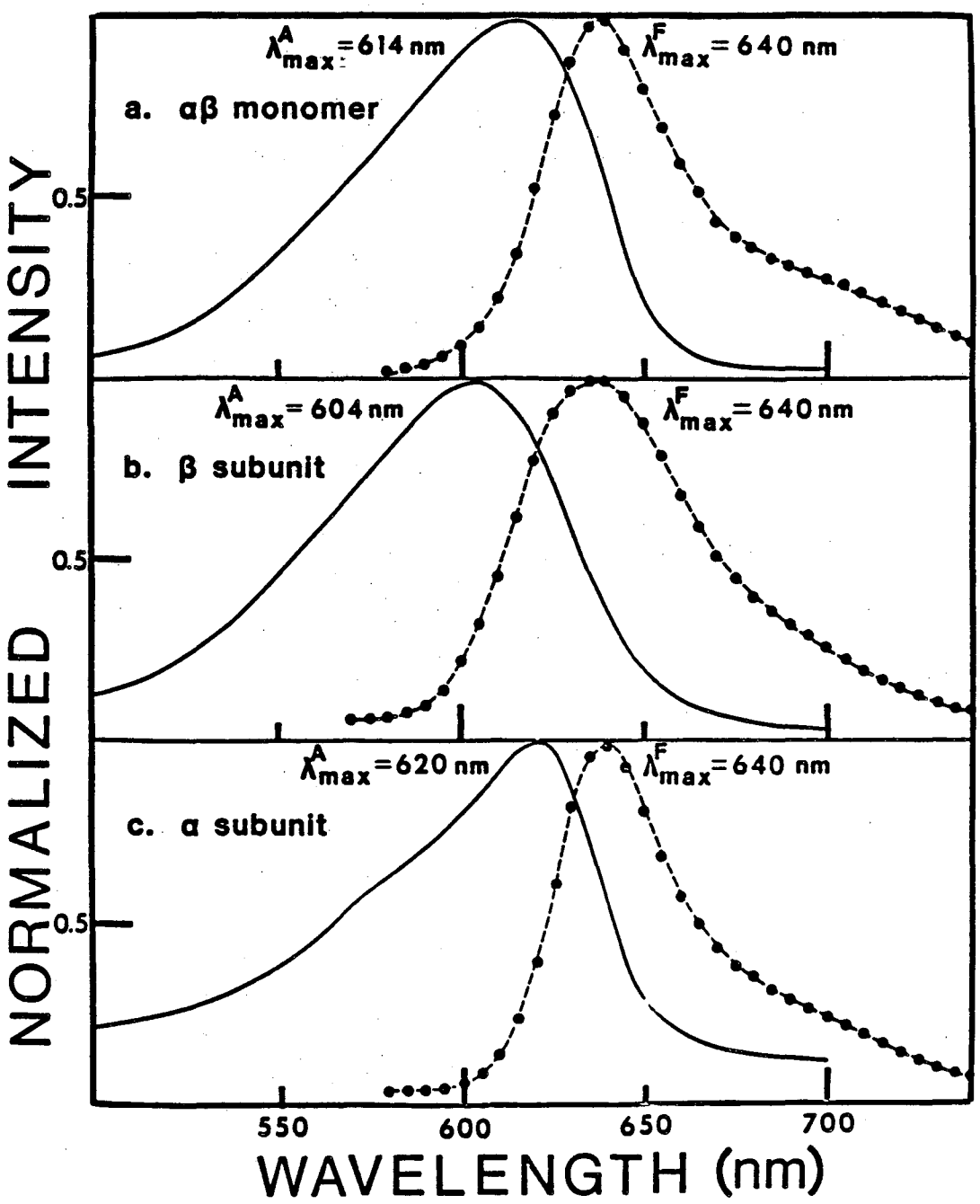

XBL 838-11280A

of the distance between the donor and acceptor. In summary, energy transfer is most efficient when the overlap is the largest, the donor-to-acceptor distance is the shortest, and the dipole moments are parallel. The largest spectral overlap occurs when the donor has an absorption maximum that is blue shifted from that of the acceptor. The Stokes shift of the donor fluorescence provides a large donor fluorescence--acceptor absorbance overlap. For phycobiliproteins, the donor (s) chromophore has a shorter absorption wavelength than the acceptor (f) chromophore for the most efficient Forster energy transfer. In addition, s chromophores have a shorter emission maximum than f chromophores for the most efficient energy transfer case. This is discussed in Section II.Clc.

Increasing protein concentration causes aggregation. However, decreasing the concentration below 1×10^{-6} M does not alter the absorption spectra of C-phycocyanin, which can be taken as evidence that no major aggregation changes occur in solutions with 0.005 M potassium phosphate, pH 7.0. From these results and circular dichroism (see Section II.Cle), the monomer is the predominant species below 1×10^{-6} M at low salt and neutral pH. Absorption spectra of the subunits (Figs. II.C-1b and c) do not change upon dilution below 5×10^{-6} M, which can be taken as evidence that aggregation at these concentrations is not likely. The presence or absence of buffer constituents, such as NaN_3 and β-mercaptoethanol, do not change the absorption spectra.

Salt concentration (ionic strength), however, is very important in determining the aggregation state. As seen in Fig. II.C-2, increasing the concentration of potassium phosphate causes a red shift of the absorption spectra, a rise in the extinction coefficient, and a change in band shape. The wavelength maximum shifts to 621 nm with 0.2 M phosphate, 624 nm with 0.4 M phosphate, 625 nm with 0.8 M phosphate, and 626 nm with 1.6 M phosphate. This is all consistent with the formation of hexamer, dodecamer, and higher assembly forms at high salt. The assembly geometry of these salt-induced aggregation forms may not be identical to the *in vivo* geometry.

Absorption spectra of denatured subunits and of denatured monomer are superimposable and have an absorption λ_{max} at 660 nm with a very broad bandshape compared to that of the native protein (Fig. II.C-3). The band remains asymmetric. The change in absorption λ_{max} and the drop in extinction coefficient is explained by the loss of the special protein-chromophore interaction. This explains why the monomer and separated subunits--which have different absorption spectra when native--exhibit identical spectra when denatured. Because only phycocyanobilin is present in all three species, removal of the protein interaction causes the spectra to become superimposable. It is interesting, however, that some asymmetry and structure is retained in the absorption spectra. This is consistent with a complex vibrational manifold composed of many chromophore conformations

Fig. II.C-2: Normalized absorption spectra of C-phycocyanin from Anabaena variabilis in 0.2 M potassium phosphate (——) and 1.6 M potassium phosphate (---). λ_{max} = 621 nm. for 0.2 M potassium phosphate, λ_{max} = 626 nm for 1.6 M potassium phosphate. Spectra were normalized at the absorption maximum.

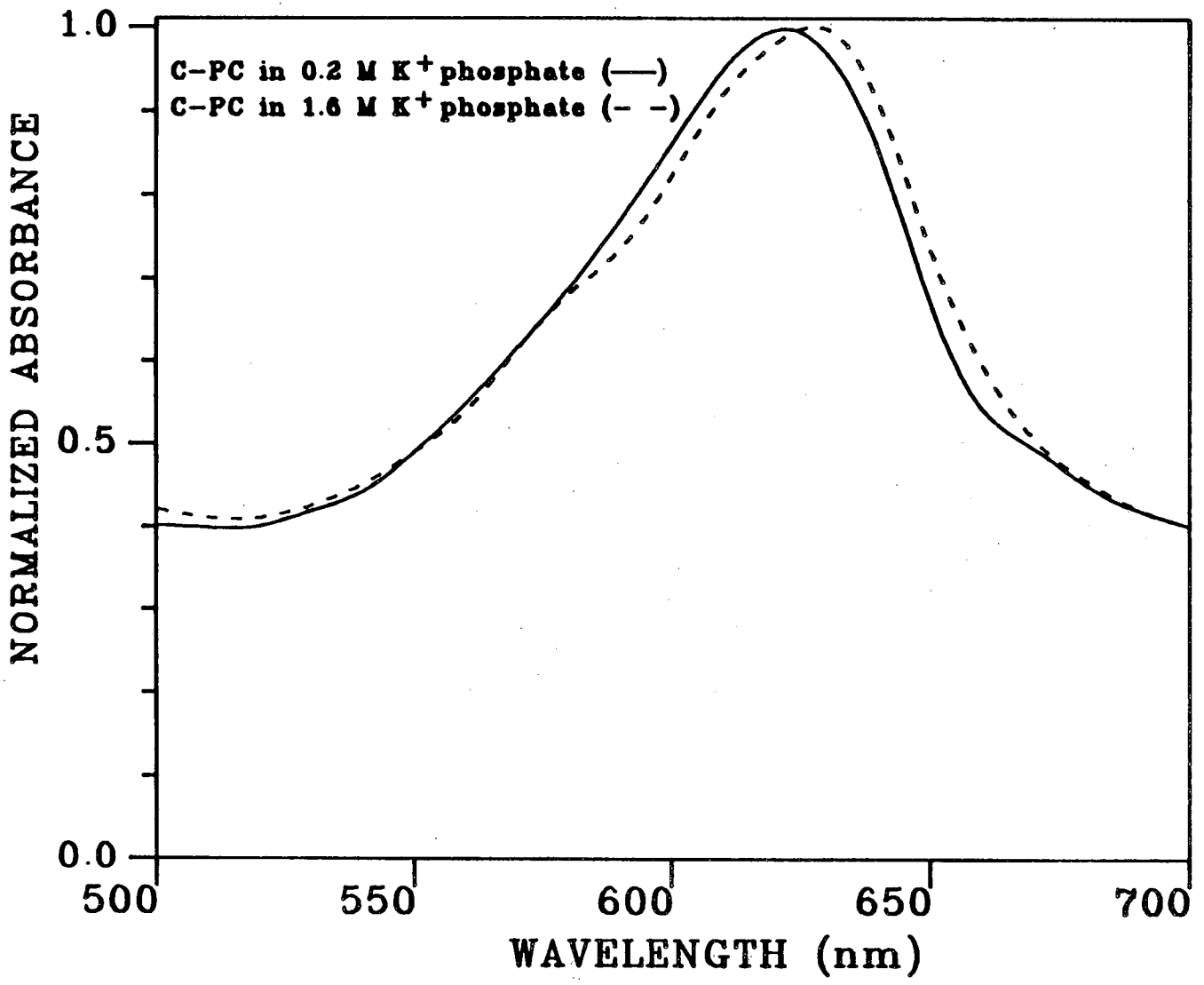
C-PC in 0.2 M K+ phosphate (——)
C-PC in 1.6 M K+ phosphate (- -)
NORMALIZED ABSORBANCE
1.0
0.5
0.0
500
550
600
650
700
WAVELENGTH (nm)

Fig. II.C-3: Normalized absorption (λ_{max} = 660 nm) and normalized fluorescence emission spectra (λ_{max} = 680 nm) for 1 X 10^{-6} M C-phycocyanin in 8 M urea, pH 3.0. Spectra were normalized at the maximum.

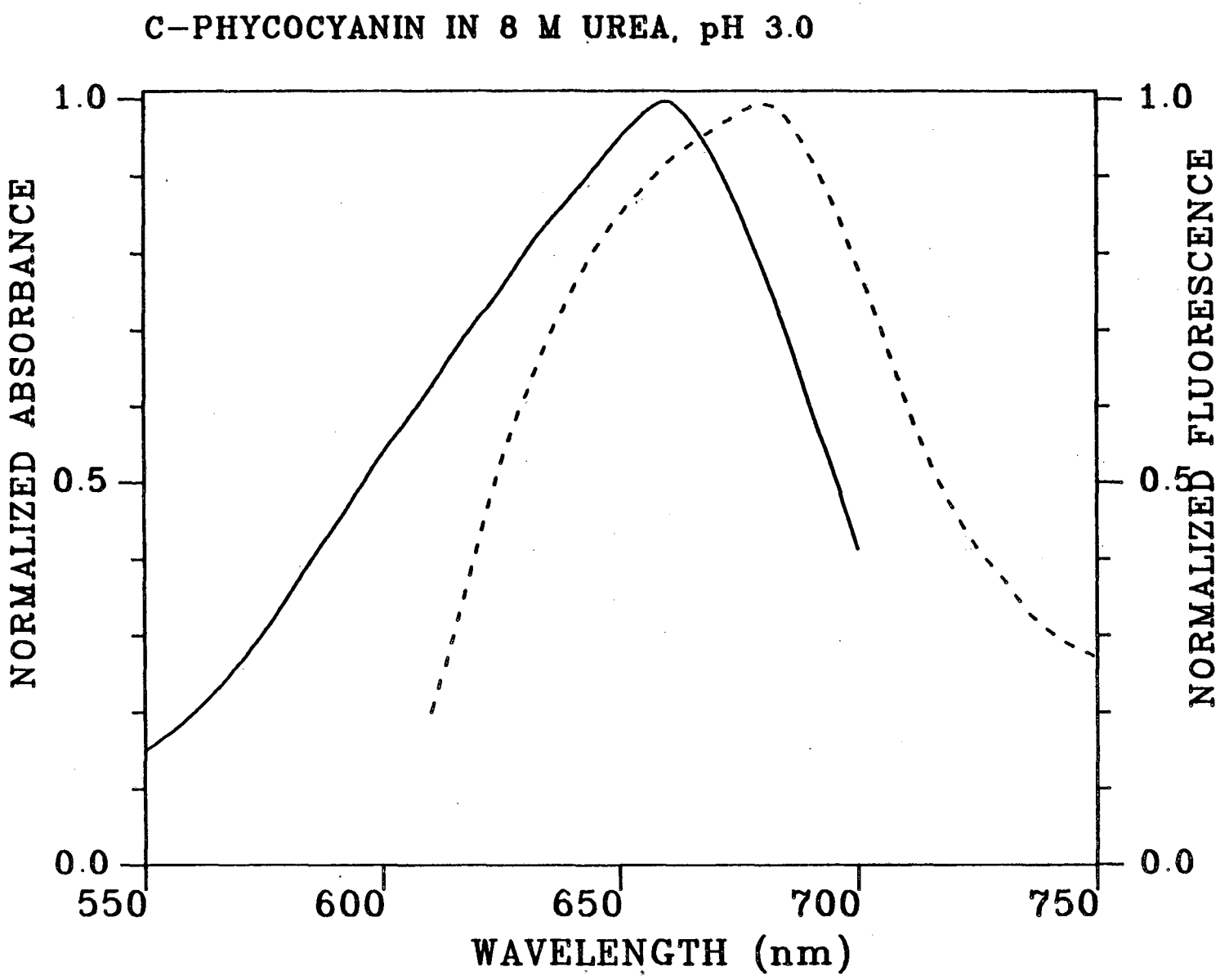
C-PHYCOCYANIN IN 8 M UREA, pH 3.0
NORMALIZED ABSORBANCE
NORMALIZED FLUORESCENCE
1.0
0.5
0.0
550
600
650
700
750
WAVELENGTH (nm)

that has been claimed for phycobiliproteins. A-ring and D-ring linked chromophores are present but, because the denatured spectra are superimposable, we can conclude that a similar distribution of conformers are present. The presence of a number of conformers has been proposed from photochemical hole-burning experiments and low temperature absorption spectra (see Section II.A2a[4]). Whether the conformers are in equilibrium and how fast they may interconvert are questions that have not been resolved (Section II.A).

Absorption spectra of pepsin-digested monomer and subunits are not so easily explained (Fig. II.C-4). The red shift in the absorption maximum is less than that of the urea-denatured protein. Enough of the backbone may still be present to provide some protein-chromophore interaction. Chromophore oxidation may also occur during digestion. However, the general trends that occur upon disruption of these interactions are still present. Namely, the extinction coefficient is decreased, the absorption λ_{max} is red shifted (but in general not so red as 660 nm), and the band becomes broad and structureless (as compared to the native protein, also shown in Fig. II.C-4).

Absorption and fluorescence emission spectra are shown in Fig. II.C-5a, b, and c for the $\alpha\beta$ monomer, separated α, and separated β subunits of C-phycocyanin from <u>Anacystis nidulans</u>, respectively. As in the case of <u>Anabaena</u>, and in the results of Glazer et al.[48], the added spectra of the subunits can be superimposed on that of the monomer. The

Fig. II.C-4: Absorption spectra of the pepsin-digested (4 hrs., pH 3.0, 37°C.) (- -) and the native (——) β subunit of C-phycocyanin. Determined at pH 7.0, 0.005 M phosphate, 25°C.

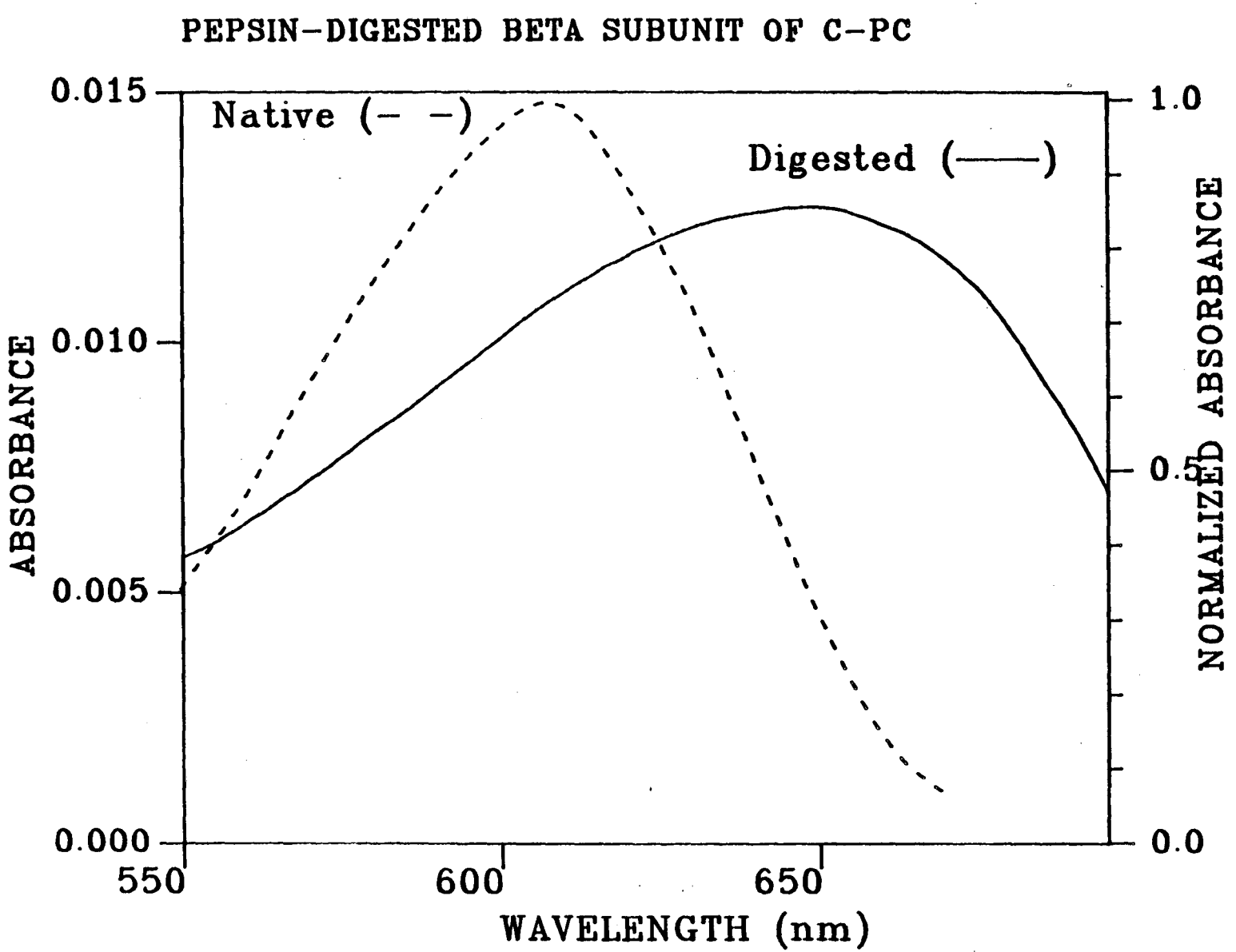
PEPSIN-DIGESTED BETA SUBUNIT OF C-PC
Native (- -)
Digested (——)
ABSORBANCE
0.015
0.010
0.005
0.000
NORMALIZED ABSORBANCE
1.0
0.5
0.0
550
600
650
WAVELENGTH (nm)

Fig. II.C-5: Absorption (——) and fluorescence (---) spectra for C-phycocyanin from Anacystis nidulans in 0.005 M potassium phosphate, pH 7, 0.001 M NaN_3, 0.001 M β-mercaptoethanol. Absorbance is 0.05 at the absorption wavelength maximum; fluorescence excitation at 550 nm. (a) αβ monomer, absorption λ_{max} = 615 nm, fluorescence emission λ_{max} = 640. (B) α subunit, absorption λ_{max} = 620 nm, fluorescence emission λ_{max} = 640. (C) β subunit, absorption λ_{max} = 608 nm, fluorescence emission λ_{max} = 645 nm.

Absorption (——) and Fluorescence Emission (– – –)
of C-phycocyanin from *Anacystis nidulans*.
A_{max} = 0.05 , λ_{ex} = 550 nm.

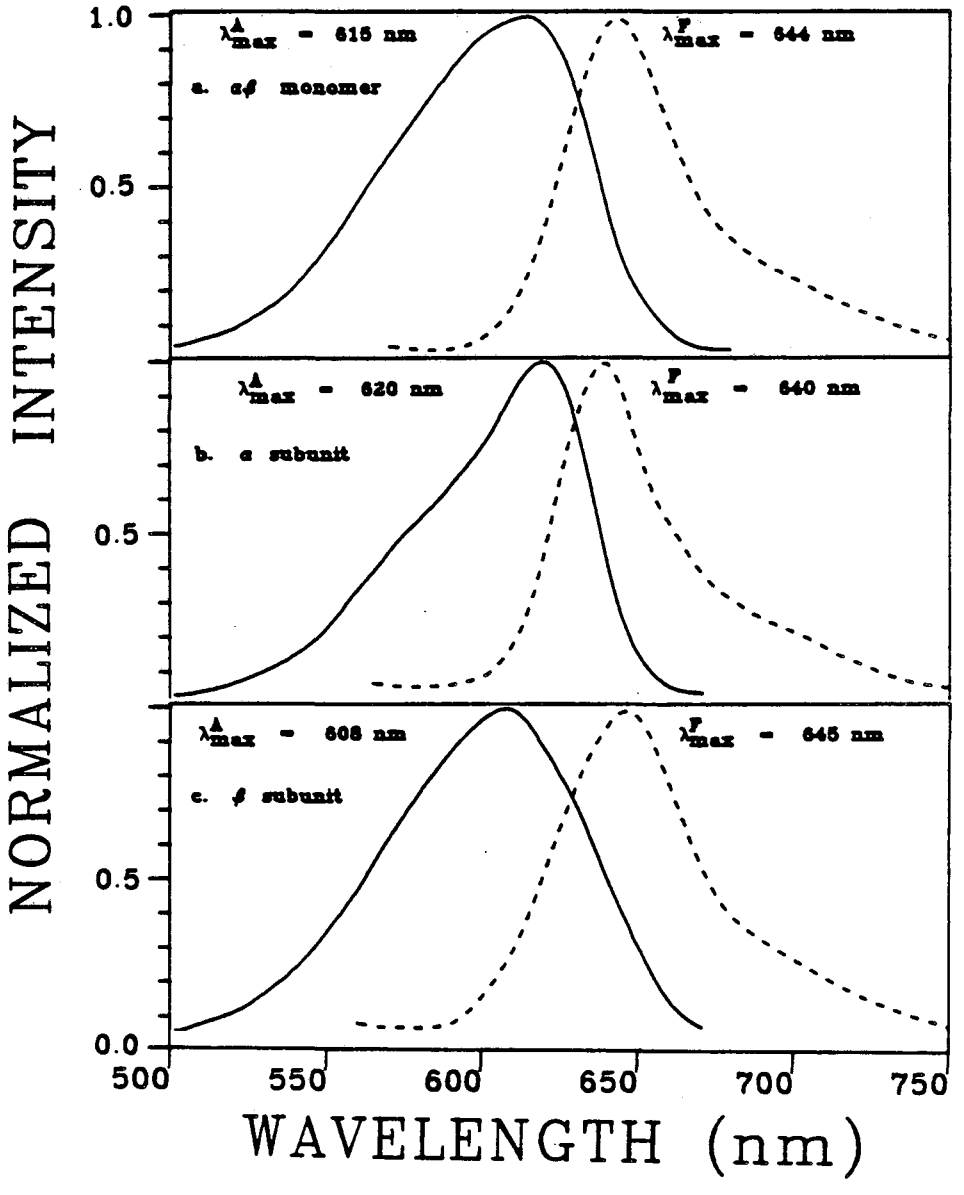

absorption maxima for the α (620 nm) and β (608 nm) subunits are identical to those of Glazer et al.[16] Concentration of protein, salt concentration, buffer constituents, and denaturation all have the same effects on Anacystis nidulans C-phycocyanin that they have on Anabaena variabilis C-phycocyanin.

Absorption spectra of R-phycocyanin dimers, with and without the 32 kD linker protein, are shown in Fig. II.C-6. The absorption λ_{max} shifts from 617 to 625 nm and the long wavelength to shorter wavelength peak height ratio increases upon addition of linker. This has been seen in the C-phycocyanin system by Yu et al.[131] and can be directly attributed to the conformational perturbation of the linker protein. Again, the same trend is observed, i.e. that further aggregation causes a red shift in the λ_{max}, etc. It should be noted that the aggregation with linker produces some of the most dramatic changes. It is at this level that native phycobiliprotein spectral characteristics begin to be observed.

These absorption spectra illustrate the main features of phycobiliprotein spectroscopy. The extinction coefficient rises as the proteins renature and then aggregate. The λ_{max} shifts to the red upon aggregation. It also shifts to the red, but much further than upon aggregation, when the protein-chromophore interaction is disrupted. In addition, the band is very broad upon denaturation or digestion. All of

Fig. II.C-6: Normalized absorption spectra of R-phycocyanin dimer from Griffithsia tenuis, with (---) and without (——) the 32 kD linker polypeptide, in 0.100 M potassium phosphate. Absorption λ_{max} = 617 nm without linker, λ_{max} = 625 nm with linker.

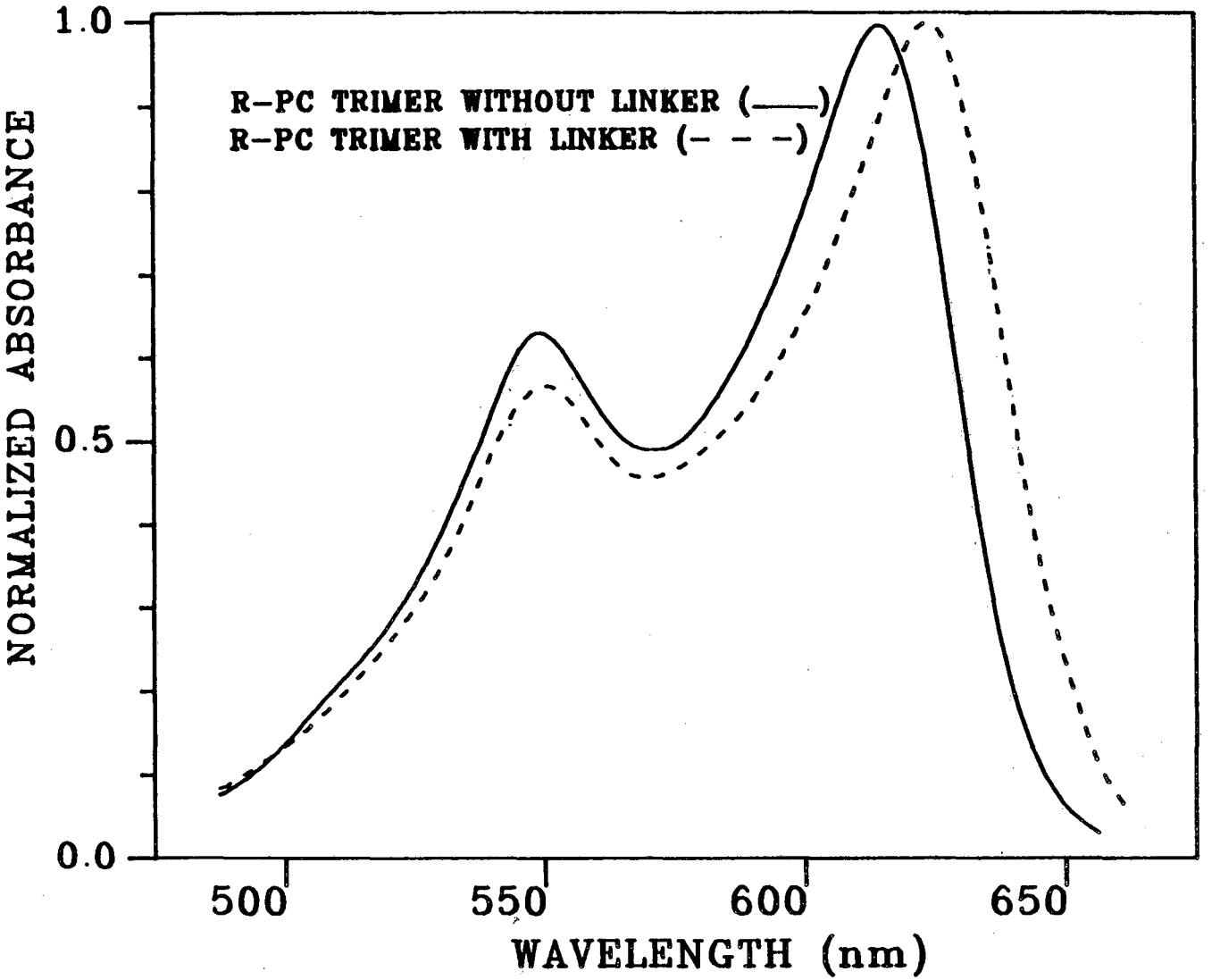
R-PC TRIMER WITHOUT LINKER (——)
R-PC TRIMER WITH LINKER (- - -)
NORMALIZED ABSORBANCE
1.0
0.5
0.0
500
550
600
650
WAVELENGTH (nm)

these results are consistent with the previous hypothesis that the main function of the protein-chromophore interactions is to provide a more rigid chromophore with less conformational heterogeneity and fewer paths for nonradiative decay.[106,107]

II.C1b Fluorescence excitation

Basically, the same things that affect absorption spectra also affect fluorescence excitation spectra. Indeed, for the αβ monomer and separated α and β subunits, the λ_{max} and bandshapes of fluorescence excitation spectra are identical to those of the absorption spectra. The λ_{max} and bandshapes are independent of the emission (observation) wavelength within the error of the instrument (± 2 nm, noise < 1% of signal, dark count < 0.1% of signal). We conclude that energy transfer is very efficient (>99%) in these samples, because energy emitted as fluorescence is directly proportional to the extinction coefficient of the sample at the particular excitation wavelength. This also implies that there is one emitting state or, if there is more than one, that these states have the same fluorescence emission spectra and cannot be distinguished on the basis of emission wavelength (for Fluorescence emission results, see Section III.C1c).

Fluorescence excitation spectra were also obtained at low temperatures (Fig. II.C-7). The excitation maxima of the subunits and the monomer are all red shifted from their room

Fig. II.C-7: Normalized fluorescence excitation (——) and fluorescence emission (- - -) spectra of the β subunit of C-phycocyanin from Anabaena variabilis at 77K in 50% glycerol and 50% 0.005 M potassium phosphate, 0.001 M NaN_3, 0.001 M β-mercaptoethanol glass. Fluorescence excitation λ_{max} = 615 nm, λ_{em} = 690 nm; fluorescence emission λ_{max} = 636 nm, λ_{ex} = 550 nm. Absorbance = 0.05, pathlength = 1 cm.

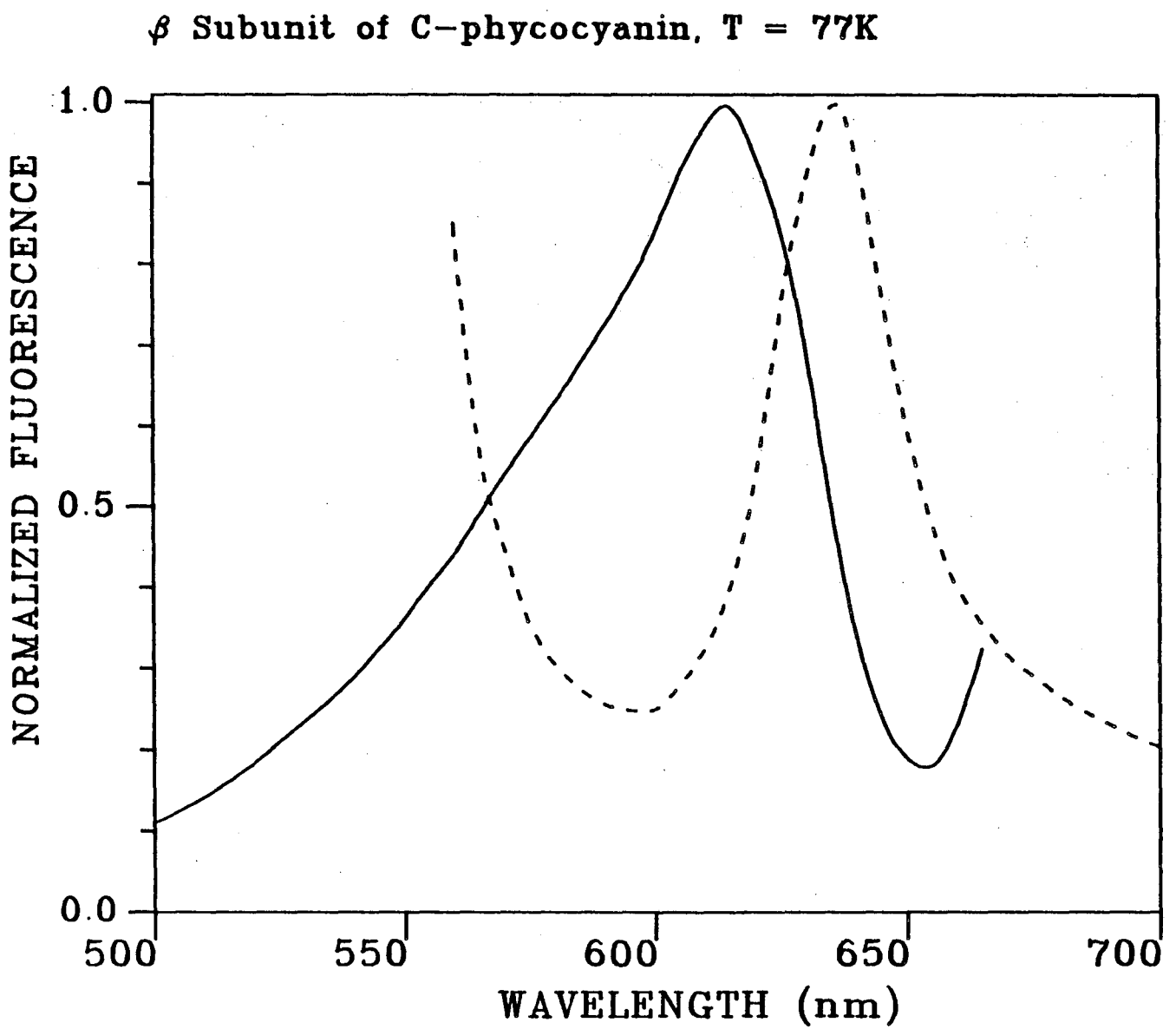
β Subunit of C-phycocyanin, T = 77K
NORMALIZED FLUORESCENCE
1.0
0.5
0.0
500
550
600
650
700
WAVELENGTH (nm)

temperature excitation maxima (Table II.C-1). There is a large contribution from scatter in the spectrum, with a maximum at the emission (observation) wavelength (not shown). Attempts were made to lower the scatter and prevent shifts of the maxima due to the overlapping peaks. The maxima were independent of emission wavelength.

These shifts in the maximum are commonly seen in the fluorescence spectra of dyes when the temperature is decreased. At room temperature, solvent relaxation is fast on the fluorescence time scale. Emission occurs from lower energy states in which the solvent dipoles have had sufficient time to reorder about the excited state dipole of the solute. At 77K, the solvent may not be able to reorder on the time scale of the fluorescence, and the emission may occur from higher energy non-relaxed solvent-solute states. Therefore, the emission is blue shifted. A Boltzmann distribution at lower temperatures has the lower vibrational levels more highly populated, and the excitation maximum is red shifted toward the $\nu_{0,0}$ vibrational band wavelength. This applies to the emission maxima as well, producing a red shift. We also observe these shifts for phycobiliproteins, and solvent-solute interactions and Boltzmann populations are sufficient to explain these results. However, these conclusions are tempered by the knowledge that the bilin photochemistry is dependent on the protein and that the aggregation state and conformation of the phycobiliproteins may be affected by temperature changes.

Table II.C-1: Fluorescence emission and excitation maxima of the αβ monomer and α and β subunits of C-phycocyanin from *Anabaena variabilis* at 298 and 77K in a 0.005 M phosphate buffer, pH 7.0.

Sample	Excitation λ_{max}, 298K	Excitation λ_{max}, 77K	Emission λ_{max}, 298K	Emission λ_{max}, 77K
α subunit	620	623	640	633
β subunit	604	615	640	636
αβ monomer	614	620	640	636

Fluorescence excitation of R-phycocyanin resembles the absorption spectra, even to the separate peak at 555 nm and maximum at 617 nm, again consistent with efficient energy transfer.

II.C1c Fluorescence emission

The fluorescence emission maximum (Figs. II.C-1a, b, and c) is at 640 nm ± 2 nm, with a long tail beyond 750 nm, for the (αβ) monomer and for the separated α and β subunits of C-phycocyanin from Anabaena variabilis. The fluorescing states or emission transition energies of the αβ monomer and separated α and β subunits are the same because the three proteins have identical (within the instrumental resolution) emission maxima. This does not fit well with a Forster energy transfer mechanism, which predicts that the β subunit should have a fluorescence maximum blue-shifted from that of the α subunit and, with a lack of strong chromophore coupling upon subunit combination, the αβ monomer should have a maximum between those of the α and β subunit. The maxima of the αβ monomer and separated α and β subunits of C-phycocyanin from Anacystis nidulans (Figs. II.C-5a, b, and c) are less consistent with a Forster mechanism than those of Anabaena variabilis. The α subunit of Anacystis nidulans fluoresces maximally at 640 nm (bluest) and the β subunit fluoresces maximally at 645 nm (reddest). These results do not support an assignment of the s chromophores to those on the β subunit, which is the assignment

based on the absorption spectra and a Forster mechanism. Clearly, the labels "s" and "f" are limited concepts at best and are not easily related to absorption or fluorescence emission maxima.

The α subunit fluorescence emission bandwidth is significantly narrower than that of β , with the combination in the αβ monomer falling within these 2 widths for C-phycocyanin from both Anabaena variabilis (Fig. II.C-1a, b, and c) and Anacystis nidulans (Fig. II.C-5a, b, and c). This width is related more strongly to the vibrational manifold than to the chromophore interaction, since the αβ monomer width is a weighted sum of the α and β subunit fluorescence linewidths.

The fluorescence emission spectra are affected by aggregation similarly as the absorption spectra: The maximum is red-shifted upon aggregation and the quantum yield increases. This is shown by increasing the concentration of salt. The bandshape does not change and the wavelength shifts have been summarized in Table II.C-2. The maximum shifts to the red upon aggregation of the protein induced by higher salt concentration. Minor buffer constituents have no effect on the quantum yield, fluorescence λ_{max}, or fluorescence emission or excitation bandshape of these proteins. In addition, there is no evidence of O_2 quenching: purged samples have the same quantum yield as aerated samples. (Care must be taken on purging or aeration, because rapid bubbling tends to denature protein with a resultant loss in

Table II.C-2: Fluorescence emission maximum of C-phycocyanin as a function of potassium phosphate concentration, pH 7, 25°C.

[Phosphate] (M)	Emission λ_{max}
0.005	640
0.2	645
0.4	647
0.8	648
1.6	649

extinction coefficient and quantum yield.

Denaturation results in a large red shift, to 680 nm, for the fluorescence emission λ_{max} of the αβ monomer and α and β subunits of C-phycocyanin, accompanied by a decrease (from 2-3 orders of magnitude) in quantum yield. Again, digestion leaves enough protein backbone and protein-chromophore interaction to complicate the spectra. The general red shift and quantum yield decrease are still observed, however.

Low temperature studies were also performed (Fig. II.C-7). The emission maxima of the subunits and the monomer are all blue-shifted from their room temperature maxima (Table II.C-1). There is a large contribution from scatter in the spectrum with a maximum located at the excitation wavelength. The maxima were independent of excitation wavelength. As previously noted, these results are consistent with non-relaxed solvent-solute states and the change in the Boltzmann distribution at low temperature.

II.C1d Fluorescence excitation polarization

For the separated α subunit of C-phycocyanin from Anabaena variabilis, the fluorescence excitation polarization is constant at 0.40 across the absorption band; however, for the β subunit, the polarization increases from 0.23 to 0.35 from short to the long wavelength across the absorption band, and increases similarly from 0.15 to 0.25 for the αβ monomer (Fig. II.C-8). For the separated α subunit of C-phycocyanin

Fig. II.C-8: Absorption and fluorescence excitation polarization of the αβ monomer (——) and separated α (– —— –) and β (---) subunits of C-phycocyanin of *Anabaena variabilis*; fluorescence emission at 694 nm. Similar values were obtained at 680 and 720 nm. Absorbance ≈ 0.05 in a 0.005 M phosphate buffer, pH 7.0.

Absorption and Fluorescence Excitation Polarization of C-phycocyanin from *Anabaena variabilis.*

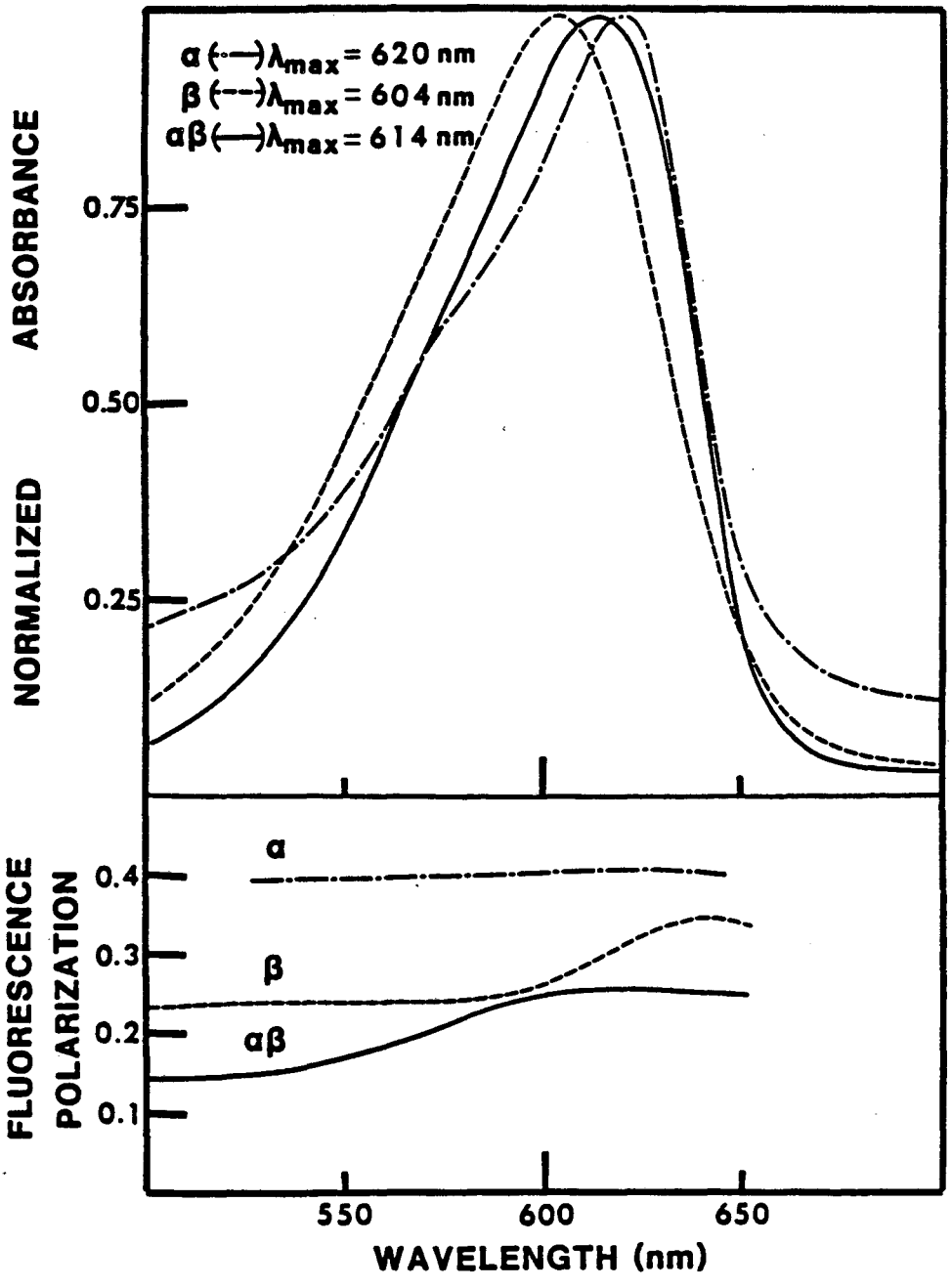

-- XBL 838-11281A --

from Anacystis nidulans, the fluorescence excitation polarization is also constant at 0.4, the polarization increases from 0.27 to 0.37 for the β subunit, and increases from 0.24 to 0.34 from short to long wavelength across the absorption band for the αβ monomer (Fig. II.C-9). We attribute the rise of polarization across the absorption band toward longer wavelength for the β subunit and the αβ monomer to energy transfer among the 3 chromophores in the αβ monomer and between 2 chromophores in the β subunit. The constant polariztion of the α subunit, with one chromophore, is consistent with the lack of any possibility of energy transfer. The polarization decreases with the increasing number of chromophores in the sample. These results are consistent with a model of s and f chromophores, as presented by Dale and Teale.[16,115] However, care must be taken in assigning "s" or "f" to a chromophore. The fluorescence excitation polarization of the αβ monomer is lower than the polarization of either the separated α or β subunits, suggesting that the emitting chromophores on the β subunit must acquire some sensitizing character upon association with the α subunit in the αβ monomer. Again, the labels s and f are relative terms.

Protein concentration affects the polarization. In these experiments, as the protein concentration increases to greater than 1×10^{-6}, the aggregation state changes, and the number of chromophores participating in the energy transfer increases, lowering the overall polarization.

Fig. II.C-9: Absorption and fluorescence excitation polarization of the αβ monomer (——) and separated α (···) and β (---) subunits of C-phycocyanin from Anacystis nidulans; fluorescence emission at 694 nm. Similar values were obtained at 680 and 720 nm. Absorbance ≈ 0.05 in a 0.005 M phosphate buffer, pH 7.0.

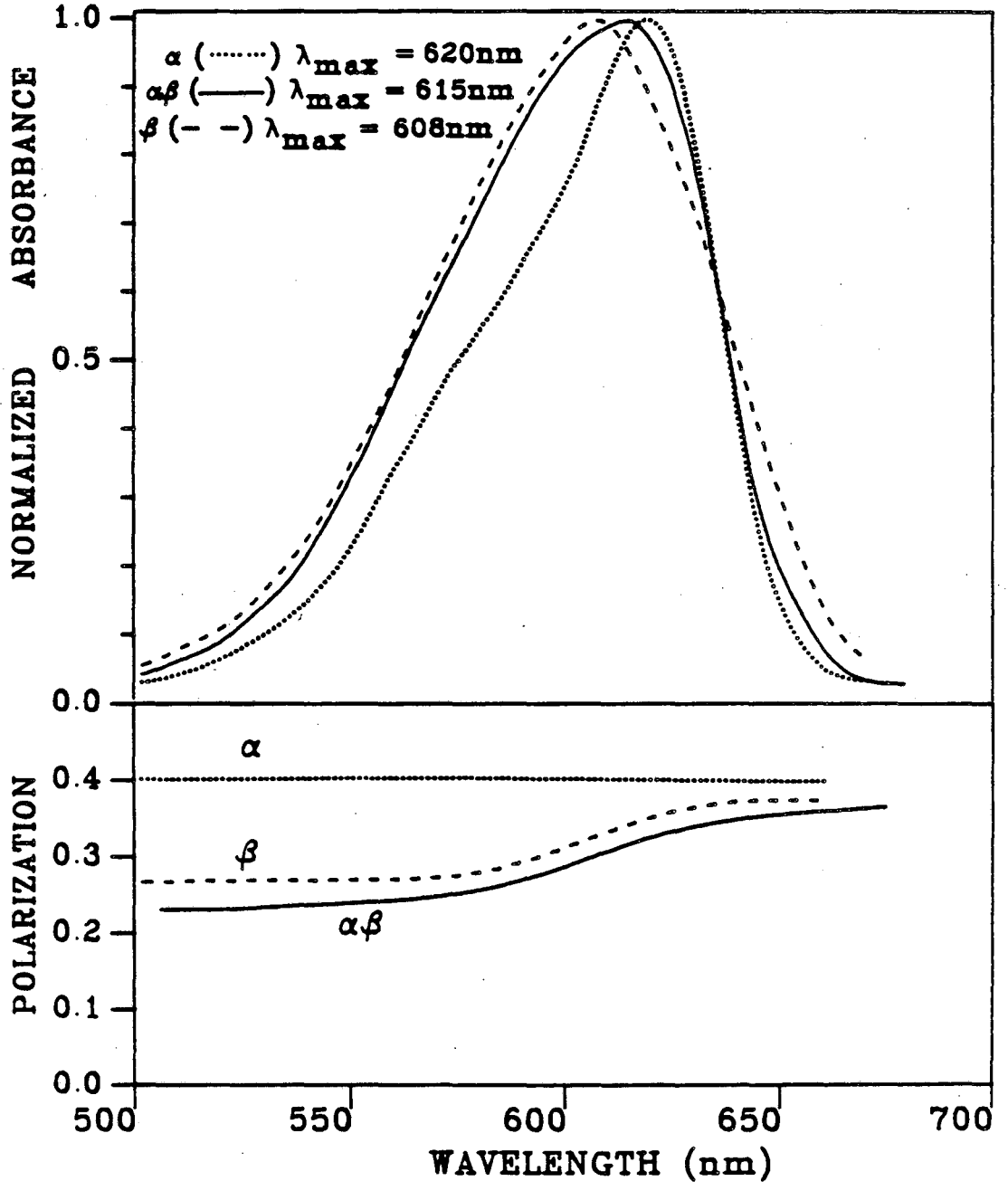
1.0
0.5
0.0
NORMALIZED ABSORBANCE
α (·····) λmax = 620nm
αβ (——) λmax = 615nm
β (– –) λmax = 608nm
α
β
αβ
0.4
0.3
0.2
0.1
0.0
POLARIZATION
500
550
600
650
700
WAVELENGTH (nm)

II.C1e Circular dichroism

Circular dichroism spectra of the αβ monomer and separated α and β subunits of C-phycocyanin from Anabaena variabilis are shown in Fig. II.C-10. The peak wavelength maxima correspond well with the absorption maxima, as in the work by Glazer et al. on Anacystis nidulans C-phycocyanin.[48] This would normally be taken to indicate that exciton coupling does not occur at this level of aggregation. (There also are no negative excursions in the CD between 500 and 700 nm.) This is not consistent with the results of Stadnichuk et al.[109], who deconvoluted the absorption spectra into a series of bands assigned to exciton states. It is consistent with either an intermediate coupling or weak, Forster coupling energy transfer mechanism. An observation in agreement with the results of Stadnichuk et al.[109] is the difference between the absorption and CD maxima. The samples that have a greater number of chromophores and the possibility of strong coupling (the β subunit and the αβ monomer) also have the largest difference between the absorption and CD maxima.

CD spectra are very sensitive to aggregation state, as shown in Fig. II.C-11. In this experiment, protein concentration was decreased by serial dilution. The shoulder at 625 nm at a concentration of 2.4×10^{-6} M, which does not appear in absorption spectrum, is due to trimer and hexamer. This shoulder is not present at a protein concentration below $\approx 5 \times 10^{-7}$ M, which is evidence that the predominant

Fig. II.C-10: Normalized circular dichroism spectra of the $\alpha\beta$ monomer (——) and separated α (···) and β (---) subunits of C-phycocyanin from Anabaena variabilis. $\alpha\beta$, λ_{max} = 598 nm; α , λ_{max} = 618 nm; β λ_{max} = 588 nm. Absorbance ≈ 0.05 in a 0.005 M phosphate buffer, pH 7.0.

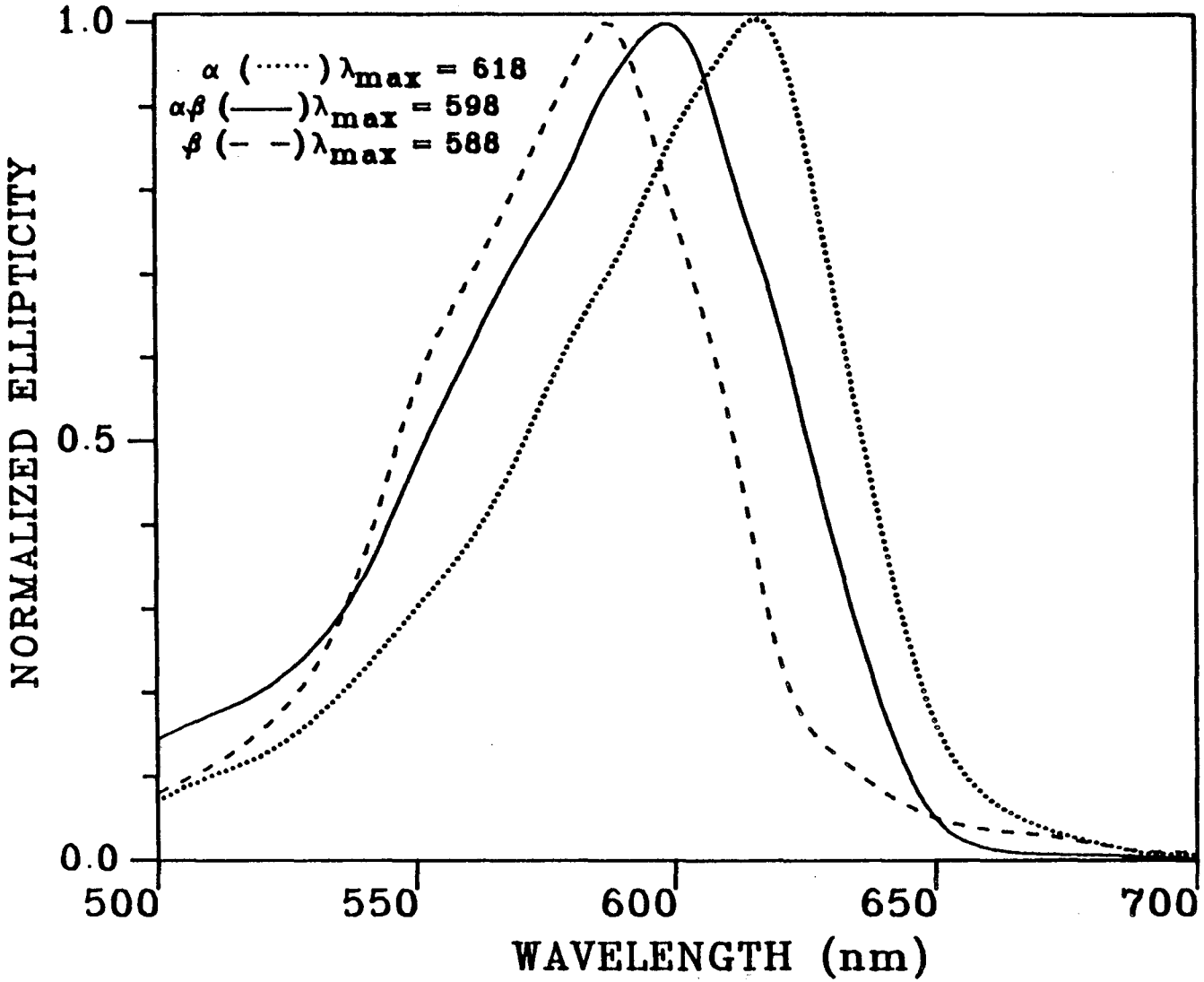
α (·····) λmax = 618
αβ (——) λmax = 598
β (– –) λmax = 588
1.0
0.5
0.0
NORMALIZED ELLIPTICITY
500
550
600
650
700
WAVELENGTH (nm)

Fig. II.C-11: Normalized circular dichroism spectra of 2.4 X 10^{-6} M (——) and 1.7 X 10^{-6} M (---) C-phycocyanin from <u>Anabaena variabilis</u>. λ_{max} = 598 nm. Shoulder at ≈ 626 nm. Absorbance ≈ 0.05 in a 0.005 M phosphate buffer, pH 7.0.

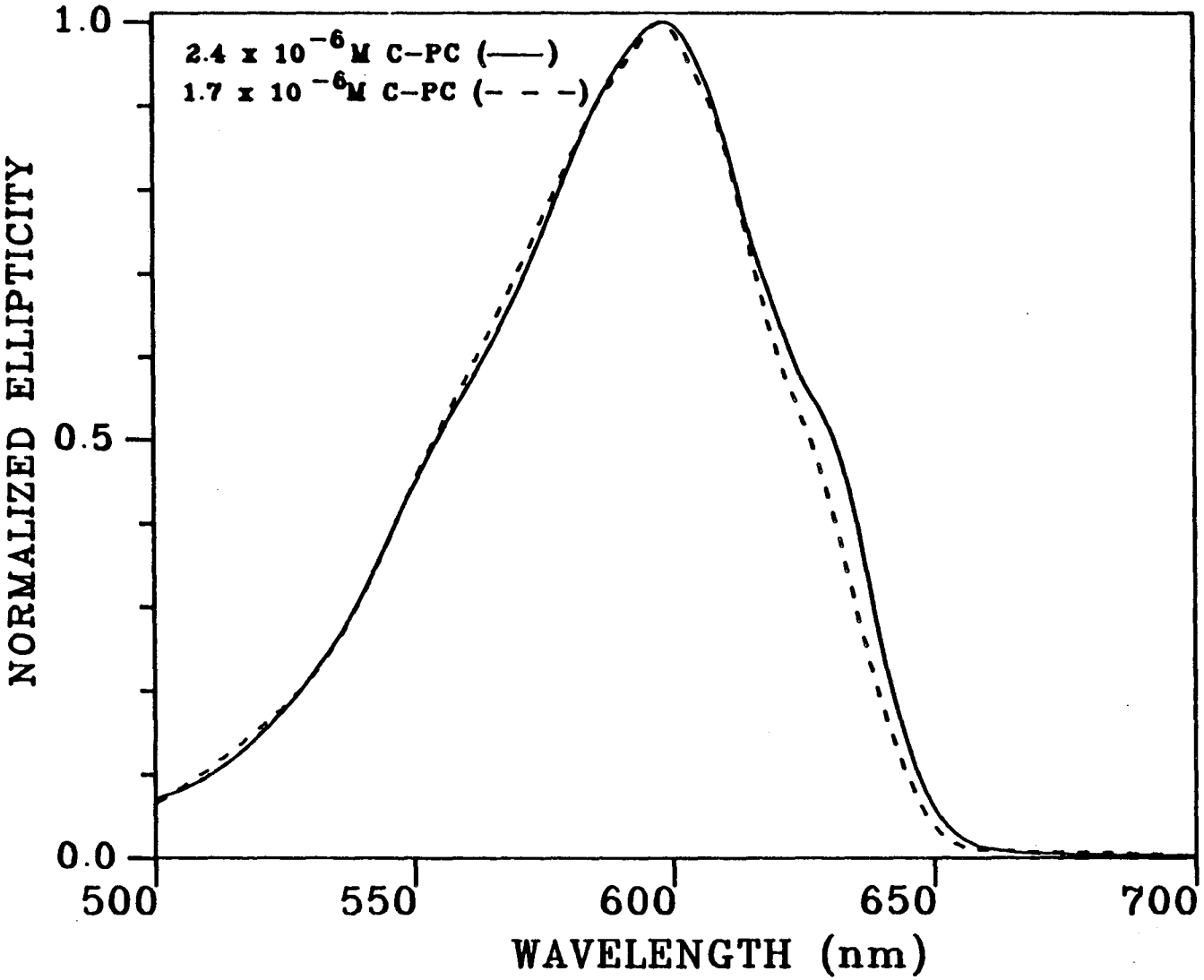
2.4 x 10^{-6}M C-PC (——)
1.7 x 10^{-6}M C-PC (- - -)
NORMALIZED ELLIPTICITY
1.0
0.5
0.0
500
550
600
650
700
WAVELENGTH (nm)

species is monomer. Increasing salt concentration also causes aggregation, as shown in Fig. II.C-12. The peak maximum is shifted and the bandshape changes as the aggregation state increases with increasing salt concentration. A band develops at 626 nm and increases with increasing salt concentration. This is evidence for hexamer formation. However, the band at 626 nm begins to shift and large negative excursions occur in the spectra above 0.8 M salt (not shown). Aggregations greater than hexameric are likely to occur above 0.8 M salt. The negative excursions above 0.8 M and shifts in band maximum are consistent with an exciton state resulting from strong coupling in trimer and hexamer aggregation states. This is similar to results of Glazer et al.[48] and MacColl et al.[83] on C-phycocyanin and allophycocyanin, respectively.

II.C2 Time-resolved fluorescence

II.C2a Monomer and subunits

The fluorescence decay from the α subunit of C-phycocyanin from Anabaena variabilis is shown in Fig. II.C-13; it is fitted poorly with one exponential component, but reasonably well with two. The (αβ) monomer and separated α and β subunits of C-phycocyanin from both Anabaena variabilis and Anacystis nidulans all exhibited a clear biexponential decay. (Throughout this section, and Section III.C, only representative decay curves will be displayed and data summarized in tables or graphs.) Table II.C-3 summarizes the

Fig. II.C-12: Normalized circular dichroism spectra of C-phycocyanin, 1 X 10^{-6} M, from Anabaena variabilis in 0.1 M (——), 0.2 M (- -), 0.4 M (···), and 0.8 M (---) potassium phosphate, pH 7, 0.001 M NaN_3, 0.0001 M β-mercaptoethanol. λ_{max} = 598 nm (0.1M), 590 nm (0.2M), 580 nm (0.4M), 576 nm (0.8M). Shoulders are present at 626 nm (0.1M), 627 nm (0.2M), 632 nm (0.4M), and 640 nm (0.8M).

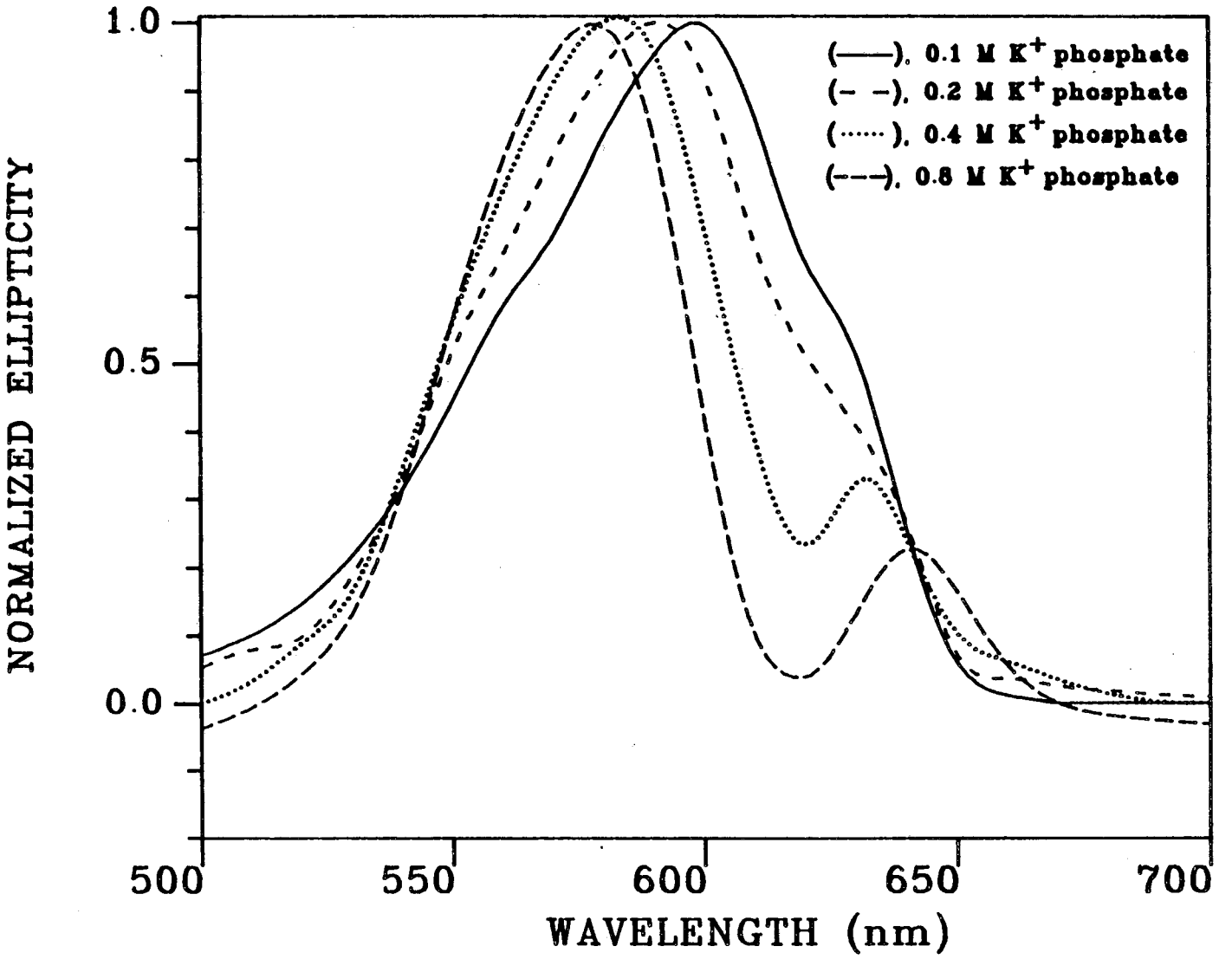
(——), 0.1 M K+ phosphate
(– –), 0.2 M K+ phosphate
(·····), 0.4 M K+ phosphate
(–·–), 0.8 M K+ phosphate
NORMALIZED ELLIPTICITY
1.0
0.5
0.0
500
550
600
650
700
WAVELENGTH (nm)

Fig. II.C-13: Fluorescence decay kinetics for the α subunit of C-phycocyanin using a C31034A photomultiplier tube. A_{620} = 0.03, $\lambda_{excitation}$ = 620 nm, $\lambda_{emission}$ = 640 nm. The narrow profile (full width, half maximum = 320 ps) is the excitation pulse shape. The experimental fluorescence decay (noisy) curve is fit with a two-exponential (smooth) curve. Middle and bottom, deviations in counts per channel of the calculated fit of a one-or-two exponential decay from the experimental decay, on a linear scale. A plot of deviations from the experimental decay for a three-exponential fit is not distinguishable from that for a two-exponential fit. Decay kinetic parameters τ (lifetime), α (amplitude), and ϕ (relative yield) are α_1 = 0.809, τ_1 = 1.470, ϕ_1 = 0.934, α_2 = 0.191, τ_2 = 0.438, ϕ_2 = 0.066. Kinetics were obtained at 25°C in a 0.005 M phosphate buffer, pH 7.0.

Fluorescence Decay Kinetics of the α subunit of C-phycocyanin from *Anabaena variabilis*

λ_{ex} = 620nm λ_{em} = 640nm

$\alpha_1 = 0.809$	$\alpha_2 = 0.191$
$\tau_1 = 1.470$	$\tau_2 = 0.438$
$\phi_1 = 0.934$	$\phi_2 = 0.066$

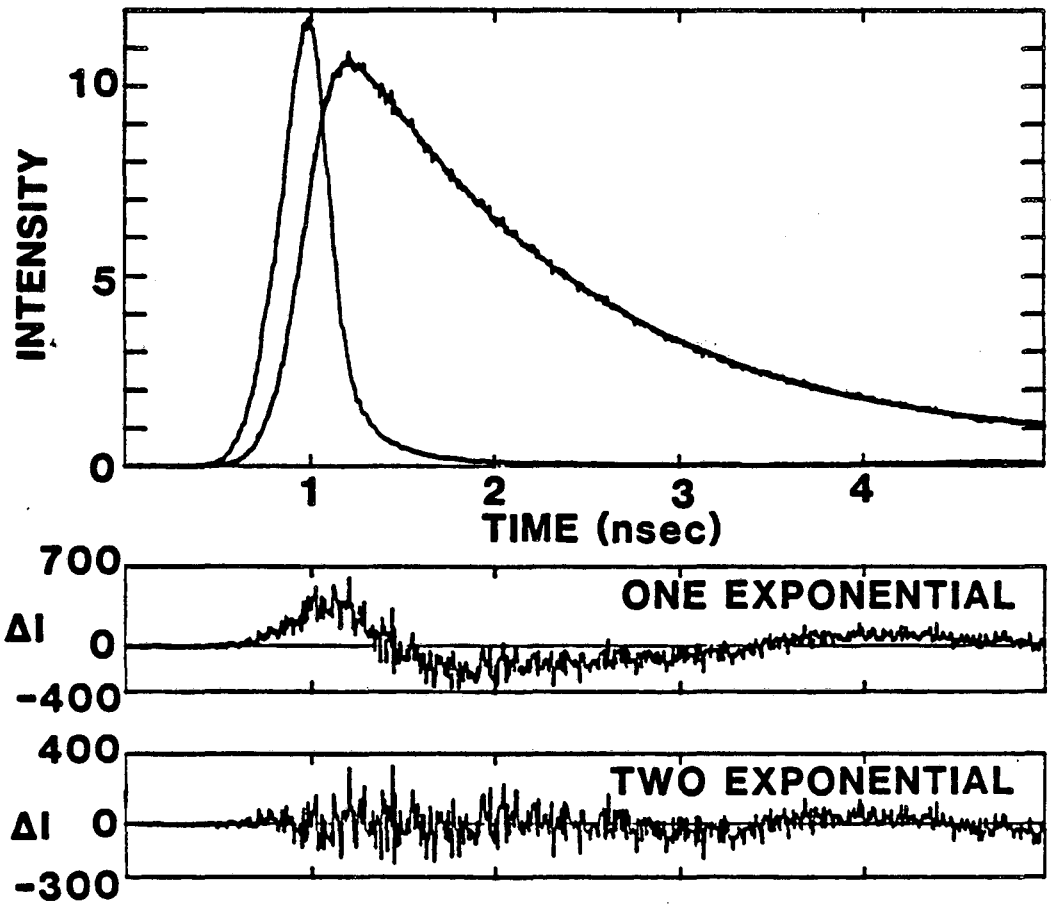

-- XBL 8312-2510 --

data for the αβ monomer and the α and β subunits of C-phycocyanin from Anabaena variabilis at different emission wavelengths. Differences, if any, as a function of wavelength are at the measurement error limits. Excitation at 600, 613, or 620 nm did not result in significant changes in the decay parameters, nor did alteration of the buffer components (0.01-0.002 M phosphate, ± NaN_3, ± $HSCH_2CH_2OH$, ± O_2) or changes in concentration. Addition of NH_4SCN (final concentration of 0.5-1.0 M) did not significantly alter the fluorescence decay parameters of the monomer or subunits.

The biexponential decay kinetics of the α subunit is unexpected, because there is only one chromophore per subunit. An explanation of the two lifetime components using the s-f model is not possible, because the α subunit has only a single chromophore. The decay parameters were not affected by changes in concentration or in buffer components, such as the chaotropic agent NH_4SCN. Chaotropic salts are known to dissociate multimers to monomer and, in some cases, monomer to separated subunits.[83,133] This suggests that aggregation and quenching by buffer components do not cause the biexponential kinetics. Invoking the s-f model and aggregation to explain the biexponential kinetics is also inconsistent with the conclusion, drawn from fluorescence excitation polarization data, that there is no energy transfer in α subunit preparation. The (αβ) monomer and β subunit decay parameters are similar to those of the α subunit, which is suggestive that similar decay mechanisms are

Table II.C-3: Decay kinetic parameters τ (lifetime), α (amplitude), and ϕ (relative yield) vs. emission wavelength (λ_{em}) for the $\alpha\beta$ monomer and α and β subunits of C-phycocyanin from *Anabaena variabilis* in a 0.005 M phosphate buffer, pH 7.0, 25°C, using a C31034A photomultiplier tube.

Protein	λ_{em}* (nm)	τ_1 (ns)	α_1	ϕ_1 (%)	τ_2(ns)	α_2	ϕ_2(%)
α subunit	640	1.48	0.80	93	0.44	0.20	7
	650	1.47	0.82	94	0.45	0.18	6
	680	1.51	0.76	87	0.50	0.24	13
β subunit	640	1.28	0.55	82	0.34	0.45	18
	650	1.30	0.57	82	0.38	0.43	18
	680	1.30	0.55	81	0.38	0.45	19
$\alpha\beta$ monomer	640	1.31	0.64	86	0.38	0.36	14
	650	1.30	0.66	87	0.40	0.34	13
	680	1.33	0.65	84	0.45	0.35	16

*λ_{ex} = 620 nm

operative in the αβ monomer and separated α and β subunits.

Table II.C-4 lists the decay parameters for the αβ monomer and separated α and β subunits of C-phycocyanin from Anacystis nidulans. Again, biexponential kinetics were required to fit these decay curves, including those of the separated α subunit. There are some differences between the decay kinetics of C-phycocyanin from Anabaena variabilis and those of C-phycocyanin from Anacystis nidulans, but these can be ascribed most simply to species difference and are not an indication of any major differences in the decay mechanism.

Decay kinetics obtained using either the photomultiplier or the MCP detector could be fit with biexponential kinetics with values given in Tables II.C-3 and II.C-4 (a representative decay using the MCP can be seen for R-phycocyanin in Fig. II.C-14). Therefore, we conclude that lifetimes that reflect energy transfer are faster than 10-15 ps, the time resolution of our present apparatus. This applies to decay times representing leakage fluorescence from "s" chromophores and rise times reflecting the delay in transferring excitation energy to "f" chromophores, or decay times representing average residence times for other transfer mechanisms. The transfer times may also have a relative fluorescence quantum yield much less than 1%, in which case they would not be detected even if the lifetime were greater than 30 or 40 ps. Remember, the time resolution refers to

Table II.C-4: Fluorescence decay kinetic parameters of the αβ monomer and separated α and β subunits of C-phycocyanin from *Anacystis nidulans* in a 0.005 M phosphate buffer, pH 7.0, 25°C, using a C31034A photomultiplier tube. $\lambda_{excitation}$ = 620 nm, $\lambda_{emission}$ = 680 nm.

Protein	α	τ	φ
α subunit	0.86	1.44	0.93
	0.14	0.56	0.07
β subunit	0.67	1.20	0.92
	0.33	0.22	0.08
αβ monomer	0.73	1.21	0.91
	0.27	0.34	0.09

the shortest, single lifetime that can be determined. When decay is heterogeneous, a low relative yield component (< 1%) may be impossible to analyze reliably with the current signal-to-noise ratio.

A possible explanation for the biexponential decay kinetics is that the chromophore exists in two (or more) conformations. These conformations may, in fact, have been formed in the isolation procedure. If so, they have similar wavelength dependences for their absorption and fluorescence spectra (Table II.C-3). Using the MCP detector, studies were performed from 570-630 nm for excitation and 610-760 nm for emission, with no significant wavelength dependence observed. As pointed out in Section II.A1, conformational heterogeneity in bilin chromophores has been used to explain their steady-state spectra. In addition, Holzwarth et al., have demonstrated that phycobilin chromophores can exist in different conformations and give rise to complex decay kinetics with model chromophore systems (e.g. biliverdin ester)[60] and with phycocyanin 645 from Chroomonas sp.[59]

To investigate the possible presence of conformational heterogeneity, we obtained the decay kinetics for both denatured protein and digested protein. The decay parameters for denatured and digested protein are listed in Tables II.C-5 and II.C-6, respectively. The two major changes from the native protein are a decreased lifetime and an increased number of lifetime components. The increase in the number of lifetime components is consistent with claims that the

chromophore has a larger number of conformations available when the protein-chromophore interaction is disrupted. The decrease in quantum yield and lifetime are consistent with an increase in the number of radiationless routes for decay.

Temperature was varied from room temperature to 0°C and the relative yield of the 2 lifetime components was seen to vary. Table II.C-7 shows the decay kinetics for the β subunit of C-phycocyanin from Anabaena variabilis as an example. We note that the amplitude of the long lifetime component (which is a measure of the initial excited state population) increases monotonically with decreasing temperature. However, no simple relationship between temperature and ratio of components is apparent. A model for a simple equilibrium between 2 conformers was tested by looking for a linear relationship in a log plot of yield vs 1/T. A linear relation could be observed for the αβ monomer and α and β subunits, but the sign of the slope was not the same for the three samples. In addition, the change in the amplitude is just within the instrument resolution. Therefore, no clear conclusions can be drawn about any conformational equilibrium.

Decay kinetics at 77K are listed in Table II.C-8. Clearly, when the solution is cooled beyond the glass point, the decay kinetics are altered. The nonradiative decay rates have probably decreased, because the lifetimes are longer than those at room temperature. Two lifetime components are still observed, as at room temperature, but these at 77K may

Table II.C-5: Fluorescence decay of denatured C-phycocyanin from *Anabaena variabilis* in a 0.005 M phosphate buffer, pH 7.0, 25°C, using a C31034A photomultiplier tube. Denaturation was obtained with 8 M urea. λ_{ex} = 620 nm, λ_{em} = 680 nm.

Protein	α	τ	ϕ
$\alpha\beta$ monomer	0.03	1.16	0.20
	0.26	0.33	0.48
	0.71	0.08	0.32
α subunit	0.03	1.67	0.24
	0.19	0.38	0.38
	0.78	0.10	0.39
β subunit	0.02	1.30	0.16
	0.21	0.30	0.38
	0.77	0.10	0.45

Table II.C-6: Fluorescence decay kinetics of pepsin-digested C-phycocyanin from *Anabaena variabilis* using a C31034A photomultiplier tube. λ_{ex} = 620 nm, λ_{em} = 680 nm.

Protein	α	τ	ϕ
$\alpha\beta$ monomer	0.03	1.38	0.30
	0.19	0.36	0.47
	0.77	0.05	0.24
α subunit	0.01	0.97	0.15
	0.10	0.27	0.34
	0.89	0.05	0.51

Table II.C-7: Temperature Dependence of the Fluorescence Decay Kinetics of the subunit of C-phycocyanin from *Anabaena variabilis* in a 0.005 M phosphate buffer, pH 7.0, using a C31034A photomultiplier tube. λ_{ex} = 620 nm, λ_{em} = 680 nm.

T(± 0.1°C)	α	τ	ϕ
23.8	0.560	1.229	0.853
	0.440	0.270	0.147
14.5	0.576	1.254	0.840
	0.424	0.325	0.160
10.3	0.585	1.241	0.861
	0.414	0.283	0.139
5.6	0.591	1.257	0.860
	0.409	0.296	0.140
1.0	0.600	1.276	0.856
	0.400	0.322	0.144

Table II.C-8: Fluorescence decay kinetics at 77K for *Anabaena variabilis* (λ_{ex} = 620 nm, λ_{em} = 680 nm), 0.005 M phosphate buffer, pH 7.0, using a C31034A photomultiplier tube.)

Sample	α	τ	ϕ
$\alpha\beta$ monomer	0.17	1.82	0.25
	0.83	1.13	0.75
β subunit	0.40	1.32	0.60
	0.60	0.57	0.40
α subunit	0.56	1.45	0.74
	0.44	0.65	0.26

not be of the same origin as those at room temperature because the protein motion and conformation may now be highly constrained by the solvent molecules. Experiments at low temperatures are complicated by scatter of the solution glass, which broadens the FWHM of the instrument response and decreases the signal to noise. Reflections from the dewar produce additional peaks in the decay data. Finally, the aggregation state of the protein at lower temperatures is unknown.

Possible exciton-exciton annihilation or excited state photochemistry was investigated by varying the excitation intensity from 10^6 to 10^9 photons/cm^2. No change in decay kinetics was observed using the PMT or MCP detector.

An attempt was made to quench the fluorescence and alter the lifetimes with potassium iodide. Concentrations as high as 1.0 M KI had no effect on the decay parameters, illustrating that the fluorescence is short enough ($\approx$ 0.5 ns) and the chromophore sufficiently protected that diffusion-controlled quenching by agents such as O_2 or KI is not effective. (The decay kinetics of deaerated and air-bubbled protein samples can be fit with the parameters in Tables II.C-3 and 4.) In addition, the lack of change in decay kinetics shows that high salt concentration with low protein concentration does not cause aggregation.

We also obtained the decay kinetics of R-phycocyanin from <u>Porphyridium cruentum</u> in the hopes that the more clearly separated sensitizing absorption at 577 nm would provide a

large risetime component in the fluorescence of an "f" chromophores (Fig. II.C-14). Again, no change in kinetics was observed with changes in excitation (570-630 nm) or emission wavelength (620-760 nm). We conclude therefore that the biexponential kinetics are due to conformational heterogeneity and not due to energy transfer.

II.C2b Dimer

An experiment to investigate the effect the linker polypeptide on decay kinetics was performed with the dimer of R-phycocyanin, with and without linker protein. The decay kinetics are summarized in Table II.C-9. Again, biexponential decay kinetics are observed for R-phycocyanin with and without linker, almost identical to those obtained for C-phycocyanin monomer and subunits and for R-phycocyanin monomer. No emission wavelength dependence is observed, but there is a slight excitation wavelength dependence for R-PC 617, the dimer without linker protein. The relative fluorescence quantum yield of the long lifetime component increases with longer excitation wavelength. The major repeatable difference between the dimer with and without linker protein is that the dimer with linker has slightly longer lifetimes for both components and a higher relative fluorescence quantum yield for the longest lifetime component. This would imply that the mobility and conformational heterogeneity of the phycobilin has been further restricted by addition of the linker protein. This is

Fig. II.C-14: Fluorescence decay kinetics for the $\alpha\beta$ monomer of R-phycocyanin from Porphyridium cruentum using a ITT 4129f microchannel plate detector. A_{617} = 0.05, in a 0.005 M phosphate buffer, pH 7.0, 25°C, $\lambda_{excitation}$ = 620, $\lambda_{emission}$ = 740. The narrow profile (full width, half maximum = 150 ps) is the excitation pulse shape. The experimental fluorescence decay (noisy) curve is fit with a two-exponential (smooth) curve. Bottom, weighted residuals ($\Delta I/I$) for the 2 exponential fit on a linear scale. A plot of deviations from the experimental decay for a three-exponential fit is not distinguishable from that for a two-exponential fit. χ^2 = reduced chi square.

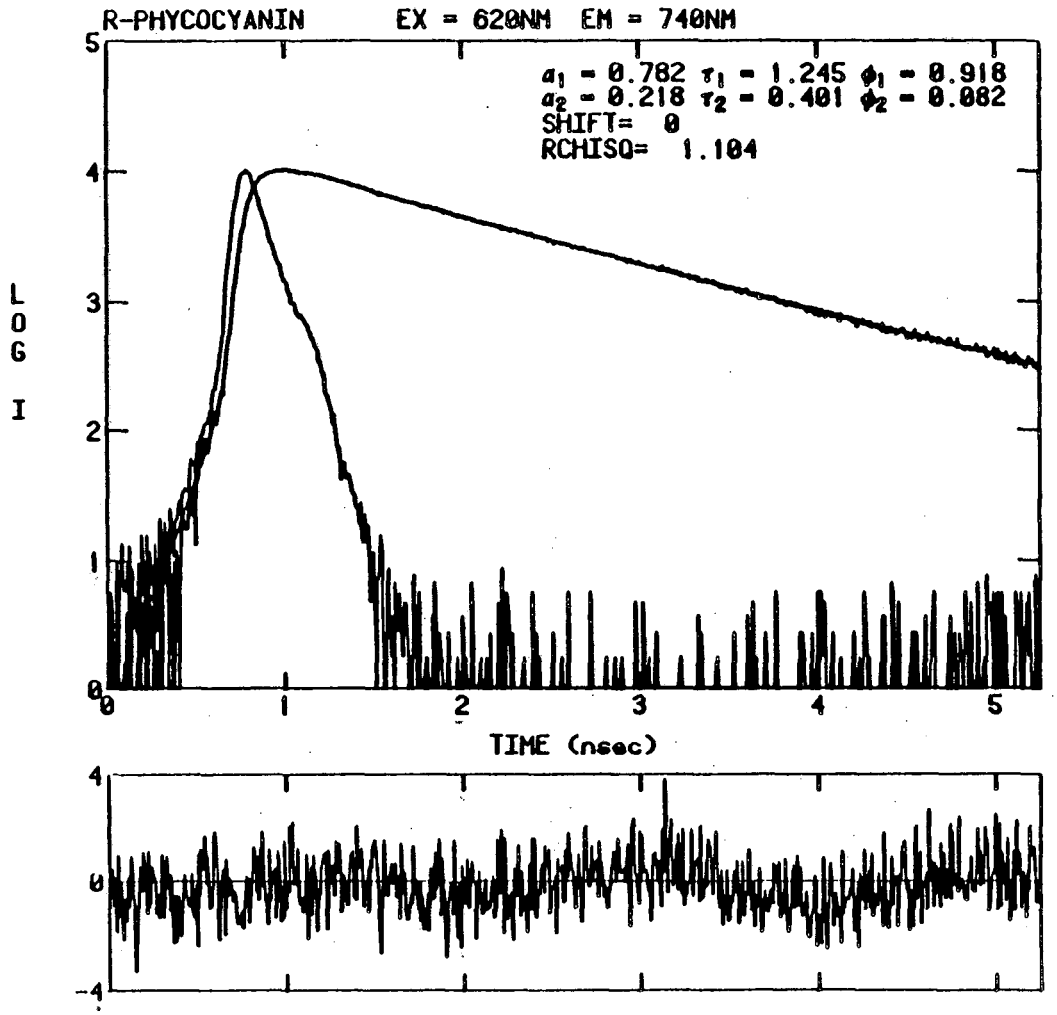
R-PHYCOCYANIN EX = 620NM EM = 740NM
a_1 = 0.782 τ_1 = 1.245 ϕ_1 = 0.918
a_2 = 0.218 τ_2 = 0.401 ϕ_2 = 0.082
SHIFT= 0
RCHISQ= 1.104
LOG I
TIME (nsec)

Table II.C-9: Wavelength dependence of fluorescence decay parameters for R-phycocyanin dimers from *Griffithsia tenuis* in a 0.005 M phosphate buffer, pH 7.0, 25°C, using a MCP.

Species	λ_{ex}*	α	τ	ϕ
R-PC 625	580	0.82 ± 0.02	1.43 ± .04	0.95 ± 0.01
		0.18 ± 0.02	.35 ± .07	0.05 ± 0.01
	620	0.83 ± 0.03	1.43 ± .03	0.95 ± 0.01
		0.17 ± 0.03	.33 ± .06	0.05 ± 0.01
R-PC 617	580	0.76 ± 0.01	1.23 ± .01	0.91 ± 0.01
		0.24 ± 0.01	.38 ± .05	0.09 ± 0.01
	620	0.78 ± 0.02	1.25 ± .01	0.93 ± 0.01
		0.22 ± 0.02	.35 ± .06	0.07 ± 0.01

* Decay parameters are independent of λ_{em} = 640-760 nm.

consistent with the steady state spectra of R-phycocyanin dimer (Fig. II.C-6) and the general trend of increasing energy transfer and decreasing alternate photochemical pathways with increasing aggregation of phycobiliproteins (Section II.A).

The decay kinetics of the native protein forms (subunits, monomer, and dimer) are quite similar, even though they have been isolated with different preparation techniques. We conclude that the heterogeneous decay kinetics (biexponential with our resolution) are characteristic of phycobilins attached to proteins and are not the result of preparation technique.

II.D Conclusion

We have obtained some steady-state results that are consistent with an s-f model for energy transfer in isolated phycobiliproteins and some that are not. We attribute the rise in polarization across the absorption band towards longer wavelength for the β subunit and the αβ monomer to energy transfer among the three chromophores in the αβ monomer and between the two chromophores in the β subunit. The constant polarization of the α subunit, with one chromophore, is consistent with a lack of any possibility of energy transfer. The wavelength dependence of the polarization is consistent with the s-f model of Dale and Teale, based on a resonance energy transfer model.[16,115] However, fluorescence emission maxima were at 640 nm for the αβ monomer and the separated subunits of Anabaena variabilis, and at 645 nm for the β subunit and 640 nm for the α subunit of Anacystis nidulans. If the s chromophores are assigned to the β subunit, then the s chromophores have the longest wavelength emission. Efficient Forster transfer is possible because of the breadth of the absorption and fluorescence bands involved. The labels s and f, however, are not easily related to the fluorescence maxima.

An examination of Fig. II.C-1 reveals that there is a lack of mirror symmetry between the absorption and fluorescence emission spectra. The lack of mirror symmetry between the absorption and fluorescence emission spectra has

been attributed to chromophore states that are active in absorption but not in emission, i.e. sensitizing chromophores (Zickendraht-Wendelstadt et al., 1980).[132] We observed a lack of mirror symmetry in the αβ monomer, the β subunit, and also the α subunit (Fig. II.C-1). With only a single chromophore, the α subunit does not have a sensitizing chromophore. The mirror image relation between the absorption and fluorescence emission spectra is expected only if there is little change in geometry of the chromophore between the ground and excited state. A change in geometry could account for the lack of mirror symmetry in the α subunit, and also the lack of mirror symmetry in the β subunit and αβ monomer. This lack of symmetry is not a conclusive sign of sensitizing chromophores.

In Section II.A, it was noted that some workers have suggested a strong coupling exists between chromophores even at the level of the monomer. Geometries are possible in which exciton interactions are present without an apparent CD exciton signature. On the other hand, shifts in CD band maxima and Cotton effects can be the result of overlapping bands due to centers of different chirality and not necessarily due to a strong exciton interaction.[51] At present, steady-state results do not provide a clear choice among the energy transfer mechanisms for isolated phycobiliproteins. The conclusive method to test for an s-f energy transfer mechanism is wavelength-resolved decay kinetics.

We observed biexponential decay kinetics for the subunits and the monomer of C-phycocyanin. The biexponential decay kinetics of the α subunit fluorescence is unexpected, because there is only one chromophore and no possibility of energy transfer. Changes in buffer components, protein concentration, and excitation and emission wavelength do not affect the decay parameters. We also found biexponential kinetics for R-phycocyanin from Porphyridium cruentum and R-phycocyanin from Griffithsia tenuis. We conclude that these lifetimes are not due to energy transfer but propose that the chromophore may exist in at least two different conformations, which have similar fluorescence excitation and emission spectra (within the resolution of our instrument). Disruption of the protein-chromophore interaction through either digestion or denaturation of the protein results in an increased number of lifetimes. The chromophores appear to have increased conformational heterogeneity, based on our assignment of the lifetimes to different conformations. Lifetimes for R-phycocyanin with the linker protein were longer and the relative fluorescence yield of the long component higher than R-phycocyanin without the linker, indicating that the linker protein alters the amounts of the heterogeneous conformations.

The steady-state spectroscopic results are consistent with the conclusions drawn from the time-resolved results. The steady-state results presented in Section II.C1 support

the proposal that the function of the apoprotein in phycobiliproteins is at least threepart. First, the protein limits the large conformational heterogeneity of phycobilin chromophores and selects the conformations providing the appropriate absorption and fluorescence wavelength maxima for a thermodynamically favored energy transfer. Second, the allowed conformations are also those with restricted nonradiative decay pathways and, therefore, increased fluorescence quantum yields. These conformations also have higher extinction coefficients. The third function is that of protection of the chromophore from destructive photochemistry, such as redox reactions, photooxidation, and reaction with other solution components.

Our results lead us to conclude that the energy transfer time is faster than 10-14 ps, the time resolution of our instrument, or that the relative fluorescence yield of the decay components attributable to energy transfer is so small (< 0.5%) that we cannot resolve them from the other fluorescence decay components.

The literature contain some claims for the s-f energy transfer time. Gillbro et al. have measured transient absorption recovery, absorption anisotropy kinetics, and fluorescence decay kinetics in phycobilisomes of Synechococcus 6301 and a mutant of Synechococcus 6301, AN112, and have observed a fast decay component of 10 ± 2 ps in all these measurements.[34,35,35a] They attribute these lifetimes to s-f transfer. Although this lifetime is reasonable

for Forster energy transfer, the assignment is not conclusive. In fact, as Glazer points out, the 10 ps component most probably represents the transfer from allophycocyanin to the terminal emitters. The bleaching is independent of excitation wavelength in these samples, which is inconsistent with an s to f transfer over this wavelength range (≈ 585-630 nm), because s chromophores would have very little absorbance at 630 nm. A change in the χ^2_ν of 0.003 to justify a fourth decay component of 12 ps (assigned to s-f energy transfer) is not statistically valid. In general, the heterogeneity and number of chromophores with overlapping absorption and fluorescence emission spectra does not allow a conclusive assignment of the short lifetime components.

This is also the case for a 25 ps fluorescence anisotropy decay component measured by Hefferle et al.[56] In this case, a 25 ps depolarization was assigned to s-f transfer in C-phycocyanin, but could also be explained by transfer from C-phycoerythrocyanin to the adjoining phycocyanin disk.

Wendler et al. measured an absorption anisotropy decay component of 12 ± 5 ps and assigned this to s-f transfer in B-phycoerythrin. The excitation wavelength was 567 nm, where f chromophores would have the largest extinction coefficient. The transfer time could also represent an f to f transfer from one disk to an adjoining disk.

Wehrmeyer et al. found a 15 ps risetime in hexameric and dodecameric B-phycoerythrin.[125] This is not consistent with results of Glazer et al.[50] They observed that the

risetimes of the fluorescence from R-phycoerythrin and from trimeric allophycocyanin were independent of excitation wavelength and were ≤ 8 ps, the time resolution of their instrument. The rate-determining step for transfer in phycobilisomes was shown to be the disk-to-disk transfer time of ≈ 25 ps. The streak camera instrumentation of Glazer et al.[50] is much more sensitive to short risetimes than the single-photon timing instrumentation used by Wehrmeyer et al.[125] when the sample has complex rise and decay kinetics. Wong et al., also using a streak camera, found the risetime to be < 12 ps (the time resolution of their instrument) for mixed aggregation state samples of C-phycocyanin, C-phycoerythrin, and allophycocyanin.[127]

To summarize, there is no reliable value for the energy transfer time among the chromophores of a disk, trimer, monomer, or subunit. We propose that the transfer time is less than 10-14 ps, in agreement with recent results of Glazer et al.[50] Reported energy transfer times of > 100 ps are probably not transfer times but indicate the conformational heterogeneity that we have observed as an inherent function of phycobilin-protein interactions. The s-f transfer model is still open to question. For transfer times much shorter than 10 ps, the s-f transfer model becomes less tenable and the excitation should be considered as delocalized over an ensemble of molecules with intermediate or strong coupling.

References

1. Badea, M. G. and L. Brand, Methods Enzymol., 61 (1979) 378.

2. Bennett, A. and L. Bogorad, Biochemistry, 10 (1971) 3625.

3. Bennett, A. and L. Bogorad, J. Cell Biol., 58 (1973) 419.

4. Bevington, P. R., "Data Reduction and Error Analysis for the Physical Sciences", McGraw-Hill, N.Y. (1969).

5. Bjorn, L. O., Quart. Rev. Biophysics., 12 (1979) 1.

6. Bogorad, L., Rec. Chem. Prog., 26 (1965) 1.

7. Bogorad, L., Ann. Rev. Plant Physiol., 26 (1975) 369.

8. Bolt, J. D. and K. Sauer, Biochim. Biophys. Acta, 637 (1981) 342.

9. Braslavsky, S. E., Holzwarth, A. R. , Schaffner, K., Angew. Chem. Int. Ed. Engl., 22 (1983) 656.

10. Bryant, D. A., Int. Symp. Prokaryotic Photosynth. Org. 3rd, 1979, D17.

11. Bryant, D. A., Hixson, C. S., and Glazer, A. N., Biol. Chem., 253 (1978) 220.

12. Canaani, O. D. and E. Gantt, Biochemistry, 19 (1980) 2950.

13. Ceckowski, D. H., E. Eberhardt, and E. Carney, IEEE Trans., Nucl. Sci., NS-28 (1981) 677.

14. Cohen-Bazire, G., S. Beguin, S. Rimon, A. N. Glazer, and D. M. Brown, Arch. Microbiol., 111 (1977) 225.

15. Colson, W. B., J. McPherson, and F. T. King, Rev. Sci. Instrum., 44 (1973) 1694.

16. Dale, R. E. and F. W. J. Teale, Photochem. Photobiol., 12 (1970) 99.

17. Demas, J. N., "Excited State Lifetime Measurements", Academic Press, N.Y. (1983).

18. Eiserling, F. A. and A. N. Glazer, J. Ultrastruct. Res., 47 (1974) 16.

19. Falk, H. and F. Neufingerl, Monatsh. Chem., 110 (1979) 987.

20. Frank, G., W. Sidler, H. Widmer, and H. Zuber, Hoppe-Seyler's Z. Physiol. Chem., 359 (1978) 1491.

21. Freidenreich, P., G. S. Apell, and A. N. Glazer, J. Biol. Chem., 253 (1978) 212.

22. Friedrich, J., H. Scheer, B. Zickendraht-Wendelstadt, and D. Haarer, J. Am. Chem. Soc., 103 (1981) 1030.

23. Friedrich, J., H. Scheer, B. Zickendraht-Wendelstadt, and D. Haarer, J. Chem. Phys., 74 (1981) 2260.

24. Gantt, E., Photochem. Photobiol., 26 (1977) 685.

25. Gantt, E., in "Biochemistry and Physiology of Protozoa", M. Levandowsky, S. H. Hutner, eds., Academic Press, N.Y. (1979) 121.

26. Gantt, E., Int. Rev. Cytol., 66 (1980) 45.

27. Gantt, E., Ann. Rev. Plant Physiol., 32 (1981) 327.

28. Gantt, E. and S. F. Conti, Brookhaven Symp. Biol., 19 (1966) 393.

29. Gantt, E., and S. F. Conti, J. Cell Biol., 29 (1966) 423.

30. Gantt, E. and C. A. Lipschultz, Biochem., 13 (1974) 2960.

31. Gantt, E. and C. A. Lipschultz, J. Phycol, 13 (1977) 185.

32. Gantt, E., C. A. Lipschultz, and B. Zilinskas, Biochim. Biophys. Acta, 430 (1976) 375.

33. Gantt, E., C. A. Lipschultz, J. Grabowski, and B. K. Zimmerman, Plant Physiol., 63 (1979) 615.

34. Gillbro, T., A. Sandstrom, V. Sundstrom, and A. R. Holzwarth, FEBS Lett., 162 (1983) 64.

35. Gillbro, T., A. Sandstrom, and V. Sundstrom, in "Ultrafast Phenomena", ed. D. H. Auston, K. B. Eisenthal, Springer, N.Y. (1984).

35a. Gillbro, T., A. Sandstrom, V. Sundstrom, J. Wendler, and A. R. Holzwarth, Biochim. Biophys. Acta, 808 (1985) 52.

36. Glazer, A. N., Photochem. Photobiol. Rev., ed. Smith, K. C., 1 (1976) 71.

37. Glazer, A. N., Mol. Cell. Biochem., 18 (1977) 125.

38. Glazer, A. N., in "The Biochemistry of Plants", eds. Stump, P. K. and Conn, E. E. (series eds.), M. D. Hatch and N. K. Boardman (eds. for Vol. 8), Vol. 8. (1981) Academic Press, N.Y., 51.

39. Glazer, A. N., Ann. Rev. Biochem., 52 (1983) 125.

40. Glazer, A. N., Biochim. Biophys. Acta, 768 (1984) 29.

41. Glazer, A. N., Ann. Rev. Biophys. Chem., 14 (1985) 47.

42. Glazer, A. N. and Apell, G. S., FEBS Lett., 1 (1977) 113.

43. Glazer, A. N., G. S. Apell, C. S. Hixson, D. A. Bryant, S. Rimon, and D. M. Brown, Proc. Natl. Acad. Sci. U.S.A., 73 (1976) 428.

44. Glazer, A. N. and D. A. Bryant, Arch. Microbiol., 104 (1975) 29.

45. Glazer, A. N., G. Cohen-Bazire, and R. Y. Stanier, Arch. Microbiol., 80 (1971) 1.

46. Glazer, A. N. and Fang, S., J. Biol. Chem., 248 (1973) 659.

47. Glazer, A. N. and Fang, S., J. Biol. Chem., 248 (1973) 663.

48. Glazer, A. N., S. Fang, and D. M. Brown, J. Biol. Chem., 248 (1973) 5679.

49. Glazer, A. N. and C. S. Hixson, J. Biol. Chem., 252 (1977) 32.

49a. Glazer, A. N. and C. S. Hixson, J. Biol. Chem., 250 (1975) 5487.

50. Glazer, A. N., S. W. Yeh, S. P. Webb, and J. H. Clark, Science, 227 (1985) 419.

51. Godfrey, Robin E., Biophys. J., 38 (1982) 1.

52. Grabowski, J. and E. Gantt, Photochem. Photobiol., 28 (1978) 39.

53. Grabowski, J. and E. Gantt, Photochem. Photobiol., 28 (1978) 47.

54. Grinvald, A. and I. Z. Steinberg, Anal. Biochem., 59 (1974) 583.

55. Haehnel, W., J. A. Nairn, P. Reisberg, and K. Sauer, Biochim. Biophys. Acta, 680 (1982) 161.

56. Hefferle, P., M. Nies, W. Wehrmeyer, and S. Schneider, Photobiochem. Photobiophys., 5 (1983) 41.

57. Holzwarth, A. R., H. Lehner, S. E. Braslavsky, and K. Schaffner, Liebigs Ann. Chem., (1978) 2002.

58. Holzwarth, A.; K. Rousslang; J. B. A. Ross; Personal Communication.

59. Holzwarth, A. R., J. Wendler, K. Schaffner, V. Sundstrom, A. Sandstrom, and T. Gillbro, Israel J. Chem., 23 (1983) 223.

60. Holzwarth, A. R., J. Wendler, and W. Wehrmeyer, Biochim. Biophys. Acta, 724 (1983) 388.

61. Jung, J., P.-S. Song, R. J. Paxton, M. S. Edelstein, R. Swanson, and E. E. Hazen, Jr., Biochemistry, 19 (1980) 24.

62. Katoh, T. and E. Gantt, Biochim. Biophys. Acta, 546 (1979) 383.

63. Klein, G. and W. Rudiger, Liebigs Ann. Chem., (1978) 267.

64. Knight, A. E. W. and B. K. Selinger, Spectrochim. Acta, 27A (1971) 1223.

65. Kobayashi, T., E. O. Degenkolb, R. Behrson, P. M. Rentzepis, R. MacColl, and D. S. Berns, Biochemistry, 18 (1979) 5073.

66. Koller, K. P., W. Wehrmeyer, and E. Moerschel, Eur. J. Biochem., 91 (1978) 57.

67. Kufer, W. and H. Scheer, Hoppe-Seyler's Z. Physiol. Chem., 360 (1979) 473.

68. Kylin, H., Hoppe-Seyler's Z. Physiol. Chem., 69 (1910) 169.

69. Lagarias, J. C., A. N. Glazer, and H. Rapoport, J. Am. Chem. Soc., 101 (1979) 5030.

70. Langer, E., H. Lehner, W. Rudiger, and B. Zickendraht-Wendelstadt, Z. Naturforsch., 35c (1980) 367.

71. Lemasson, C., N. Tandeau de Marsac, and G. Cohen-Bazire, Proc. Natl. Acad. Sci. U.S.A., 70 (1973) 3130.

72. Leskovar, B., Physics Today, (1977) 42.

73. Leskovar, B. and C. C. Lo, Proceedings of the European Conference on Precise Electrical Measurements, Published by the Institution of Electrical Engineers, London (1977) 41.

74. Ley, A. C. and W. L. Butler, Biochim. Biophys. Acta, 462 (1977) 290.

75. Ley, A. C., W. L. Butler, D. A. Bryant, and A. N. Glazer, Plant Physiol., 59 (1977) 974.

76. Lichtle, C. and J. C. Thomas, Phycologia, 15 (1976) 393.

77. Lo, C. C. and B. Leskovar, IEEE Trans, Nucl. Sci., NS-28 (1981) 698.

78. Lotter, H., G. Klein, W. Rudiger, and H. Scheer, Tetrahedron Lett., (1977) 2317.

79. Lundell, D. J., A. N. Glazer, R. J. DeLange, and D. M. Brown, J. Biol. Chem., 259 (1984) 5472.

80. Lundell, D. J., R. C. Williams, and A. N. Glazer, Plant Physiol., 59 (1977) 974.

81. MacColl, R., Photochem. Photobiol., 35 (1982) 899.

82. MacColl, R. and D. S. Berns, Isr. J. Chem., 21 (1981) 296.

83. MacColl, R., K. Csatorday, D. S. Berns, and E. Traeger, Biochemistry, 19 (1980) 2817.

84. Morschel, E. and W. Wehrmeyer, Arch. Microbiol., 105 (1975) 153.

85. Morschel, E. and W. Wehrmeyer, Arch. Microbiol., 113 (1977) 83.

86. Morschel, E., K. P. Koller, and W. Wehrmeyer, Arch. Microbiol., 125 (1980) 43.

87. Murao, T., I. Yamazaki, and K. Yoshihara, Applied Optics, 21:13 (1982) 2297.

88. Myers, J. and W. A. Kratz., J. Gen. Physiol., 39 (1955) 11.

89. Nichols, K. E. and L. Bogorad, Bot. Gaz., 124 (1962) 85.

90. O'Carra, P. and O'hEocha, C., in "Chemistry and Biochemistry of Plant Pigments", ed. T. W. Goodwin, Academic Press, N.Y. (1976) 328.

91. Ohad, I., R. K. Clayton, L. Bogorad: Proc. Natl. Acad. Sci. U.S.A., 76 (1979) 5655.

92. Ohad, I., H.-J. A. W. Schneider, S. Gendel, and L. Bogorad, Plant Physiol., 65 (1980) 6.

93. O'hEocha, C., in "Comparative Biochemistry of Photoreaction Systems", ed. Allen, M. B., Academic Press, N.Y. (1960) 181.

94. O'hEocha, C., in "Physiology and Biochemistry of Algae", ed. Lewin, R. A., Academic Press, N.Y. (1962) 421.

95. O'hEocha, C. in "Chemistry and Biochemistry of Plant Pigments", ed. T. W. Goodwin, Academic Press, N.Y. (1965) 175.

96. O'hEocha, C., Ann. Rev. Plant Physiol., 16 (1965) 415.

97. O'hEocha, C., P. O'Carra, and D. Mitchell, Proc. R. Ir. Acad., Sect. B, (1964) 191.

98. Parker, C. A., "Photoluminescence of Solutions", Elsevier, Amsterdam (1968).

99. Pietry, G., IEEE Trans., Nucl. Sci., NS-24 (1977) 228.

100. Porter, G., L. J. Tredwell, G. F. W. Searle, and J. Barber, Biochim. Biophys. Acta, 501 (1978) 232.

101. Rippka, R., J. Deruelles, J. B. Waterbury, M. Herdman, and R. Y. Stanier, J. Gen. Microbiol., 3 (1979) 1.

102. Schoenleber, R. W., S.-L. Leung, D. J. Lundell, A. N. Glazer, and H. Rapoport, J. Am. Chem. Soc., 105 (1983) 4072.

103. Schoenleber, R. W., D. J. Lundell, A. N. Glazer, and H. Rapoport, J. Biol. Chem., 259 (1984) 5481.

104. Schoenleber, R. W., D. J. Lundell, A. N. Glazer, and H. Rapoport, J. Biol. Chem., 259 (1984) 5485.

105. Scheer, H., Angew. Chem. Int. Ed., 20 (1981) 241.

106. Scheer, H., in "Molecular Biology, Biochemistry and Biophysics", (Light React. Path Photosynth.), ed. F. K. Fong, Springer, Berlin, Vol. 35, Chap. 2 (1982) 7.

107. Scheer, H. and W. Kufer, Z. Naturforsch., 32c (1977) 513.

108. Searle, G. F. W., J. Barber, G. Porter, and C. J. Tredwell, Biochim. Biophys. Acta, 501 (1978) 246.

109. Stadnichuk, I. N. and L. A. Mineeva, Biofizika, 25 (1980) 727.

110. Stadnichuk, I. N., L. A. Mineeva, and M. V. Gusev, Biokhimiya, 45 (1980) 1560.

111. Staehelin, L. A., T. H. Giddings, P. Badami, and W. W. Krzymowski, in "Light Transducing Membranes: Structure, Function and Evolution", ed. D. W. Deamer, Academic Press, N.Y. (1978) 335.

112. Sweet, R. M., H. E. Fuchs, R. G. Fisher, and A. N. Glazer, J. Biol. Chem., 252 (1977) 8258.

113. Tandeau de Marsac, N., J. Bacteriol., 130 (1977) 82.

114. Tandeau de Marsac, N. and G. Cohen-Bazire, Proc. Natl. Acad. Sci. U.S.A., 74 (1977) 635.

115. Teale, F. W. J. and R. E. Dale, Biochem. J., 116 (1970) 161.

116. Troxler, R. F., A. S. Brown, and S. B. Brown, J. Biol. Chem., 254 (1979) 3411.

117. Turko, B. T., J. A. Nairn, and K. Sauer, Rev. Sci. Instrum., 54 (1983) 118.

118. Vernotte, C., Photochem. Photobiol., 14 (1971) 163.

119. Wang, R. J., C. L. R. Stevens, and J. Myers, Photochem. Photobiol., 25 (1977) 103.

120. Wanner, G. and H.-P. Kost, Protoplasma, 102 (1980) 97.

121. Ware, W., in "Creation and Detection of the Excited State", ed. A. A. Lamola, Dekker, N.Y., Vol. 1, Part A, (1971) 213.

122. Watson, B. A., S. D. Waaland, and J. B. Waaland, Biochemistry, Manuscript submitted January, 1986.

123. Wehrmeyer, W., Arch. Microbiol., 71 (1970) 367.

124. Wehrmeyer, W., in "Proteins and Nucleic Acids in Plant Systematics", eds. V. Jensen and D. E. Fairbrothers, Springer, Berlin, (1983) 143.

125. Wehrmeyer, W., J. Wendler, and A. R. Holzwarth, Eur. J. Cell Biol., 36 (1984) 17.

126. Wendler, J., A. R. Holzwarth, and W. Wehrmeyer, Biochim. Biophys. Acta, 58 (1984) 765.

127. Wong, D., F. Pellegrino, R. R. Alfano, and B. A. Zilinskis, Photochem. Photobiol., 33 (1981) 651.

128. Yamanaka, G., A. N. Glazer, and R. C. Williams, J. Biol. Chem., 253 (1978) 8303.

129. Yamanaka, G. and A. N. Glazer, Arch. Microbiol., 124 (1980) 39.

130. Yamazaki, I., N. Tamai, H. Kume, H. Tsuchiya, and K. Oba, Rev. Sci. Instrum., 56:6 (1985) 1187.

131. Yu, M.-H., A. N. Glazer, and R. C. Williams, J. Biol. Chem., 256 (1981) 13130.

132. Zickendraht-Wendelstadt, B., J. Friedrich, and W. Rudiger, Photochem. Photobiol., 31 (1980) 367.

133. Zilinskis, B. A., J. Grabowski, and S. Campbell, in "Advances in Photosynthesis Research", ed. C Sybesma, 2 (1984) 687.

134. Zuber, H., Ber. Deutsch Bot. Ges., 91 (1978) 459.

CHAPTER 3

TRIPHENYLMETHANE DYES

III.A Introduction

In our attempts to use triphenylmethane dyes to calibrate the picosecond fluorescence instrumentation described in Section II.B3a, we presumed, based on literature results, that a log lifetime vs. log viscosity plot would have a linear dependence. This time dependence would allow us to estimate the time resolution of the instrument. However, we found marked curvature in this plot that could not be explained by instrumental artifacts. Further studies were performed in order to map the viscosity dependence over a larger range than that used by other workers. This was attempted for 3 reasons. First, the larger viscosity range would allow us to estimate the curvature in the log-log plot and determine the instrument time resolution. Secondly, the larger viscosity range allows us to explain many of the discrepancies in previous studies. Third, the photophysics of the triphenylmethane dyes is thought to be related to its molecular rigidity, and a clearer understanding of these systems may help in the understanding of the conformationally dependent photophysics of phycobiliproteins.

This dye system was originally chosen because of the viscosity dependence reported in the literature, but it was also chosen because these dyes are stable in solution for

several months, they are stable to intense illumination, and they absorb strongly within our dye laser excitation band region (570-630 nm).

III.A1 Structure

Crystal violet (Fig. III.A-1) illustrates the basic structure of the TPM dyes. The structure consists of 3 aniline moieties, ($C_6H_5NH_2$), bonded to a central carbon atom to form a stable tertiary carbonium ion. The stability results from the delocalization of the positive charge over the conjugated π electron density of the phenyl rings and the nitrogens of the amino groups. Variation is provided by substitution on the ring or the amino group, resulting in absorption and fluorescence band shifts (dimethyl substitution on each amino group in the case of crystal violet). To be precise, these dyes should be denoted tri(aminophenyl)methane dyes. However, in keeping with the literature, the term triphenylmethane (TPM) will be used.

The ground state conformation of TPM dyes, according to X-ray crystallography, is propeller shaped with the phenyl rings rotated 32° from the central plane. The 3 central carbon-phenyl carbon bonds are coplanar and the molecule has D_3 symmetry.[11] The angle between adjacent phenyl rings is 54°, which is consistent with the value of 47-54° estimated on the basis of steric repulsion.[7]

Fig. III.A.-1: Structures of crystal violet (a) and malachite green (b) carbonium ions.

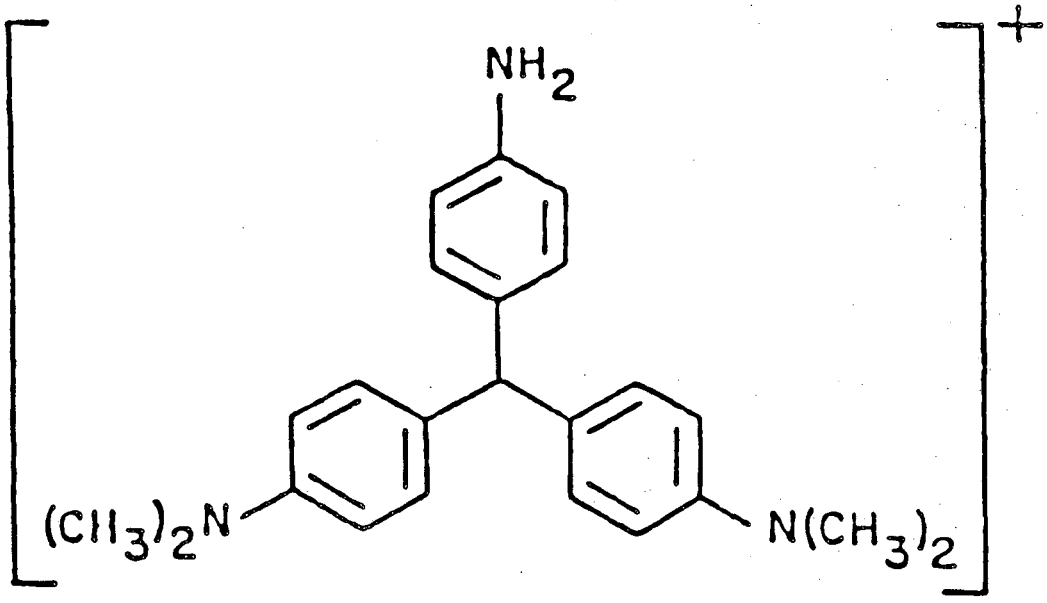

(b)

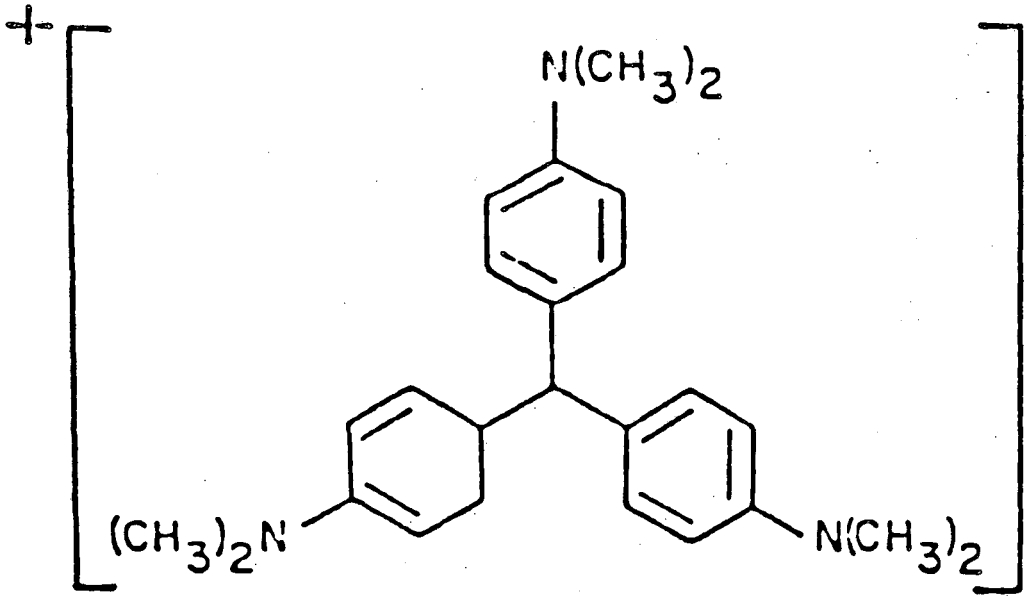

(a)

III.A2 Photophysics

The photophysics of triphenylmethane (TPM) dyes has been investigated for over 40 years. Lewis et al. studied the effects of solvent and temperature on TPM dyes.[15] They concluded that crystal violet has two ground state isomers, one with a synchronously-rotated phenyl ring propeller shape, and one with one ring rotated 90° with respect to the other two rings. They attributed the short wavelength shoulder to the isomer with one ring rotated in the opposite direction from the other two rings. The assignment of the absorption shoulder and peak to separate isomers in equilibrium was based on subtracting the spectrum of malachite green from that of crystal violet to eliminate the shoulder. This was considered appropriate because it was claimed that malachite green does not have a pronounced shoulder. Our data indicate that malachite green does have an observable shoulder in the absorption spectrum in solvents used by Lewis et al. (see Section III.C).[15] A plot of normalized absorption spectra as a function of temperature was claimed to show the reduction of only the shoulder extinction coefficient and conversion of this isomer into the isomer assigned to the peak maximum. However, the apparent reduction of the shoulder could be interpreted as narrowing of the entire absorption band, which has vibrational band substructure, and not as evidence of a separate isomer. Lewis et al. also reported that fluorescence and phosphorescence were not observed until the temperature was lowered below room temperature. No

investigation of the low quantum yield in nonviscous solutions vs. viscous solution (e.g. 10^{-4} in ethanol vs. 10^{-2} in glycerol at 25°C, Magde and Windsor[16]) was made until 1956. At that time, Oster and Nishijima proposed that phenyl ring rotational motion was responsible for the decreased fluorescence through a random thermal diffusion mechanism.[18] However, a random process is not consistent with the model of Forster and Hoffmann.

Forster and Hoffmann (FH) proposed a phenomenological model based on their studies of TPM dye fluorescence quantum yields in a variety of solvents and at various temperatures.[10] They concluded that the quantum yield for TPM dyes depends on the viscosity raised to the 2/3 power, $Q = C\,\eta^{2/3}$, for viscosities from approximately 0.6 - 10,000 cp, and approaches a limiting value at higher viscosities. The proposed model states that absorption produces a Franck-Condon excited state with the phenyl rings in the ground state conformation (Fig. III.A-2). Next, the rings synchronously rotate toward a new equilibrium on the excited state S_1 potential surface, and nonradiative depopulation of the excited state occurs with a rate proportional to the square of the displacement angle, $(\theta - \theta_0)^2$. This squared dependence on displacement angle accounts for the 2/3 power dependence on viscosity. The steric repulsion occurs between the ortho hydrogens of adjacent phenyl rings, and the restoring force is the partial double bond character of the central carbon - phenyl carbon bond.[15] The minimum of the

Fig. III.A-2: Potential energy surface corresponding to the Forster-Hoffmann model for the viscosity dependence of fluorescence quantum yield in triphenylmethane dyes. From Ref. 5.

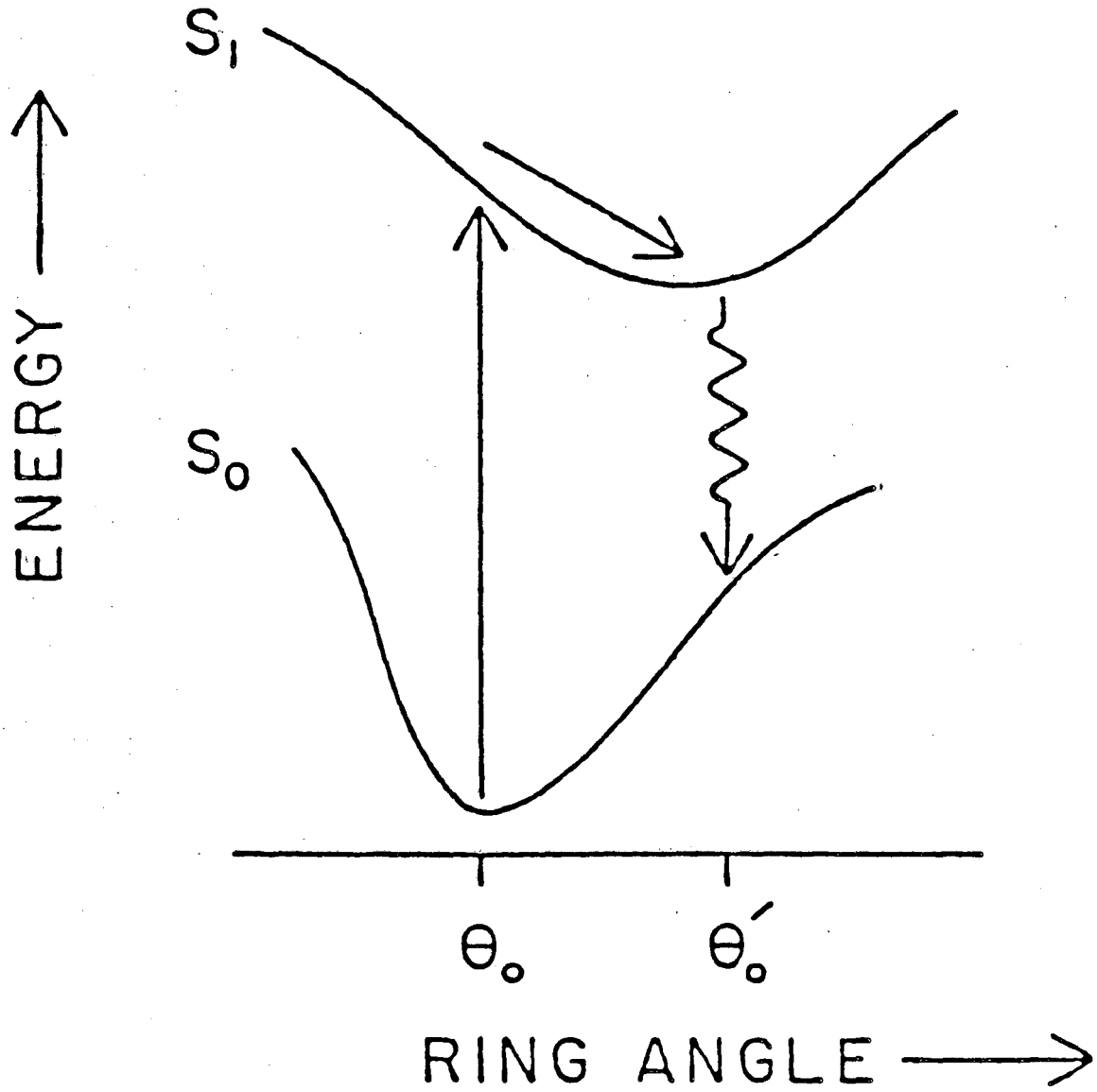
S1
S0
ENERGY
θ0
θ0´
RING ANGLE

excited state potential surface is shifted to a larger displacement angle because the excited state loses the double bond character of the central carbon - phenyl carbon bond and, hence, the associated restoring force.

The assumptions here are that the molecules are sterically driven by ring repulsion towards the minimum of the excited state potential curve, which allows for enhanced nonradiative decay by internal conversion, and that the rate of this excited state rearrangement is dependent only on the viscosity of the solvent. The claim is that there is also a nonradiative decay which is angle and viscosity independent, accounting for the limit of Q at high viscosities. In addition, fluorescence emission rates are claimed to be independent of ring rotation. According to the FH model, the excited state population, N(t), decay as

$$N(t) = e^{-(at)^3}$$

Experimentally, this has not been observed.

Magde and Windsor (1974) determined that the ground state recovery (GSR) lifetime of crystal violet showed a 1/3 power viscosity dependence over the viscosity range of 1-12,000 cp.[16] They concluded that either this was the time required for equilibration in S_0 in order to be consistent with the FH model or that some of the assumptions in the FH model were incorrect. The lifetime could be fit to $e^{-(at)^3}$ but simple exponential fits could not be excluded.

In 1976, Ippen et al. repeated the experiments of Magde and Windsor and found that the ground state recovery could be

resolved into one exponential to the first power of time for the viscosity range 0.6-100 cp, and into 2 simple exponentials for the range 100-1000 cp, contrary to predictions by FH and to the results of Magde and Windsor.[14] The best fit to each lifetime appears to be $\eta^{1/2}$, but an $\eta^{2/3}$ dependence cannot be excluded. The overall 1/e point of the ground state recovery was stated to depend on $\eta^{1/3}$. Their explanation for the extra component is that there is a "hot distribution" in the S_0 level which subsequently relaxes to the ground state. This explanation is not probable because vibrational relaxation within an electronic manifold ($S_0^* \rightarrow S_0$) should be faster than internal conversion between S_1 and S_0 and cannot explain the longer decay component. This vibrational relaxation is also not normally viscosity dependent.

Yu et al.[25] in 1977 found only a single exponential fluorescence decay for malachite green, the kinetics of which varied as $\eta^{2/3}$ for the range 100-6000 cp, which they compared to the slow GSR lifetime of Ippen et al. However, according to their interpretation this slow component is the result of S_1 to S_0^* internal conversion. The fast component of Ippen et al. was not observed. In the studies of both Magde and Windsor and of Yu et al., the decay times are about 4 times larger than those calculated by FH from τ_0, the radiative lifetime, and Q, the fluorescence quantum yield, using $\tau = \tau_0 Q$.

Mastrangelo and Offen[17] repeated the work of Oster and Nishijima and FH and found, by contrast, Q $\eta^{2/3}$ for auramine O and Q $\eta^{0.77}$ for crystal violet for the viscosity range 900-13,500 cp. Brey et al. found that Q $\eta^{2/3}$ for both auramine O and crystal violet.[4] However, the quantum yield became less viscosity dependent in the higher viscosity region and became more viscosity dependent in the low viscosity limit.

Hirsch and Mahr[13] (1979) found 2 exponential decays for malachite green with lifetimes and preexponential factors which separately varied as $\eta^{1/3}$. The relative fluorescence quantum yield varied as $\eta^{2/3}$. The ratio of the preexponential factors, A_1/A_2, was independent of viscosity. Time resolved spectra were taken at t=0 and t=370 ps and no change in emission spectra was observed.

Cremers and Windsor (1980) found that the GSR lifetime decreases as the size of the para substituent on the phenyl rings increases, supporting the argument that steric hindrance at this position is what drives the ring rotation in the excited state.[6] The ground state recovery was observed between 500 and 630 nm, while excited state absorption (ESA) was observed between 380-500 nm and stimulated emission between 630-860 nm for viscosities > 70 cp. The ESA extinction coefficient increased with time. Approximately 10% of the initial excited state population was converted to triplet formation in solutions with viscosity > 18,000 cp. GSR kinetics were independent of probe wavelength from

564-610 nm. Consistent with this, the time resolved difference spectrum showed no wavelength shifts from 20-80 ps. Cyclohexanol and glycerol/water solutions, at different temperatures but at the same viscosity, had similar GSR kinetics; the conclusion was drawn that solvent properties other than viscosity were not important in determining the ground state recovery. The data could be adequately fit by 2 exponentials, but it was concluded that a multiexponential decay fit was more appropriate. Cremers' thesis also contains a quantum mechanical calculation of the ground and excited state potential surfaces.[5] The analysis showed that the ground state potential surface is shallow with respect to asynchronous variation in the phenyl ring angle and that, in comparison, the excited state potential surface is much steeper and narrower. Assuming synchronous ring rotation, calculations indicated that the ground state and excited state potential surfaces had the same shape. Identical shape surfaces would not allow for the enhancement of internal conversion upon ring rotation in the excited state. The asynchronous model was adopted to explain the enhancement of internal conversion. In addition, a large number of ground state conformers were proposed, which are maintained in the initial excited state upon absorption. High viscosity solvents prevent rapid conformational changes, and many individual decay components can be observed. In low viscosity solvents, rapid conformational change is probable, the multicomponent decay collapses into 2 or a single

exponential, and only the fast decaying components remain significant. The ESA kinetics were identical to the GSA kinetics within experimental error. The conclusion was drawn that electronic relaxation proceeds directly from the excited state to the ground state without intermediate states.

Solutions with the same viscosity but at different temperatures were obtained with glycerol at 25°C, a glycerol/water solution at 0°C, and a 40% glucose/60% glycerol solution at 80°C. GSR kinetics were found to be identical at all 3 temperatures.

Beddard et al. (1980) found biexponential fluorescence decay kinetics from fluorescence upconversion in malachite green and crystal violet over the viscosity range of 80-5000 cp.[2] The ratio of the preexponential factors was not 1/1, contrary to the results of Hirsch and Mahr.[13] Crystal violet showed an $\eta^{2/3}$ dependence and malachite green an $\eta^{1/3}$ dependence. These data were explained using the model of Cremers.

Sundstrom et al. (1982) found single and biexponential ground state recovery kinetics that were wavelength and viscosity dependent with a transition between single and biexponential kinetics at an isosbestic point.[23] A critical viscosity (temperature) regime for this kinetic transition was also found for crystal violet and ethyl violet in n-alcohols. However, malachite green and brilliant green had single exponential fits (with some slight deviations due to a low intensity, long-lived component) and no significant

wavelength dependence. The data were fit to linear dependences with various slopes for the plots of log lifetime vs. log viscosity. Double exponential decays were observed above 30 cp for ethyl violet, malachite green and crystal violet in glycerol/water solutions. The lifetimes for malachite green were wavelength independent, but those for crystal violet and ethyl violet showed strong wavelength dependences. To explain the wavelength dependence, a model was proposed in which there are two ground state conformers for crystal violet and ethyl violet and one conformer for malachite green and brilliant green. A twisted state, whose formation and decay rates explained the complex kinetics observed, was also proposed.

T. Doust (1983) found biexponential kinetics for crystal violet in a series of mono and diols.[8] The long lifetime showed a log τ vs. log η dependence of approximately 0.8, and the short lifetime a log η dependence of 0.6, from 5-15 cp for the monohydric alcohols. Only two dihydric alcohols were studied so that the slope value could not be determined quantitatively. However, the two points were not on the same line as the mono alcohols and they show a distinctly lower slope. The slow lifetime matched the fast component of GSR measurements of Sundstrom et al., who also used glycerol/water mixtures. The preexponential factors were in a ratio of 1/1 except for ethane 1,2 diol, which had a ratio of 4/1 slow/fast lifetime. The delay in the fluorescence emission seen in monohydric alcohols was

explained by the possibility of some wavelength dependence of emission kinetics faster than 1 ps. However, at the limiting time resolution of the experiment, no dependence of kinetics on excitation or emission wavelength was observed.

Saiken and Sei, using absorption polarization in the frequency domain, found an $\eta^{2/3}$ dependence for log relaxation time vs. log η from 1-50 cp.[19] The magnitude of the relaxation time increased with increasing size of the TPM dye substituents. The values above 50 cp began to approach a plateau but the error in time resolution increased in this time regime. In contrast to TPM dyes, methylene blue showed a η^{1} dependence.

Bagchi, Fleming, and Oxtoby (BFO) proposed a model for electronic relaxation in the absence of an activation barrier.[1] Pinhole, position-dependent Gaussian, and position-dependent Lorentzian shaped sinks on the excited state potential surface were used to model the relaxation. The model predicts an asymptote or limit (viscosity-independent activation energy) at low viscosities for the GSR kinetics when a Gaussian or Lorentzian sink was used. The plot of the log of the quantum yield vs. the log of the viscosity was nonlinear and, in general, had a fractional slope less than 1. The decay was predicted to be single exponential at low viscosities and nonexponential at higher viscosities. An excitation wavelength dependence was predicted because of the change in the initial position of the sink with excitation wavelength.

In 1984, Sundstrom and Gillbro studied TPM dyes in a series of n-alcohols.[22] The GSR kinetics were obtained as a function of viscosity, temperature, and excitation (pump) and analyzing (probe) wavelength. They concluded that the relaxation rate of TPM dyes is not only viscosity dependent but solvent and temperature dependent. A plot of the log of the relaxation rate vs. 1/T indicated a potential barrier for rotation in the higher alcohols and almost no potential barrier in the lower molecular weight alcohols. The relaxation was described as rotational diffusion in the lower alcohols.

The dependence of GSR lifetime on wavelength was concluded to be due to the analyzing wavelength and used to support the previous model of 2 ground state isomers.[23] The barrier height was proposed to be due to the lowering of the S_1 excited state potential surface with respect to the S_2 excited state surface, which has a minimum at a twisted conformation. This was suggested to be the result of some specific solvent-solute interaction that is present in the lower molecular weight alcohols. Both the dielectric constant and solvent/solute molecular volume ratio were considered to be important for interaction.

The BFO model was discussed, and the inability of the model to explain the solvent and temperature dependence was pointed out. The BFO model predicts an excitation wavelength dependence but not the analyzing wavelength dependence observed by Sundstrom and Gillbro. The lack of excitation or

analyzing wavelength dependence of malachite green and brilliant green is also not explained by the BFO model. The low viscosity limit predicted by Bagchi et al. was not observed.

Engh, Petrich, and Fleming removed the coherent coupling artifact in GSR experiments and were able to show that the recovery lifetimes for malachite green in methanol/water mixtures were independent of viscosity from 0.6-1.8 cp and independent of the mole fraction of either water or methanol, in contrast to all previous measurements in this viscosity regime.[9] The lifetime in water was 1.29 ± 0.33 ps. Only the low viscosity limit of the BFO model was addressed, and excitation wavelength dependent studies were proposed to study the other predictions of the BFO model.

Some points of agreement among most workers are that the TPM dyes have enhanced internal conversion as a function of viscosity and that this enhanced internal conversion accounts for the low fluorescence quantum yield in nonviscous solvents. All workers have found that the fluorescence decay kinetics are independent of excitation or emission wavelength. Differences in the structure of the TPM dyes have been used to explain the reported kinetics.

The points of contention are numerous. The values for the slope of the plots of the log of the fluorescence quantum yield, the ground state recovery lifetimes, and the fluorescence decay lifetimes vs. the log of the viscosity differ from 1/3 to 2/3. Even this dependence is now open to

question because of the recent results of Engh et al.[9] Low viscosity asymptotes have been reported, but many GSR and fluorescence decay results do not show these asymptotes. The time dependence has been predicted to be an exponential of the time to the third power, to the first power, or nonexponential. (Nonexponential models are usually treated as multiexponential). Monoexponential, biexponential, and one or two exponential kinetics (dependent on the viscosity range) have been reported. The wavelength, solvent, and temperature dependence of GSR lifetimes have not been agreed upon.

The work in this thesis is consistent with most of the accepted facts about TPM dyes. The disagreements about the number of exponentials and the dependence of the lifetimes on viscosity are resolved in Section III.C. The basic difference between the wavelength dependence of GSR kinetics and the wavelength independence of fluorescence decay kinetics has not been resolved. Solvent effects are open to question.

We have concluded that there is no regime in which the log of the fluorescence decay lifetimes of TPM dyes has a linear dependence on the log of the viscosity. Rather, a continuous curve fits the results, with different low and high viscosity lifetime asymptotes for malachite green and crystal violet and with different viscosities at which the inflection points of similarly shaped curves appear. In addition, we obtained two lifetimes for crystal violet and

three for malachite green, all with different asymptotes and inflection points. Additional lifetimes may not be resolvable due to instrument limitations. The preexponential factors are not in a constant ratio, but vary as a function of viscosity and number of lifetimes resolved. These results are discussed in terms of previous viscosity regimes.

III.B Materials and methods

All solutions were 5 x 10^{-7} M in triphenylmethane dye unless otherwise indicated. Cremers has shown that, in glycerol and glycerol/water solutions, TPM dyes do not form aggregates with dye concentrations < 10^{-3} M.[5] This is also true for other solutions of high dielectric constant, such as ethanol, acetone, etc. In our experiments, concentrations from 1 x 10^{-5} to 1 x 10^{-7} gave identical results. Malachite green and crystal violet (Fig. III.A-1) were used as obtained from Aldrich (99%). Glycerol (MCB, spectroquality reagent grade) was used without further purification. Other batches of glycerol (reagent grade) gave identical results. Viscosities lower than 1500 cp were obtained with glycerol/water (wt/wt%) solutions at 25.0, 22.5, and 20.0°C and viscosities above 1500 cp were obtained by cooling 100% glycerol solutions (T = ± 0.1°C). Viscosity values were obtained from references 21 and 20.

Absorption spectra were obtained using a Cary model 118 uv-visible absorption spectrophotometer. Steady-state fluorescence excitation and emission spectra were obtained using a previously described spectrophotofluorimeter.[3] Fluorescence decay kinetics were obtained from a previously described synchronously pumped mode-locked picosecond pulse dye laser system using single-photon timing.[12,24] (See Section II.B3a.) The average full width at half maximum (FWHM) of the instrument response (Section II.B) obtained for these

measurements was 140 ps (Fig. III.B-1). The time resolution of this system is estimated to be 10-14 ps.

Fig. III.B-1: Fluorescence decay kinetics of malachite green in glycerol, 5×10^{-7} M, T = 6.0°C, λ_{ex} = 580 nm, λ_{em} = 640 nm. Top, the narrow profile (full width at half maximum = 140 ps) is the instrument response function. The experimental fluorescence decay (noisy) curve is fit with a 3 exponential (smooth) curve. Bottom, the weighted ($\Delta I/I$) residuals in counts of the calculated fit of a 3 exponential decay from the experimental decay, on a linear scale. χ^2_ν = reduced chi square = 1.059.

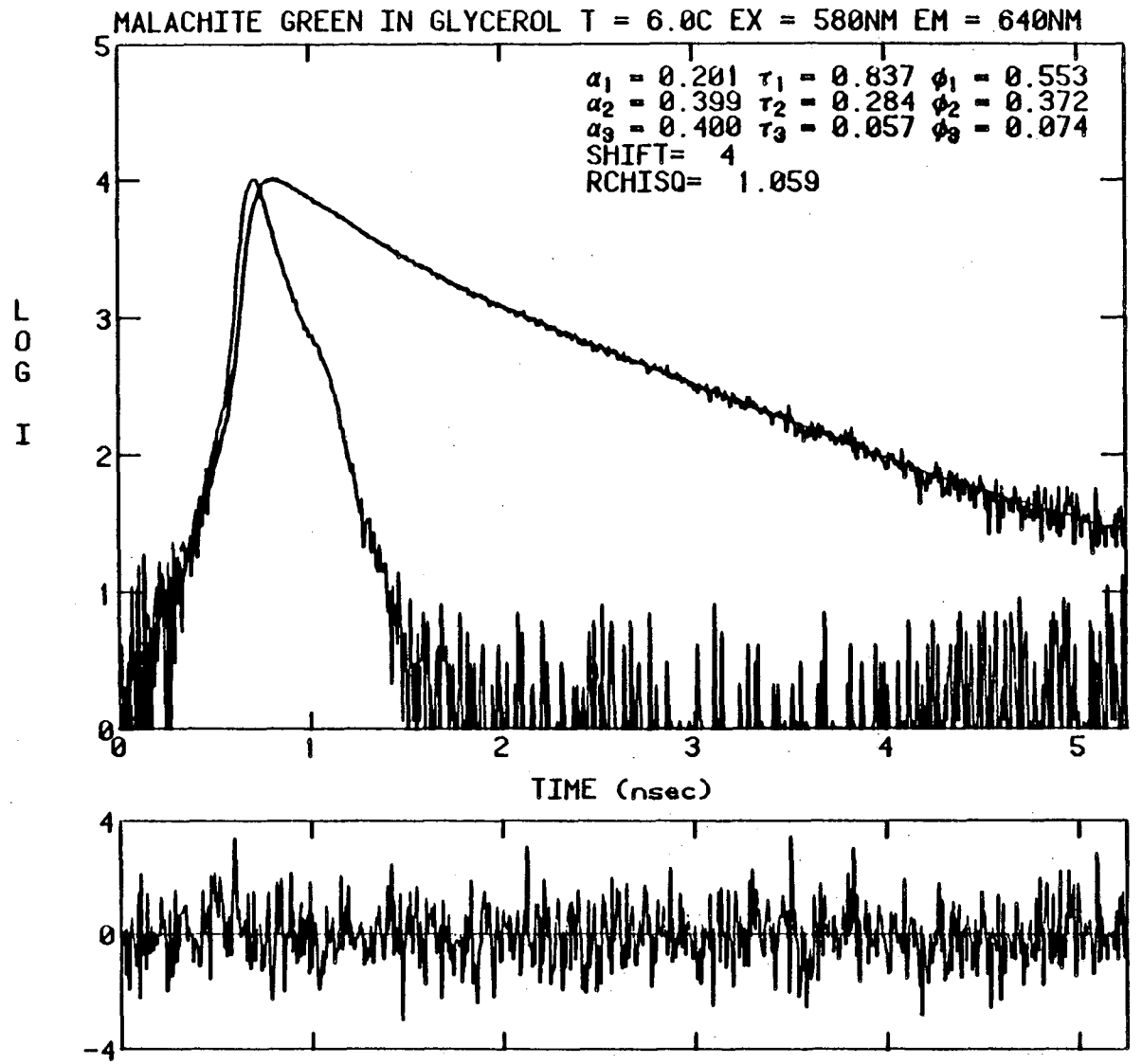
MALACHITE GREEN IN GLYCEROL T = 6.0C EX = 580NM EM = 640NM
α_1 = 0.201 τ_1 = 0.837 ϕ_1 = 0.553
α_2 = 0.399 τ_2 = 0.284 ϕ_2 = 0.372
α_3 = 0.400 τ_3 = 0.057 ϕ_3 = 0.074
SHIFT= 4
RCHISQ= 1.059
LOG I
TIME (nsec)
0
1
2
3
4
5
-4

III.C Results

Absorption and fluorescence emission spectra for malachite green and crystal violet are presented in Fig. III.C-1. It is clear that, in the case of both dyes, the absorption maximum changes as a function of solvent composition in glycerol/water solutions (Fig. III.C-2), contrary to some previous literature reports. However, all kinetics presented in this work are independent of excitation wavelength from 580-620 nm and emission wavelength from 610-760 nm. The absorption spectra are superimposable on the fluorescence excitation spectra (not shown).

Log lifetime vs. log viscosity plots of the 2 fluorescence lifetimes resolved for crystal violet and the 3 fluorescence lifetimes of malachite green are shown in Figs. III.C-3 and III.C-4, respectively. The size of the points indicates the fractional contribution ϕ_i to the relative fluorescence quantum yield ϕ, $\Sigma_i \phi_i = \phi = \Sigma_i \alpha_i \tau_i$, where α_i is the preexponential factor (defined as A_i in some references), τ_i is the lifetime of the ith component, and ϕ is normalized to 1.0. The data are fit to a smooth curve for all lifetime components presented. The smooth curve fit to the third lifetime component of malachite green is not significant considering the error bars on the points. In general, errors in lifetime were ± 5% or 5 ps, whichever is greater.

Fig. III.C-1: Absorption and fluorescence emission spectra of malachite green (- - -) and crystal violet (——) in 100% glycerol, room temperature, normalized to 1.0 at the λ_{max} peak height. Absorption λ_{max} = 631 nm for malachite green and 598 nm for crystal violet. Fluorescence emission λ_{max} = 665 nm for malachite green and 644 nm for crystal violet. Dye concentration = 5×10^{-7}; pathlength = 1 cm.

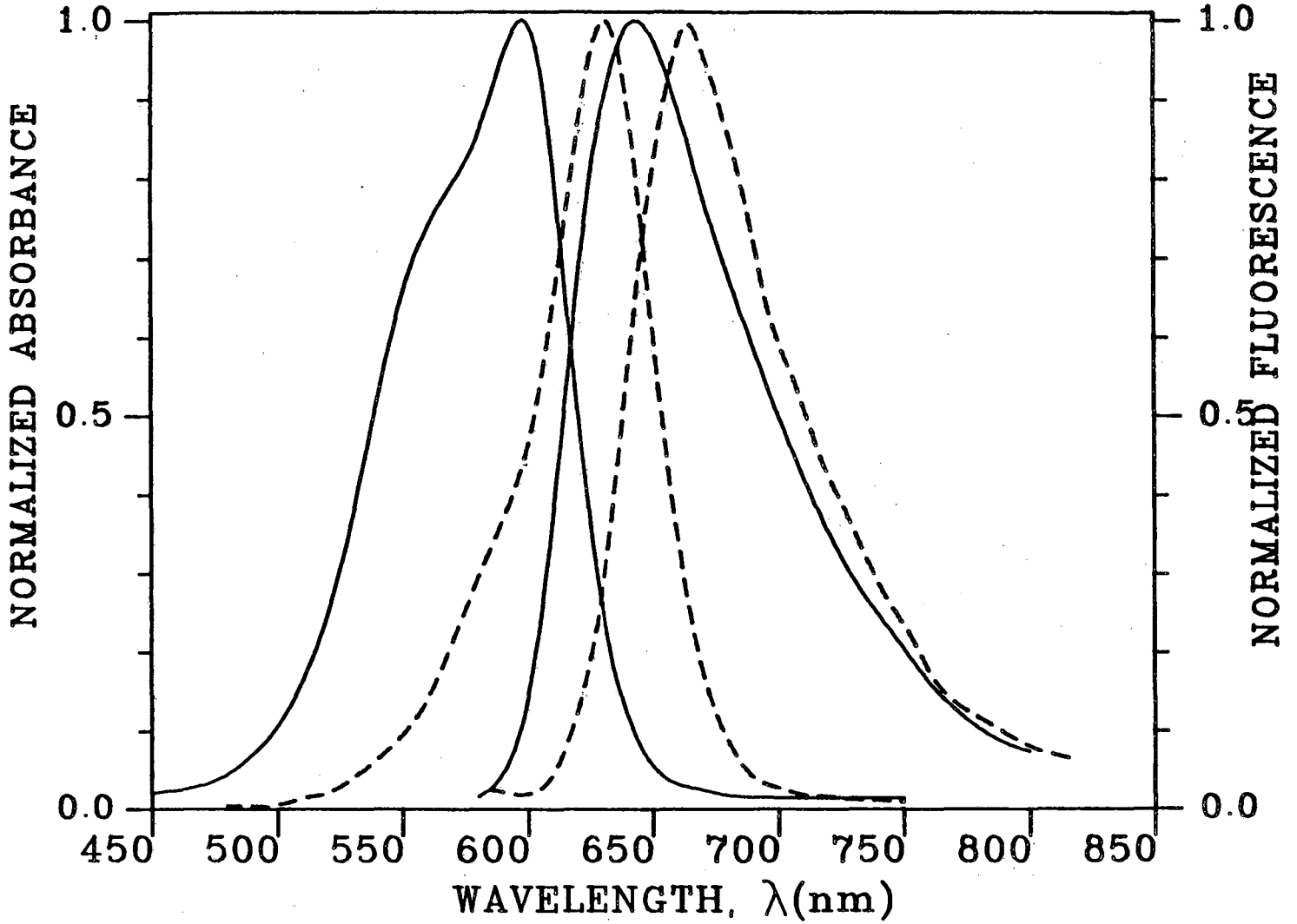
1.0
0.5
0.0
NORMALIZED ABSORBANCE
1.0
0.5
0.0
NORMALIZED FLUORESCENCE
450
500
550
600
650
700
750
800
850
WAVELENGTH, λ(nm)

Fig. III.C-2: Absorption spectra for malachite green in 27% glycerol/water (- - -) and 100% glycerol/water (——) solutions, normalized to 1.0 at the maximum peak height. Absorption λ_{max} = 622 nm for 27% and 631 nm for 100% glycerol/water solutions. Dye concentration = 5 x 10^{-7}; pathlength = 1 cm.

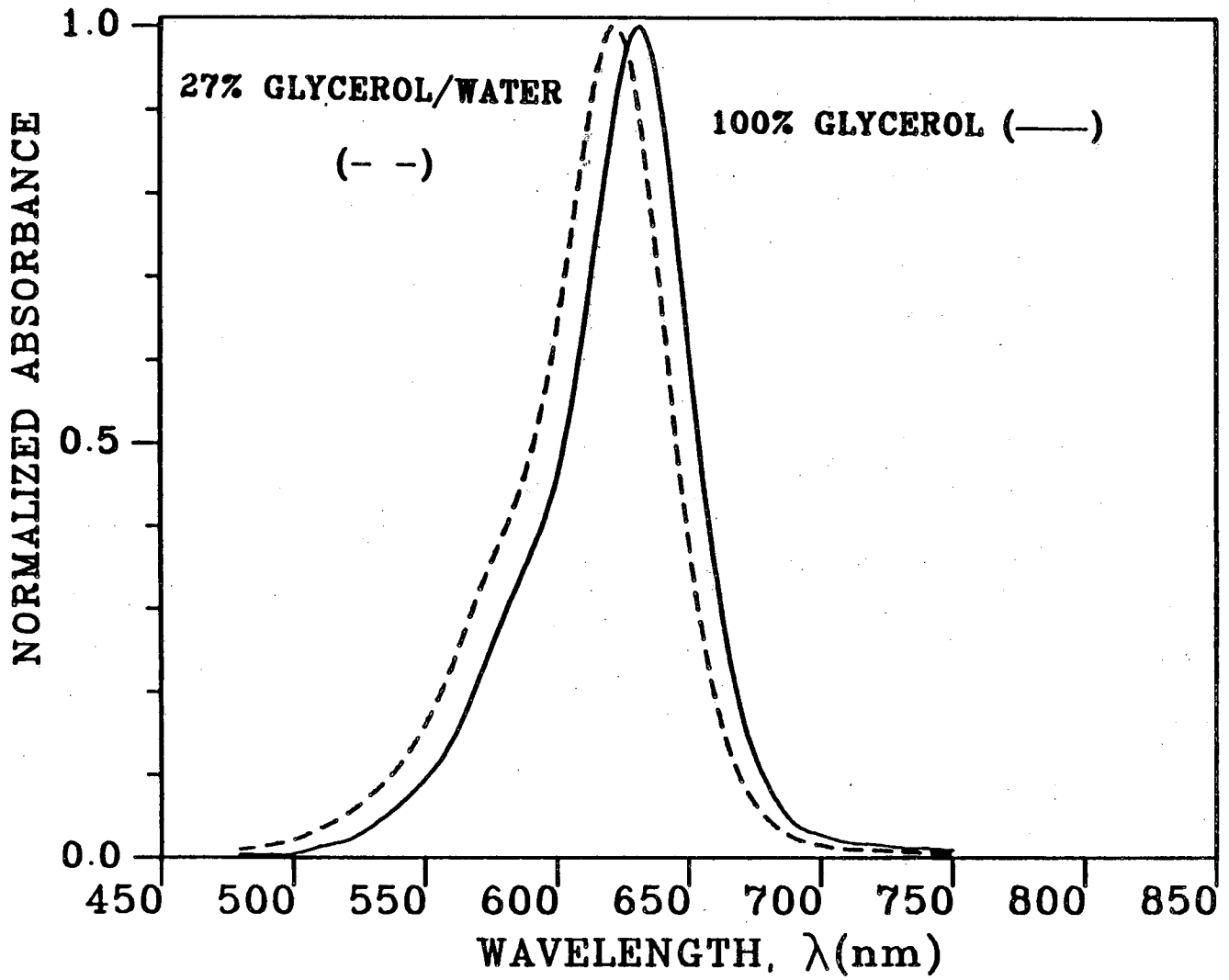
1.0
0.5
0.0
NORMALIZED ABSORBANCE
27% GLYCEROL/WATER
(- -)
100% GLYCEROL (——)
450
500
550
600
650
700
750
800
850
WAVELENGTH, λ(nm)

Fig. III.C-3: Log fluorescence decay lifetime, τ (ps) vs. log viscosity, η (cp) for the 3 lifetime components of malachite green in glycerol/water solutions. The size of each circle symbol is proportional to the relative quantum yield, $\phi_i = \alpha_i \tau_i$ of the ith component. One standard deviation is assigned for the error bar with an average of approximately 9 measurements. Curves are based on spline fits to the average values.

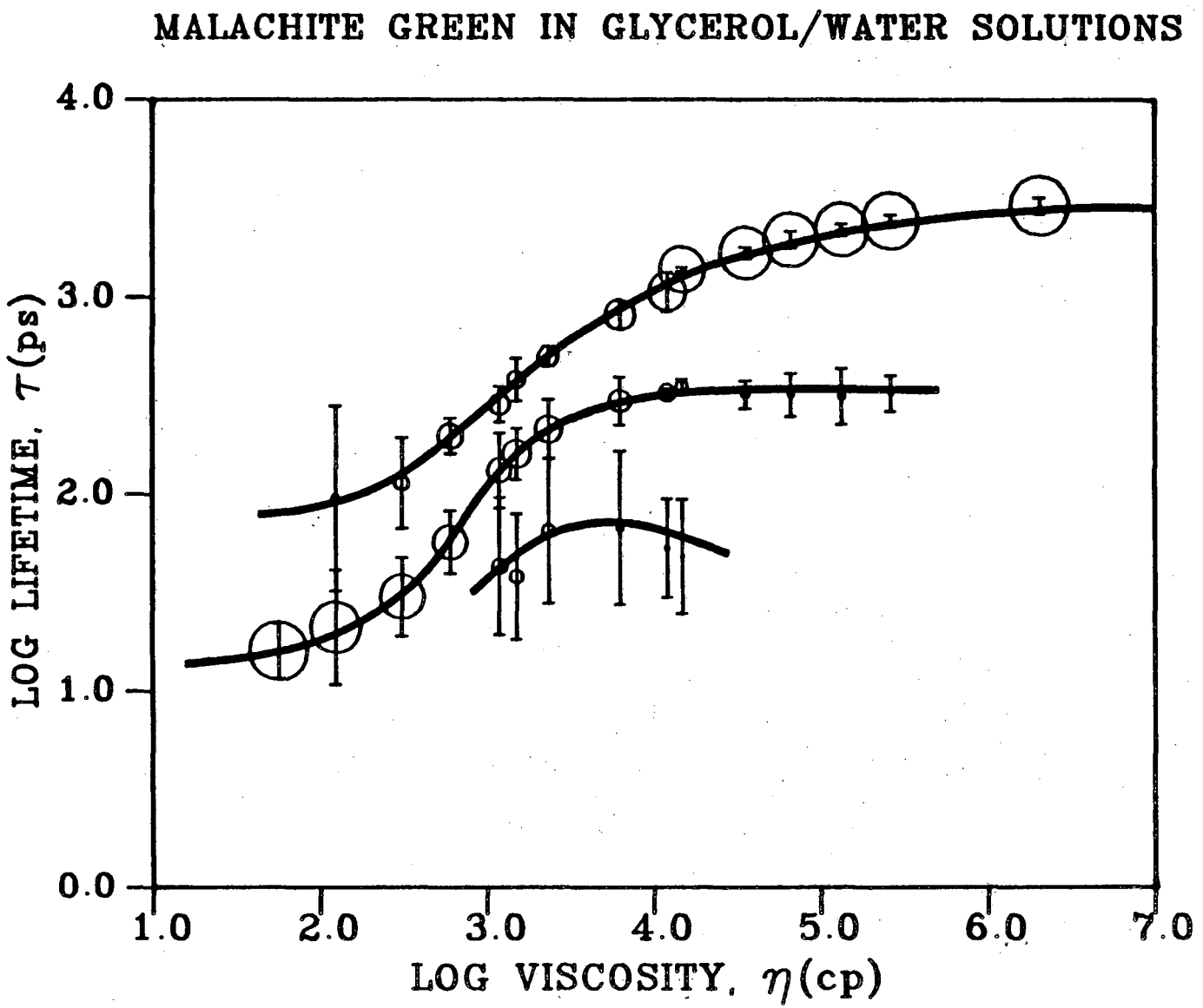
MALACHITE GREEN IN GLYCEROL/WATER SOLUTIONS
4.0
3.0
2.0
1.0
0.0
LOG LIFETIME, τ(ps)
1.0
2.0
3.0
4.0
5.0
6.0
7.0
LOG VISCOSITY, η(cp)

Fig. III.C-4: Log fluorescence decay lifetime, τ (ps) vs. log viscosity, η (cp) for the 2 lifetime components of crystal violet in glycerol/water solutions. The size of each circle symbol is proportional to the relative quantum yield, $\phi_i = \alpha_i \tau_i$ of the ith component. One standard deviation is assigned for the error bar with an average of approximately 9 measurements. Curves are based on spline fits to the average values.

CRYSTAL VIOLET IN GLYCEROL/WATER SOLUTIONS

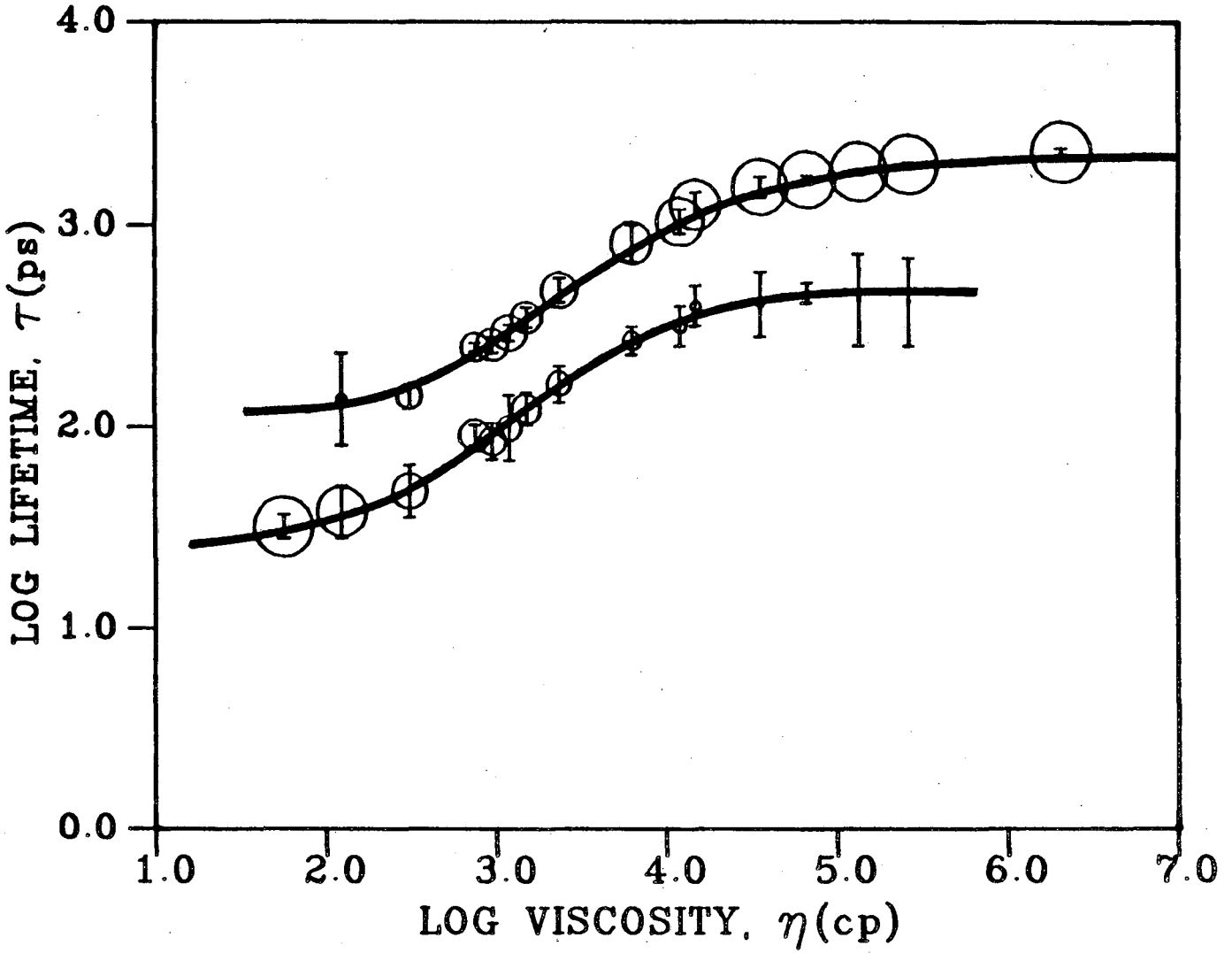

The approximate asymptotes and inflection points, for the curves corresponding to each lifetime component in Figs. III.C-3 and 4, are listed in Table III.C-1. The data were also fit by a linear regression analysis over various viscosity ranges, and the slopes are presented in Table III.C-2 and Table III.C-3 for malachite green and crystal violet, respectively.

The fluorescence quantum yield Q, calculated by collection time and integrated counts and normalized (for filters and laser intensity) to 1.0 for 100% glycerol at 25°C, is presented as a function of viscosity in Figs. III.C-5 and III.C-6 for malachite green and crystal violet, respectively. Again, the data are fit to a smooth curve. For both dyes, a plot of log Q vs. log η was fit by a linear regression analysis. Tables III.C-4 and III.C-5 contain the slopes from linear fits to various viscosity regimes for malachite green and crystal violet, respectively.

Fluorescence decay kinetics were fit to single exponential kinetics in the other solvents tested. The single lifetime components are presented with the viscosity of the solvent in Table III.C-6. These results fit the curve of Fig. III.C-3 within the error (± one standard deviation) of the measurement.

Table III.C-1: Estimated Asymptotes and Inflection Points from Figures III.C-3 and 4 for the Fluorescence Decay Lifetime Components of Malachite Green and Crystal Violet.

Molecule	Lifetime Component, τ_i	High Viscosity Asymptote (ps)	Low Viscosity Asymptote (ps)	Inflection Point (ps,cp)
Malachite Green	1	3000	80	325,1233
	2	345	12	74,614
	3	75	--	--,--
Crystal Violet	1	2330	110	389,2009
	2	440	22	100,1000

Table III.C-2: Linear Regression Fits of Log Lifetime vs. Log Viscosity for Malachite Green in Glycerol/Water Solutions.

Lifetime Component, τ_i	Viscosity Range (cp)	Slope	Correlation Coefficient, r
1	124 - 602	0.445	0.9306
2	56 - 602	0.513	0.9689
1	124 - 1186	0.507	0.9684
2	56 - 1186	0.668	0.9594
2	124 - 1186	0.811	0.9686
1	124 - 6260	0.590	0.9881
2	124 - 6260	0.760	0.9778
3	1186 - 6260	0.318	0.8132
1	602 - 6260	0.617	0.9921
2	602 - 6260	0.675	0.9449
1	124 - 12110	0.572	0.9910
2	56 - 12110	0.645	0.9747
2	124 - 12110	0.667	0.9655
3	1186 - 12110	0.142	0.5606
1	602 - 12110	0.568	0.9919
2	602 - 12110	0.534	0.9283
1	1186 - 12110	0.542	0.9888
2	1186 - 12110	0.381	0.9690
1	124 - 14900	0.579	0.9932
2	56 - 14900	0.613	0.9738
3	1186 - 14900	0.076	0.3677

Table III.C-3: Linear Regression Fits of Log Lifetime vs. Log Viscosity for Crystal Violet in Glycerol/Water Solutions.

Lifetime Component, τ_i	Viscosity Range (cp)	Slope	Correlation Coefficient, r
1	124 - 750	0.330	0.8909
2	56 - 750	0.390	0.9552
1	124 - 945	0.343	0.9309
2	56 - 945	0.383	0.9683
1	124 - 6260	0.480	0.9735
2	124 - 6260	0.516	0.9887
1	750 - 6260	0.591	0.9953
2	750 - 6260	0.560	0.9855
1	124 - 12110	0.489	0.9832
2	56 - 12110	0.462	0.9879
1	124 - 14900	0.502	0.9871
2	56 - 14900	0.472	0.9902

Fig. III.C-5: Log normalized quantum yield, Q vs. log viscosity, η (cp) for malachite green in glycerol/water solutions. The quantum yield is normalized to 1.0 at 100% glycerol at 25°C (1499 cp). Curves are based on spline fits.

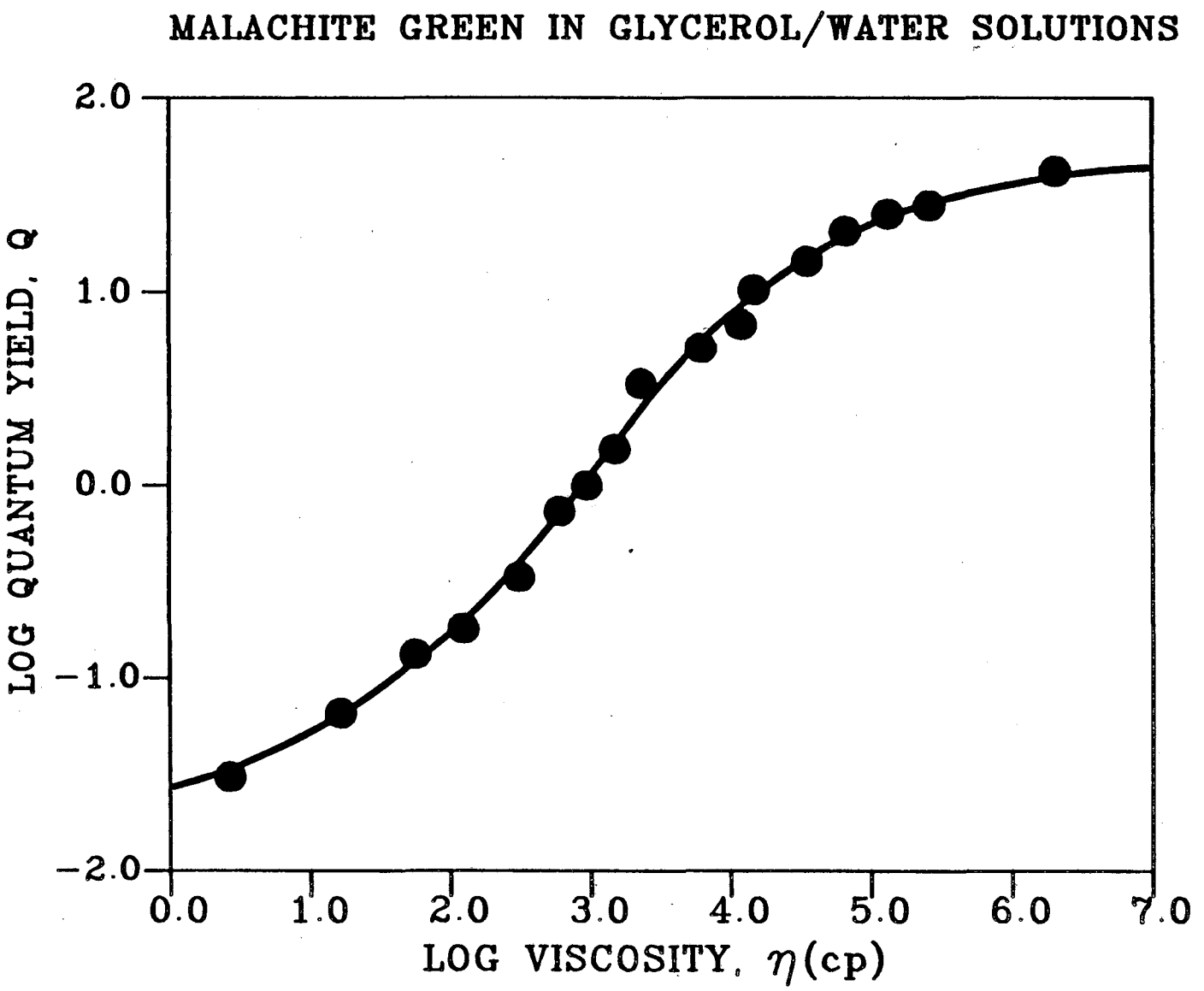
MALACHITE GREEN IN GLYCEROL/WATER SOLUTIONS
LOG QUANTUM YIELD, Q
2.0
1.0
0.0
−1.0
−2.0
0.0
1.0
2.0
3.0
4.0
5.0
6.0
7.0
LOG VISCOSITY, η(cp)

Fig. III.C-6: Log normalized quantum yield, Q vs. log viscosity, η (cp) for crystal violet in glycerol/water solutions. The quantum yield is normalized to 1.0 at 100% glycerol at 25°C (1499 cp). Curves are based on spline fits.

CRYSTAL VIOLET IN GLYCEROL/WATER SOLUTIONS

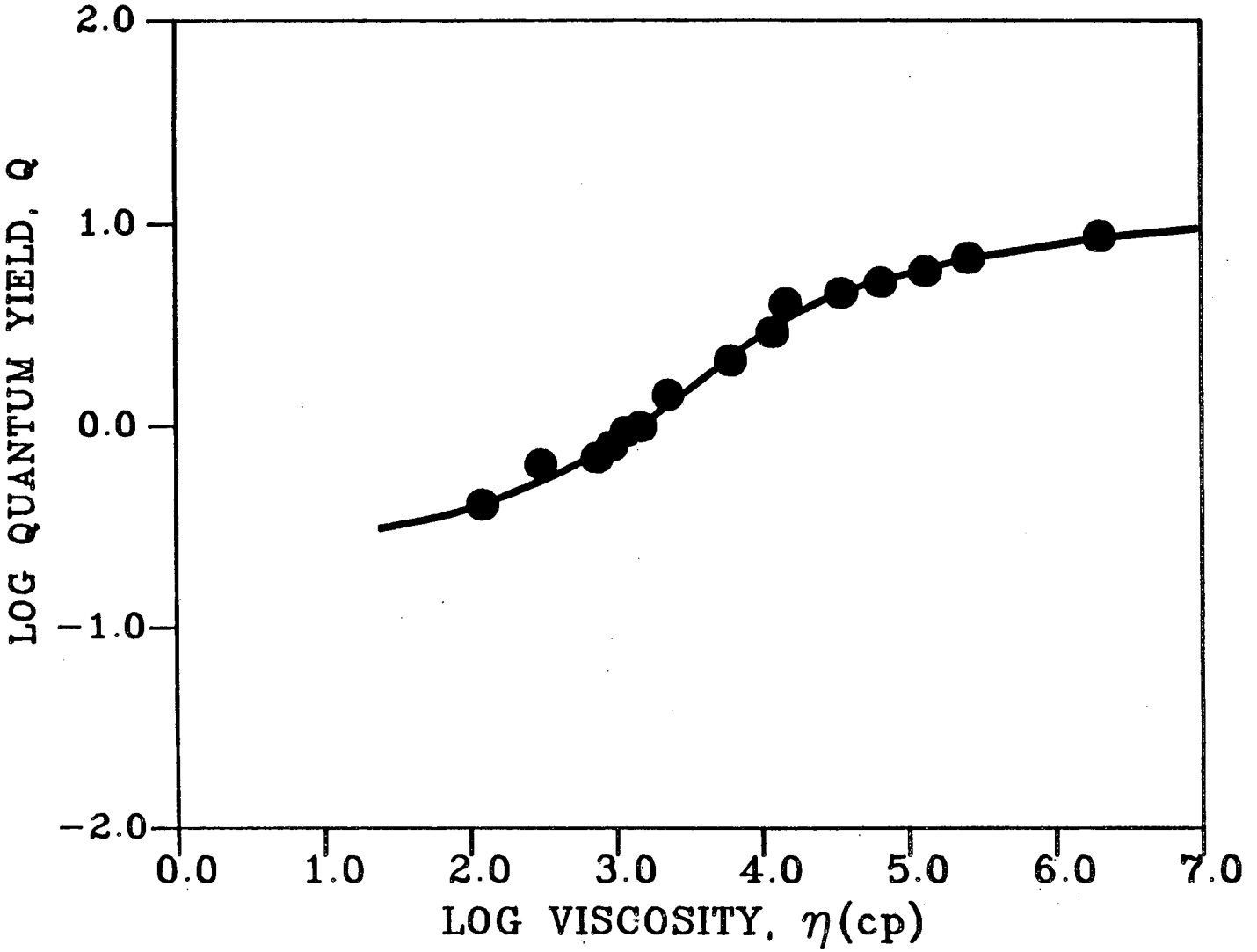

Table III.C-4: Linear Regression Fits of Log Quantum Yield vs. Log Viscosity for Malachite Green in Glycerol/Water Solution.

Viscosity Range (cp)	Slope	Correlation Coefficient, r
2.7 - 56	0.474	0.9958
2.7 - 602	0.558	0.9849
2.7 - 945	0.590	0.9851
56 - 945	0.742	0.9846
124 - 945	0.868	0.9927
124 - 6260	0.909	0.9904
602 - 6260	0.887	0.9748
945 - 12110	0.744	0.9610
602 - 12110	0.775	0.9739
124 - 12110	0.843	0.9877
2.7 - 12110	0.694	0.9857
2.7 - 14900	0.707	0.9875

Table III.C-5: Linear Regression Fits of Log Quantum Yield vs. Log Viscosity for Crystal Violet in Glycerol/Water Solutions.

Viscosity Range (cp)	Slope	Correlation Coefficient, r
124 - 750	0.302	0.9297
124 - 945	0.301	0.9536
124 - 6260	0.410	0.9767
750 - 6260	0.530	0.9920
124 - 12110	0.431	0.9845
124 - 14900	0.463	0.9831

Table III.C-6: Fluorescence Decay Lifetimes of Crystal Violet (10^{-6} M) in Various Solvents.

Solvent	Viscosity, η (cp)	Lifetime, τ (ps)
undecanol	14.6	30 ± 4
dodecanol	16.6	36 ± 4
cyclohexanol	33.0	40 ± 13
1,3-propanediol	40.8	29 ± 4
1,5-pentanediol	98.4	47 ± 3

III.D Discussion

Previous related studies by earlier workers, presented in the Introduction, can be summarized as follows:

1. The log of the fluorescence quantum yield, GSR relaxation lifetime and fluorescence decay lifetime for TPM dyes have been fit to a linear dependence on log viscosity.
2. Various fractional slope values have been obtained from the linear treatment of the log Q vs. log η and log τ vs. log η dependences (1/3, 1/2, 2/3, 0.58, 0.68, etc.), except for the results of Engh, Petrich, and Fleming which showed no dependence of GSR lifetimes on viscosity.
3. One and two exponentials and nonexponential fits have been reported for the various instrumental methods used.
4. Preexponential constants have been reported to be independent of viscosity.
5. Differences in the lifetime and quantum yield dependences on viscosity, number of lifetimes, value of the lifetime, etc. between malachite green and crystal violet have been reported and attributed to the differences in substitution of the phenyl ring and amino groups.
6. All previous models attempt to fit the region between the low and high viscosity asymptotes to a model in which τ, Q, or both τ and Q are proportional to a

power of viscosity. Some models attempt to fit the high viscosity region to a limiting value.

From Figs. III.C-3 and 4 and Tables III.C-2 and 3, it is apparent that the dependence of malachite green and crystal violet lifetimes on viscosity is complex. Except in the asymptotic regimes, the use of a model that describes the lifetime as dependent upon a simple power of the viscosity is questionable. The general shape of the curves between malachite green and crystal violet are the same. None of the results points to an effect clearly attributable to the different ring substitution of the two TPM dyes.

The asymptotic lifetime values and inflection points are important parameters that reflect the photophysics of the TPM dye. One interpretation using the FH model would suggest that, in the low viscosity regime, fluorescence lifetime values approach a limit because of the minimum in the excited state potential surface. At this minimum, internal conversion and the nonradiative decay rate have reached a maximum, and no further quenching of fluorescence can occur. The quenching of fluorescence by the enhanced internal conversion has reached an upper limit and the fluorescence lifetimes do not continue to decrease as a function of viscosity. This is consistent with the observation that the molecular systems with long lifetime decay components reach this nonradiative limit at higher viscosities than systems with short lifetime components (Table III.C-1). The systems

with long lifetime components have longer times to probe the potential surface to find the minimum in the excited state potential surface. Because the phenyl ring rotation drives the molecules to this minimum, and ring rotation is hindered at high viscosity, only the systems with long lifetimes will remain in the excited state long enough to find the minimum at higher viscosities.

The high viscosity lifetime limit reflects a hindrance of rotation by solvent friction to the extent that no enhancement of internal conversion occurs on the time scale of fluorescence. This also explains why the systems with shorter lifetime components reach this radiative limit at lower viscosities than the systems with long lifetime components.

Almost all previous functional relations of log Q vs. log η and log τ vs. log η can be reconciled with the restricted viscosity region that was studied and the predominant lifetime component that was measured (Tables III.C-2 and 3). Especially informative is the result of Engh, Petrich, and Fleming who showed a limit (independence) of GSR lifetimes vs. viscosity in the low viscosity regime provided by the solvents water and methanol.[11] This viscosity regime corresponds well with the nonradiative regime determined from our fluorescence decay data.

The dependence of crossover between the nonradiative and radiative limits should be contained in the shape of the curves and in the inflection points. FH modeled this region

with a damped solvent friction but were not able to fit the curvature.[10]

The multi-component nature of the decay can be explained by a heterogeneous emitting population, the heterogeneity arising from differences in displacement from the S_1 potential surface minimum. These differences in displacement are continuous, however. The multicomponent exponential fit most likely represents a nonexponential decay of a continuum in the excited state, rather than a discrete set of excited state conformations. Such differences in displacement would be expected to result in differences in gap energy between S_0 and S_1 and a wavelength dependence of kinetics on emission wavelength. The lack of dependence of fluorescence lifetime on wavelength and the dependence of GSR lifetime on wavelength demonstrated by Sundstrom et al.[23] can be accounted for if the fluorescence occurs to a vibrationally excited state of the ground electronic state surface, S_0^*, that does not have a displaced minimum from that of the S_1 surface, and then nonradiative relaxation occurs to S_0. However, if the fluorescence occurs to a surface that does not have a displaced minimum from the S_1 surface, the enhancement of the internal conversion as a function of viscosity will not occur.

Intermediate states have been proposed and appear to be necessary to explain both ground state recovery and fluorescence lifetime results. Sundstrom et al.[23] proposed a rapid

equilibrium between 2 excited states to explain the biexponential emission kinetics together with the observation of emission from only one of the two conformers (the long wavelength absorbing conformer). However, our lifetimes correspond more closely with the ground state recovery lifetimes of the short wavelength absorption conformer that they have proposed. This conformer was proposed to be absent in malachite green, but even for this dye our results are consistent with this short wavelength absorbing conformer. In addition, the kinetics that we observe are multiexponential and have a complex viscosity dependence.

Expanding on this last point, we do not conclude that only 2 or 3 lifetimes exist in the TPM dye system. Clearly, as viscosity changes, the percentage of the initial excited state population (amplitude, α_i) due to each decay component changes (Figs. III.C-3 and 4), and the ability to resolve very small yields of fast components dictates the number of components detected. The fitting criterion used was the reproducibility of the data, the reduced χ^2, and the examination of the weighted residuals for systematic deviations, as shown in Fig. III.B-1. In some analyses, a third, faster component could be resolved for crystal violet in the same viscosity range as the third (fastest) component of malachite green. However, this component for crystal violet is not shown because the fits were not significantly improved over two component fits and the resolution of the third lifetime component was not satisfactorily reproducible. Faster time

resolution and an increased signal-to-noise ratio may result in additional resolved components.

There are many inconsistencies between the model of Sundstrom et al.[23] and our fluorescence decay kinetics. First, our data show no excitation or emission wavelength dependence. Second, the kinetics appear to be independent of solvent, with regard to size or dielectric constant (Table III.B-6). Third, there are no discriminating features of the decay data between crystal violet and malachite green. Our results are supported by some previous fluorescence decay results, if the viscosity regime and error bars are considered. Our results are also supported by GSR kinetics of Cremers and Windsor and of Engh et al.[5,6,9] In fact, from our results we predict the low viscosity asymptotic region observed by Engh et al. (which was also independent of solvent composition).

In general, the BFO and FH models predict the proper viscosity dependence for our data but not the data of Sundstrom et al. These models are not consistent with the analyzing wavelength dependence of the GSR kinetics of Sundstrom et al. nor with the lack of excitation or emission wavelength dependence of our fluorescence data. No model currently fits both the GSR and fluorescence decay kinetics and the various GSR and fluorescence lifetime-viscosity dependences. A new model will clearly have to be more complex to account for the viscosity dependence, and a

treatment using a two-dimensional potential surface seems necessary to explain the various wavelength correlations.

The low viscosity asymptote points from log quantum yield vs. log viscosity are not as clear. Errors result from our inability to fit to short lifetimes and detect low yields at these lower viscosities. These errors are probably due to instrument limitations or the mathematical limitations of multiexponential curve-fitting. The data of FH more clearly indicate the asymptotic behavior if a system similar to ours is considered (e.g. room temperature glycerol/methanol solutions and low temperature glycerol solutions). Nevertheless, the viscosity regions are apparent in the quantum yield plots (Figs. III.C-5 and 6) and confirm results of FH and our fluorescence lifetime analysis.

III.E Conclusion

From the foregoing synopsis, it is clear that there is no general agreement on the viscosity dependence of the fluorescence lifetimes of TPM dyes. Further, it is unclear whether there is any viscosity regime over which the TPM fluorescence lifetimes obey a simple equation based on a power of the viscosity. Rather, we have presented results over a wide range of viscosity, in which the fluorescence lifetimes are related to the viscosity by a smooth sigmoid-shaped curve. In particular, we examined crystal violet, which exhibits a double exponential decay, and malachite green, from which we obtained three decay lifetimes, and find that (with the exception of one decay time in malachite green) the curves are smooth and sigmoid-shaped. In addition, we find that the coefficients for the exponentials in each dye vary with the viscosity. No conclusion can be drawn that relates differences in fluorescence decay kinetics with differences in ring substitution between these two TPM dyes. No dependence of the fluorescence decay kinetics on solvent, excitation wavelength, or emission wavelength is observed.

References

1. Bagchi, B., G. R. Fleming, and D. W. Oxtoby, J. Chem. Phys., 78 (1983) 7375.

2. Beddard, G. S., T. Doust, and M. W. Windsor, in "Picosecond Phenomena II", R. M. Hochstrasser, W. Kaiser, and C. V. Shank, eds., Springer, N.Y. (1980) 167.

3. Bolt, J. D. and K. Sauer, Biochim. Biophys. Acta, 637 (1981) 342.

4. Brey, L. A., G. B. Schuster, and H. G. Drickamer, J. Chem. Phys., 67 (1977) 2648.

5. Cremers, D. A., Ph.D. Thesis, Washington State University, 1980.

6. Cremers, D. A. and M. W. Windsor, Chem. Phys. Letters, 71 (1980) 27.

7. Deno, N. C., J. J. Jarulselski, and A. Schriesheim, J. Org. Chem., 19 (1954) 155.

8. Doust, T., Chem. Phys. Letters, 96 (1983) 522.

9. Engh, R. A., J. W. Petrich, and Graham R. Fleming, J. Phys. Chem., 89 (1985) 618.

10. Forster, Th. and G. Hoffmann, Z. Physik. Chem. NF, 75 (1971) 63.

11. Gomes de Mesquita, A. H., C. H. MacGillavry, and K. Eriks, Acta Crystallogr., 18 (1965) 437.

12. Haehnel, W., J. A. Nairn, P. Reisberg, and K. Sauer, Biochim. Biophys. Acta, 680 (1982) 161.

13. Hirsch, M. D. and H. Mahr, Chem. Phys. Letters, 60 (1979) 299.

14. Ippen, E. P. , C. V. Shank, and A. Bergman, Chem. Phys. Letters, 38 (1976) 611.

15. Lewis, G. N., T. T. Magel, and D. Lipkin, J. Am. Chem. Soc., 64 (1942) 1774.

16. Magde, D. and M. W. Windsor, Chem. Phys. Letters, 24 (1974) 144.

17. Mastrangelo, C. J. and H. W. Offen, Chem. Phys. Lett., 46 (1977) 588.

18. Oster, G. and Y. Nishijima, J. Am. Chem. Soc., 78 (1956) 1581.

19. Saiken, S. and J. Sei, J. Chem. Phys., 79 (1983) 4154.

20. Segur, J. B., in "Physical Properties of Glycerol and Its Solutions", from Glycerol, Carl S. Miner and N. N. Dalton, eds., Reinhold Publishing Corporation, N.Y. (1953) 238.

21. Sheeley, M. L., Ind. Eng. Chem., 24 (1932) 1060.

22. Sundstrom, V. and T. Gillbro, J. Chem. Phys., 81:8 (1984) 3463.

23. Sundstrom, V., T. Gillbro, and Hans Bergstrom, Chem. Phys., 73 (1982) 439.

24. Turko, B. T., J. A. Nairn, and K. Sauer, Rev. Sci. Instrum., 54 (1983) 118.

25. Yu, W., F. Pellegrino, M. Grant, and R. R. Alfano, J. Chem. Phys., 67 (1977) 1766.

CHAPTER 4

CONCLUSION AND FUTURE EXPERIMENTS

IV.A Methods and Instrumentation

The improvement of the time-resolved techniques used to monitor energy transfer can aid in the determination of the energy transfer mechanism in phycobiliproteins. In addition, the development of fluorescence decay kinetics provides another tool to study the photosynthetic process.

IV.A1 Deconvolution

Improvements can be made in deconvoluting fluorescence decay data. Laplace and Fourier transforms are being developed as replacement methods for real time domain methods.[1,6] They offer the advantage of more efficient computer execution, the use of a fractional shift, and fewer model assumptions. Currently, we allow the excitation profile to shift by an integral number of channels to correct for differences between the excitation E(t) file and experimental F(t) file. The differences may occur because of instrumental drift with time or other systematic differences (excitation wavelength dependent shifts, etc.). Instrumental drift is a more probable explanation for the observed shift because excitation files collected close in time to fluorescence files will fit without a shift. This suggests that instrument time is the most important factor.

However, deviations in the weighted residuals still usually occur at shorter times. These deviations usually cannot be reduced by adding another lifetime component. We have been able to reduce the deviations by calculating a fractional shift through a linear interpolation. In many cases, however, the fits are unstable and converge to different values depending upon which direction the E file is shifted.

An important advantage of transform methods is that they allow the fractional shift to be performed in the transformed domain. The fractional shift becomes even more critical with narrower instrument responses. Another method that can be used is splining. A splined E file can be fractionally shifted fairly easily. In addition, Dr. Robert Ross (Ohio State Univ., Dept of Biochemistry) is developing methods to use splined E and F files for deconvolution.

The transform methods involve an actual deconvolution, a solution of the convolution integral equation of Section II.B3c. No model need be assumed to obtain the initial solution but the interpretation of the decay parameters still involves the use of a model.

All of these methods lend convenience but do not change the basic fact that the signal-to-noise ratio determines the number and accuracy of the lifetime components.[7] This leads us to Section IV.A2 and a discussion of methods to improve the amount of information obtained from the data.

IV.A2 Component analysis

The most promising technique for obtaining more information from fluorescence decay data is called factor analysis. If a species in solution has decay kinetics (lifetimes or amplitudes) that vary linearly and continuously with some other variable, such as excitation or emission wavelength, then a matrix of data can be collected and used to resolve each species, or factor, more precisely.[9,2,11] This is an excellent way to improve the apparent signal-to-noise by obtaining correlated data and using these correlations to define the system. Spectra and individual decay profiles are obtainable for each factor. The factors are determined uniquely if 3 variable (or 3 dimensional) matrices are used. A common choice in fluorescence decay studies includes the decay, the excitation wavelength, and the emission wavelength. This is also a good choice and an important method for studying energy transfer in systems where the Forster mechanism is operative. As applied to phycobiliproteins, this implicates s and f chromophores whose fluorescence decay kinetics would be excitation wavelength dependent. However, for very efficient transfer, transfer times would be short (< 50 ps) and the quantum yield for the leakage fluorescence from s chromophores could be 1% or less. Such short, small yield components would be impossible to detect with currently available signal-to-noise ratios and with the heterogeneous, multiexponential decays of phycobiliproteins (including separated subunits). Therefore, a

technique, such as factor analysis, which is very sensitive to wavelength dependences and other correlated data, is necessary for the unequivocal determination of energy transfer factors, e.g. factors assignable to s and f chromophores, or factors assignable to resolvable chromophore conformations. Dr. Bruce Holmer (U. C. Berkeley, Computer Sciences Dept.) and Dr. Robert Ross are developing 3 dimensional factor analysis techniques.

Phycobiliproteins are a prime example of the need and utility of factor analysis, but other systems will benefit from this technique. Of course, all photosynthetic systems and most biophysical systems (even isolated amino acids, such as tryptophan) have multiexponential decay kinetics. Reasonably, we can assume that some of these lifetime components are wavelength dependent and belong to resolvable factors that can be correlated to structurally distinct species. Dye systems, such as the TPM dyes, have also been suggested to show wavelength dependent photophysics. Apparently, wavelength-resolved decay curves are very important for further energy transfer studies. Suggestions concerning the efficient collection of wavelength dependent data are presented in Section IV.A3. Other variables, such as electrochemical potential, polarization, temperature, etc. can be combined with wavelength to comprise the 3 (or more!) dimensional data matrix.

IV.A3 Wavelength-resolved decay kinetics

From previous sections, it is clear that the solution of many of the questions in photosynthesis, energy transfer, and photophysics depends on accurate wavelength resolution of the picosecond fluorescence decay kinetics. Starting on the excitation side of the sample, the pumped dye laser is still one of the best sources of tunable, high repetition, variable power pulses necessary for single-photon timing. On the emission side, the 10 nm bandpass (FWHM) interference filters currently used will be replaced by a high thruput, low scatter, high resolution monochromator. These have already been developed in other systems with high gain PM tube detectors (Holzwarth and Yamazaki, References in Sections II.A and II.C). These detectors have been shown to approach the time resolution of current MCP's when the emission is carefully focussed on the photocathode. (However, see Section IV.A4.) Moreover, gains are larger and tube life longer than MCP detectors. The unique spatial resolution of the MCP, however, can be utilized to provide wavelength resolution.

The MCP has spatial resolution on the order of 1 or 2 channels (10-100 μm). A segmented anode could easily provide 10 different segments and can take advantage of the entire photocathode and anode surfaces (usually 10-20 mm diameter).[4] The output of a monochromator can be imaged on the photocathode and the current pulse outputs from the distinct anodes delayed and gated. This would provide, for

example, 10 separate wavelength bands that can be collected. The bandwidth and interval spacing would be provided by the monochromator dispersion and anode spacing. Since almost the entire photocathode area of an MCP is useable, the expected gain would be about five times the current focussed configuration. Our tests of the MCP indicated that the use of the whole surface of the photocathode did not appreciably change the FWHM, but also did not increase the gain in a direct proportion to the new surface area. However, there is some increased gain and, therefore, instead of having to collect 10 separate decays, decays could be collected simultaneously in 1/2 to 1/5 the time needed at present. In addition, the bandwidth could be reduced. Also, since excitation files would be collected closer in time to multiple fluorescence files, fewer time shifts and instrument drift errors would be encountered.

IV.A4 Time resolution

Time resolution remains an important consideration because energy transfer times and important conformational photophysics can occur in < 10 ps. Pulse-probe measurements are now approaching the 0.5-1 ps time regime but still suffer from low signal-to-noise ratios when distinguishing among the numerous lifetime components in biophysical systems.

New technology in MCP's is now being developed by Hamamatsu and ITT. In particular, ITT is developing new electrode configurations which provide more efficient signal

collection and faster time response.[3] These developments promise MCP's with FWHM of 50-70 ps which could provide time resolution of 5-7 ps with the advantage of high signal-to-noise and multicomponent analysis. New Canberra TAC's provide digitization of the voltage ramp that gives ≦ 1 ps per channel resolution. In addition, MCA's also now provide A to D conversion to collect over an 8 ns range with 1 ps per channel resolution. Currently, CFD's and fast amplifiers have now become the bottleneck for faster time resolution. However, it is probably safe to predict that these roadblocks will also be removed and time resolution in single-photon counting will drop below 5-10 ps, providing time resolution necessary to test for intermediate and strong coupling energy transfer in photosynthetic systems. One of the promising systems for study in this time domain is the isolated phycobiliproteins of cryptomonads which have been shown to exhibit strong coupling among the chromophores (Section II.A2).

IV.B TPM dyes

Many questions still remain about TPM dye photophysics. The wavelength, solvent, and temperature dependence of the lifetimes and number of decay components are not explainable by the available models. The existence of ground state or excited state isomers has been proposed, but the evidence is not compelling. The shape of the excited state potential surface is still unknown. Some experiments to examine these questions follow.

IV.B1 Separation of temperature, viscosity, and solvent dependence of fluorescence decay kinetics.

As indicated in Chapter 3 (and by Cremers and Windsor[5]), the most important solvent property for determining the photophysics for TPM dyes is the solvent viscosity, either macroscopic or microscopic. However, some recent GSR results (Sundstrom and Gillbro[12]) indicate that temperature and solvent are also crucial. There may be solvent-induced activation energy barriers to the rotation of the phenyl rings in the excited state. Therefore, further temperature studies on single solvent systems, such as the n-alcohols, varying the temperature but not the solvent in an experiment, should be performed to test for these solvent-dependent barriers. Our preliminary work (Table III.C-6) does not indicate an activation energy dependent on temperature or solvent, but those experiments were not performed to systematically test for the temperature or solvent dependence. Differences in lifetimes (rates), viscosity dependence of the kinetics, number of kinetic components, and wavelength dependence of those components between GSR and time-resolved fluorescence spectroscopy become apparent upon comparing previous GSR and time-resolved fluorescence experiments, including our results presented in Chapter 3. Therefore, no a priori assumptions can be made about the results of experiments to separate the temperature, solvent, and viscosity effects on fluorescence decay kinetics.

In addition to the time resolved experiments, steady-state absorption, fluorescence excitation and fluorescence emission spectroscopy could be used to monitor the band shape changes as a function of temperature, solvent, and viscosity. The last attempt at steady-state spectroscopy to systematically study the photophysics of TPM dyes was made in 1942 by Lewis et al.[10] The interpretations presented therein are not completely consistent with modern knowledge of photophysics and spectroscopy. The repetition and extension of those experiments would assist in interpreting the picosecond experiments.

In our studies, we picked crystal violet and malachite green because of their use in previous literature. This choice was fortunate, allowing us to make comparisons with literature that distinguished between two classes of TPM dyes, of which malachite green and crystal violet are representative members. Our data, however, does not indicate any classifiable characteristics. In order to carefully study the effect of substitution and to attempt any classification, further steady-state and picosecond experiments on a series of TPM dyes are necessary.

IV.B2 Time-resolved Raman spectroscopy

Because the present evidence for the change in the bond character of the central carbon-phenyl carbon bonds upon excitation is not conclusive, Raman spectroscopy on the picosecond time scale could be of some use. The time

evolution of the different conformers formed upon excitation can be followed. This would provide information about the activation barrier and the shape of the excited state potential surface. It is not clear whether actual excited state or ground state intermediates are present in TPM dyes. The distinction between the two kinds of intermediates is dependent on bond order and conformation, and time-resolved information about these characteristics is important for the description of TPM photophysics. Resonance Raman could be used to investigate the chemical structure of the ground state isomers that have been proposed.

IV.B3 Transient absorption spectroscopy

Although ground state recovery and excited state absorption kinetics have been obtained for TPM dyes in the past, much of this work is contradictory and is not readily explained by instrument differences between workers. Therefore, transient absorption studies performed on the same samples under the same conditions that we have used for fluorescence measurements would help in interpreting some of the conflicts in data. In combination with previous experiments suggested in Section IV.B1 and 2, these measurements would provide the most complete description of the TPM dyes.

IV.C Phycobiliproteins

Questions remain about the mechanism of energy transfer in isolated phycobiliproteins. The Methods and

instrumentation section contains ways to improve our ability to monitor energy transfer kinetics. We have shown that phycobiliproteins have conformational heterogeneity, but the exact chemical structure of these conformers and how they affect the function of phycobiliproteins remains unclear. Some experiments to probe the conformational heterogeneity follow.

IV.C1 Effect of temperature on decay kinetics

The results in Section II.C2a on the effect of temperature between 25 and 0°C on the fluorescence decay of the monomer and separated subunit of C-phycocyanin are not clear. These experiments should be repeated now that better temperature control and better time resolution are available. The trimer of R-phycocyanin, with and without linker, is another candidate for this kind of experiment. An extension of these experiments to temperatures between 25 and 60°C would be helpful in checking the measurements of Hefferle et al., who investigated this temperature regime using streak camera instrumentation.[8] They assigned the shorter components they observed to energy transfer, which is not consistent with our results or those of other workers. On the contrary, we would assign these intermediate (100-700 ps) lifetime components to conformational heterogeneity, and it would be interesting to resolve and quantify these components in temperature regions where the biliproteins and subunits began to denature. Metastable conformational states that

have been inferred to be related to in vivo function have been observed for partially denatured biliproteins (phycochromes; see Section II.A). The kinetics of these states as a function of temperature may tell us about their relation to the energy transfer function of phycobiliproteins. Wavelength-resolved kinetics in these temperature ranges are crucial, because the absorption, fluorescence excitation, and fluorescence emission maxima and band shapes change upon partial or complete denaturation. The model, in which the intermediate lifetime components are in a dynamic equilibrium with the long lifetime component of $\approx$ 1.4 ns, can be tested if higher sensitivity or better time resolution were available. Our initial results were not conclusive and this model may yet explain the heterogeneous decay kinetics of phycobiliproteins.

IV.C2 Time-resolved Raman spectroscopy

Resonance Raman spectroscopy is one of the most sensitive techniques available for providing dynamic structural information about subtle conformational differences. In general, quantitative structural information is available only if model compounds are available and specific band assignments are made. However, if some variable, such as temperature (suggested in Section IV.C1) can be used to vary the amount of the different conformations, the quantitative information can be gained about the ratios and equilibria among conformations in

solution. Qualitative information will also be available about the identity of the conformations. Time-resolved Raman spectroscopy can provide the same information in phycobiliproteins as that in the TPM dye system. Such experiments can be modeled after the time-resolved Raman work on visual pigments. It is becoming increasingly apparent that such protein-chromophore interactions are also important in phycobiliproteins. Raman spectroscopy has now reached the stage where techniques (CARS, antistokes Raman) to monitor highly fluorescent systems (such as isolated photosynthetic antenna) are now advanced enough for these experiments to be useful.

IV.C3 Methods and instrumentation

Of course, the material covered in Section IV.A is generally applicable to most photochemistry. However, it was presented with the TPM dye and phycobiliprotein systems as the classic cases for study. These two systems provide the fast, coupled, and heterogeneous kinetics to test any new deconvolution technique or improvement in time resolution. They also are proving ground for factor analysis and the efficient collection of wavelength-resolved decay kinetics. These dyes and phycobiliprotein systems continue to provide some of the most interesting questions about photophysics in condensed phases, especially those related to the environment of the chromophore and the chromophore-environment interactions.

References

1. Ameloot, M. and H. Hendrickx, Biophys. J., 44 (1983) 27.

2. Beechem, J. M., J. R. Knutson, J. B. A. Ross, B. W. Turner, and L. Brand, Biochemistry, 22 (1983) 6054.

3. Ceckowski, D. H., Personal communication.

4. Ceckowski, D. H., E. Eberhardt, and E. Carney, IEEE Trans, Nucl. Sci., NS-28 (1981) 677.

5. Cremers, D. A. and M. W. Windsor, Chem. Phys. Letters, 71 (1980) 27.

6. Good, H. P., A. J. Kallir, and U. P. Wild, J. Phys. Chem., 88 (1984) 5435.

7. Grinvald, J. and I. Z. Steinberg, Anal. Biochem., 59 (1974) 583.

8. Hefferle, P., W. John, H. Scheer, and S. Schneider, Photochem. Photobiol., 39 (1984) 221

9. Knutson, J. R., J. M. Beechem, and L. Brand, Chem. Phys. Lett. 102 (1983) 501.

10. Lewis, G. N., T. T. Magel, and D. Lipkin, J. Am. Chem. Soc., 64 (1942) 1774.

11. Marchiarullo, M. A. and R. T. Ross, Biochim. Biophys. Acta, 807 (1985) 52.

12. Sundstrom, V. and T. Gillbro, J. Chem. Phys., 81 (1984) 3463.

This report was done with support from the Department of Energy. Any conclusions or opinions expressed in this report represent solely those of the author(s) and not necessarily those of The Regents of the University of California, the Lawrence Berkeley Laboratory or the Department of Energy.

Reference to a company or product name does not imply approval or recommendation of the product by the University of California or the U.S. Department of Energy to the exclusion of others that may be suitable.

TECHNICAL INFORMATION DEPARTMENT
LAWRENCE BERKELEY LABORATORY
UNIVERSITY OF CALIFORNIA
BERKELEY, CALIFORNIA 94720